



UNIVERSITÀ DEGLI STUDI DI NAPOLI
FEDERICO II

Dottorato di Ricerca in
INGEGNERIA GEOTECNICA
XXIII CICLO
Coordinatore
Prof. Claudio Mancuso

Barbara Bitetti

EFFECTS OF TUNNELLING IN URBAN AREAS

RELATORE

Prof. Alessandro Mandolini

ACKNOWLEDGEMENTS

The result of an experimental work like this Thesis, is not strictly related only to the person who is in charge of presenting it officially. All the merits, hence, have to be shared among various persons which have contributed, even if with different roles and in different ways.

The first thank I have to express is in regards of my tutor, Prof. Alessandro Mandolini.

Then I would like to thank the Dutch group, in particular, Prof. Frits Van Tol, Wout Broere and Ronald Brinkgreve for their infinite availability both in hosting me in a foreign country and in guiding me wisely within the complex world of numerical analysis.

Apart from the academic world, I must thank all the persons and enterprises which allowed me to get my experimental data. In particular, a great “thank” is in regards of Ing. Mario Carastro, Geom. Michele Merlo and Ing. Michele Barbato (Riviera S.p.A.) and Ing. Andrea Belfiore (Rocksoil S.p.A.).

CONTENTS

ACKNOWLEDGEMENTS

INTRODUCTION	1
Chapter 1. BACKGROUND	3
1.1. Introduction	3
1.2. Tunnelling-induced soil movements	3
1.3. The prediction of ground movements due to tunnelling	5
1.3.1. Empirical methods	6
1.3.1.1. Transverse behavior	6
1.3.1.2. Longitudinal behavior	9
1.3.1.3. Volume loss	12
1.3.1.4. Trough width parameter	15
1.3.1.5. Subsurface movements	17
1.3.2. Numerical analyses of tunnel construction	21
1.3.2.1. Two dimensional analyses	22
1.3.2.2. Three dimensional analyses	26
1.4. Building damage assessment	30
1.4.1. Definition of structure deformation parameters	31
1.4.2. Evaluation of risk of damage	32
1.4.2.1. Preliminary assessment	33
1.4.2.2. Second stage assessment	33

1.4.2.3.	Detailed evaluation	34
1.4.3.	Category of damage	35
1.4.4.	Calculation of building strain	37
Chapter 2. LINE 6: A 3 KM TUNNEL IN A DENSELY URBANIZED ENVIRONMENT		44
2.1.	Introduction	44
2.2.	LINE 6: the design	45
2.2.1.	Ground conditions	48
2.2.1.1.	Site and laboratory investigations	50
2.2.2.	The used excavation technique	57
2.2.3.	The monitoring plan	59
2.2.3.1.	Installed monitoring instruments	63
2.3.	The empirical methods for prediction of tunnelling induced displacements	66
Chapter 3. LINE 6: ANALYSIS OF MONITORING DATA		76
3.1.	Introduction	76
3.2.	Tunnel excavation	76
3.3.	Field monitoring data	81
3.3.1.	Excavation machine performances	82
3.3.2.	Landmarks on the ground surface	83
3.3.3.	Landmarks on buildings	97

Chapter 4.	THREE-DIMENSIONAL FINITE ELEMENT ANALYSIS	111
4.1.	Introduction	111
4.2.	Plaxis 3D Tunnel: useful informations for Line 6 application	111
4.2.1.	The Hardening Soil Model	113
4.3.	Three-dimensional analyses of the Line 6 tunnel	121
4.3.1.	The input model	121
4.3.2.	The effects of soil parameters on surface subsidence	124
4.3.3.	Parametric analyses on the EPB front and grouting pressures	130
4.3.4.	Back-analysis of observed effects of Line 6 tunnelling	136

APPENDIX

REFERENCES AND BIBLIOGRAPHY

INTRODUCTION

The always increasing demand in new transportation routes in urban area, in the last years, led to the need in increasing the present road transports; by then, the need to use the underground environment for new transportation lines became always more important. New underground lines started to be excavated in many of the largest cities in the world, leading to a large number of shallow and deep excavations in the urban environment.

Many tunnels, often located at relatively shallow depth from the ground surface, started to be excavated, inducing not negligible effects on the preexisting buildings. For such a reason, methods directed to the induced tunnelling effects prediction were developed on the basis of empirical data collected all over the years. Despite such empirical methods resulted very useful and reliable for the designing process of a tunnel line, as to predict the tunnel induced displacements on the ground surface, they base on very simplified hypothesis, neglecting important phenomena such as the soil-tunnel-buildings interaction and considering in a simplified way the excavation technique influence. Indeed data collected from literature, demonstrated how the improvements in technologies in the last years allowed an important reductions in induced displacements on the ground surface. For a such a reason numerical analysis of the excavation technique influence on tunnelling induced displacements, became always more significant.

Thus, the purpose of this research is to define the importance of excavations technologies, in terms of tunnelling induced effects on the ground surface, inspired by the current construction process of the Line 6 tunnel in Naples. For this purpose, a number of numerical analyses, by means Finite Element codes, were performed as to simulate the tunnel excavation process, and to carry on a parametric study on the technology influence on the induced effects, finally compared to results of a similar parametric study concerning the geotechnical properties of the soils affected by the excavation. Results of such analyses were then used to back-analyze monitoring data collected during the Line 6 tunnelling process.

Chapter 1. BACKGROUND

1.1. Introduction

The construction of tunnels in soft ground inevitably leads to ground movements.

Since most of the excavation processes usually take place in extremely densely urbanized environment, affecting existing surface or subsurface structures, the determination of their magnitude plays an important role in designing process and in defining the most useful technique to use.

This chapter summarizes methods to estimate tunnel induced ground movements and to assess the resultant damage on buildings.

1.2. Tunnelling-induced soil movements

The displacements field (Fig. 1-1) induced by the excavation of tunnel in soft ground, is strongly affected by many phenomena, such as:

- Face deformations due to stress release, relevant in open-faced tunnels or in EPB or slurry shield excavations when the face pressure is not rightly controlled; they have been strongly reduced by the introduction of the Tunnel Boring Machine;
- movements induced by shield in advancing, due to the over-cutting, useful to reduce friction between shield and ground: they strongly depend by the over-cutting edge thickness and by any steering problems in maintaining the alignment of the shield;
- ground movements in between the lining and the shield tail, reduced by using grout injections or, in case of expanded lining used, by expanding the lining as soon as possible;

- lining deflections due to earth pressure, generally smaller than the other movements components once the final lining is installed;
- long term deformations due to consolidation process in clayey soils.

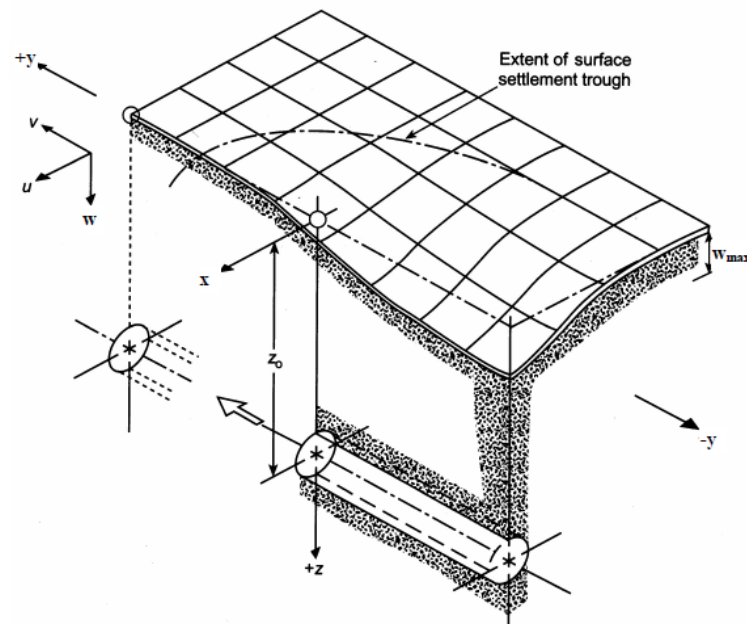


Fig. 1-1. Ground movements induced by tunnel excavations (after Attewell et al., 1986)

Time dependency in the mechanical behavior of soil influences ground movements resulting from tunnelling, leading to the classification of short, medium and long-term movements.

Short-term movements usually occur at the most the first four days after the excavation in London clay; by reporting short-term settlements over a period of 24 hour before and after the passage of the shield, Macklin and Field (1999) showed that short-term displacements occur almost instantaneously with the advance of tunnel heading, leading to a constant volume response of the ground and to a suddenly new stress regime. Because of strains are usually less than 0.1% (a part from very locally to the tunnel), not enough to cause failure or alter the soil structure, the constitutive model for the soil does not change in this phase.

Medium and long-term settlements, caused by alteration of soil properties at constant load, due to such phenomena as creep, ageing and/or consolidation. The timescale over which they occur depends on ground conditions, varying from weeks or months for sand and soft clays, to years for stiff clays.

About the magnitude of short-term compared with long-term tunnel-induced displacements, case histories suggested that for typical site on stiff clay, around 60% of the total settlements occurs in the short term (Simons and Som, 1970; Morton and Au, 1975).

Attewell and Selby (1989) observed long-term settlements up to 2.5 times the short term, but also that the long-term trough width tended to be wider than the short-term; it implies the structures are more able to accommodate long-term than short-term settlements, which consequently are the chief issue of engineering problems related to tunnel-induced displacements.

1.3. The prediction of ground movements due to tunnelling

Many methods were implemented to quantify tunnelling induced ground movements: from the analytical methods, to predict displacements in green-field conditions, going through more sophisticated numerical models (e.g. Finite Element Methods), up to the physical models, such as centrifuge tests, reproducing in small scale the in situ situation.

As for numerical analyses a sufficiently accurate constitutive model for the soil is required, for the modelling technique (either laboratory or numerical), the tunnelling process has to be represented with an acceptable degree of accuracy.

1.3.1. Empirical methods

1.3.1.1. Transverse behavior

The current and widely used empirical design methods for predicting ground surface settlements in response to tunnelling operations, can be dated back to Peck & Schmid (1960); afterwards, Peck¹ (1969) introduced the Normal Gaussian Distribution (Fig. 1-2) as the curve matching at the most the field data representing the tunnel induced settlements on ground surface in green-field conditions. Since then, its mathematical formulation expressed by (1.1) has been accepted as it allows a quite straightaway calculation of vertical displacements in transverse direction; it is given by:

$$S_v(x) = S_{v,max} \cdot e^{-\frac{x^2}{2i_x^2}} \quad (1.1)$$

where:

- $S_{v,max}$ is the maximum settlement above the tunnel axis;
- i_x is the distance between the inflection point of the curve, where the trough has its maximum slope, and the central axis of the tunnel; it separates the *sagging* from the *hogging* zone of the curve
- $S_v(x)$ is the settlement at distance x from the tunnel axis.

¹ “Ordinarily the settlements above the tunnel, unless caused by a local disturbance such as a run into the face or stopping above the crown, are more or less symmetrical about the vertical axis of the tunnel. They form a trough like depression with a shape roughly resembling the error function or probability curve” (Peck, 1969)

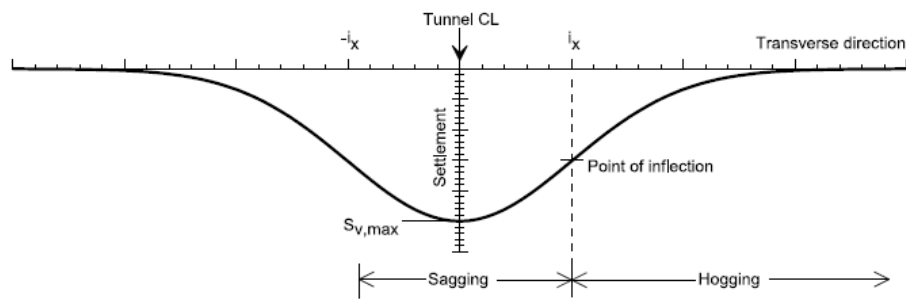


Fig. 1-2. Transverse settlements trough

As it represents the probability that the x has a value between $-\infty$ and $+\infty$, the area below the trough is by definition equal to 1, as a consequence the area enclosed by settlements trough is defined by:

$$V_s = \int_{-\infty}^{+\infty} S_v(x) dx = \sqrt{2\pi} \cdot i_x \cdot S_{v,max} \quad (1.2)$$

V_s is the volume of the settlements trough per unit length, strictly dependent by the ground affected by the excavation. In grounds with low permeability, such as stiff-clays, with initially undrained response to the excavation process, which means not allowed changing in volume, the volume of settlements trough has to correspond to the excess excavated volume of ground to the theoretical volume of the tunnel. It is usual to define the extra excavated ground as *Volume Loss*, given by:

$$V_L(\%) = \frac{V_s}{\frac{\pi \cdot D^2}{4}} (\%) \quad (1.3)$$

where D is the outer tunnel diameter. V_L is usually defined as a proportion of theoretical tunnel volume per unit length, expressed as a percentage of it.

Combining the (1.2) to (1.3), the transverse settlements profile can be expressed in terms of *Volume Loss* as:

$$(1.4)$$

$$S_v(x) = \sqrt{\frac{\pi}{2}} \frac{V_L \cdot D^2}{4 \cdot i_x} \cdot e^{-\frac{x^2}{2i_x^2}}$$

It shows that for a given tunnel diameter D , the settlements profile only depends by the *Volume Loss* V_L and by the trough width i_x , two crucial parameters that need to be defined to know the settlements field induced by tunnelling.

O'Reilly & New (1982) showed that the transverse horizontal surface displacements can be derived from the previous equations, considering their resultants pointing toward the center of the tunnel. They gave the expression to determine them:

$$S_{hx}(x) = -\frac{x \cdot S_v(x)}{z_0} \tag{1.5}$$

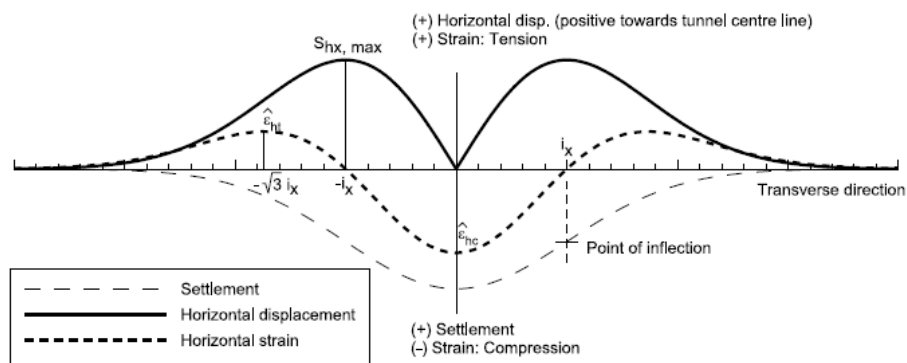


Fig. 1-3. Horizontal surface displacements and strains in transverse direction together with settlement trough

Fig. 1-3 clearly shows as the maximum horizontal displacements occur at the point of inflections of settlements trough ($x = i_x$). By differentiating the horizontal displacements with respect to x , the horizontal strains can be obtained from (1.5) as shown in equation (1.6)

(1.6)

$$\varepsilon_{hx}(x) = \frac{S_v(x)}{z_0} \cdot \left(\frac{x^2}{i_x^2} - 1 \right)$$

Equation (1.6) leads to compression being defined as negative while a positive value is assigned to tension. Fig. 1-3 shows the development of a compression zone between the two points of inflections i_x and i_y and of a tensile zone outside them; the maximum compression strain develops at $x=0$, while the maximum tensile strain develops at $x = \sqrt{3} \cdot i_x$.

1.3.1.2. Longitudinal behaviour

Attewell and Woodmann (1982) showed that even the longitudinal settlement profile can be defined through a cumulative probability curve $\phi(y)$, given by:

(1.7)

$$\phi(y) = \frac{1}{i_y \cdot \sqrt{2\pi}} \cdot \int_{-\infty}^y e^{-\frac{y^2}{2i_y^2}}$$

as a consequence the longitudinal profile is described by equation (1.8) while the generic settlement is expressed by (1.9) :

(1.8)

$$S_v(y)_{x=0} = S_{v,\max} \cdot \phi\left(\frac{y}{i}\right)$$

(1.9)

$$S_v(y) = S_v(x, y, z) \cdot \frac{\pi \cdot D^2}{4} \cdot V_L \cdot \frac{1}{\sqrt{2 \cdot \pi}} \cdot \frac{1}{K \cdot z} \cdot \exp\left[\frac{-y^2}{2 \cdot (K \cdot z)^2}\right] \cdot \left[\phi\left(\frac{x-x_0}{K \cdot z}\right) - \phi\left(\frac{x-x_f}{K \cdot z}\right) \right]$$

The shape of longitudinal displacements curve is shown in Fig. 1-4. It indicates the minimum and maximum values of the longitudinal settlements reached respectively at $y = -\infty$ (ahead the tunnel face) and $y = +\infty$ (behind the tunnel face), while above the tunnel face ($y = 0$) it is $S_v = S_{v,\max} / 2^2$.

For completely defining the longitudinal settlement profile, it is important to know about the curve width, defined by the i_y value. Attewell et al. (1986) compared the magnitudes of i_x and i_y for a range of case studies; they observed that usually i_x is bigger than i_y (the transverse settlements troughs were longer than the longitudinal ones); on the basis of field data coming from the tunnel construction of the Jubilee Line Extension beneath St. James's Park in London, Nyren (1998) observed the same behavior translated into the ratio $i_x / i_y = 1.3$. However, despite this discrepancy, it is common to consider $i_x = i_y = i$.

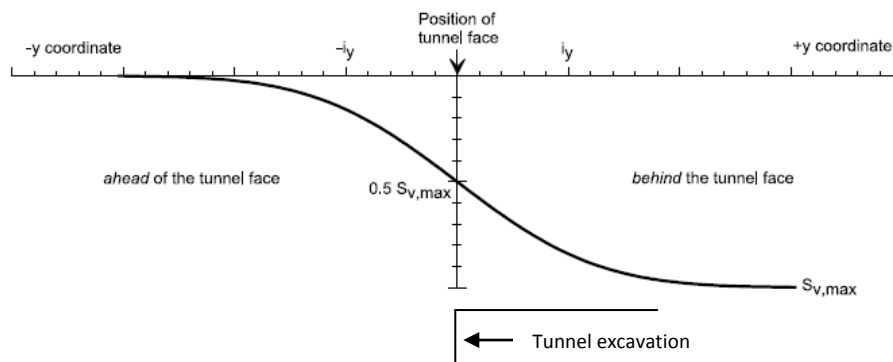


Fig. 1-4. Longitudinal settlement profile after Attewell et al., 1986

Attewell et al. (1986) assumed that for open face tunnelling, the settlement above the tunnel axis ($x = 0$) is 50% of the maximum settlement reached behind the tunnel face, while for closed face tunnelling, where significant face support is provided, the

² Attewell & Woodman (1982) showed that above the tunnel face, for stiff clays usually occurs $S_{v(y=0)} \approx 40\% S_{v,\max}$

displacements ahead the tunnel face reduce significantly. Mair and Taylor (1997) concluded that for closed face tunnelling the settlements above the tunnel axis is 25% - 30% the maximum settlement; this leads to a longitudinal displacements curve translated as shown in Fig. 1-5.

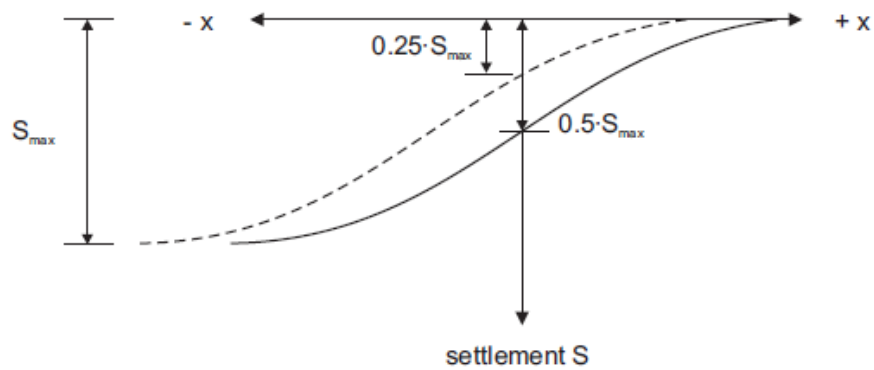


Fig. 1-5. Longitudinal settlement profile for open face and closed face tunnelling after Mair & Taylor (1997)

Based on the analyses of tunnel induced displacements in the United Kingdom, Craig & Muir Wood (1978) stated that, for each point of observation, depending on the ground, for open face tunnelling, nearly the 80% - 90% of the settlement is reached when the face is one to two times the tunnel depth.

Type of ground	Percentage of total settlement completed	
	At face of shield [%]	At passage of tail of shield [%]
Sand above water table	30-50	60-80
Stiff clays	30-60	50-75
Sand below water table	0-25	50-75
Silts and soft clays	0-25	30-50

Tab.1-1. Development of settlement profile (Craig & Muir Wood, 1978)

Observing the horizontal displacements going toward the center point of the tunnel face, Attewell & Woodman (1982) gave the expression (1.10) for determining the horizontal displacements at the ground surface in the longitudinal direction:

$$S_{hy}(y)_{x=0} = \frac{V_L \cdot D^2}{8 \cdot z_0} \cdot e^{-\frac{y^2}{2i^2}} \quad (1.10)$$

By deriving (1.10) with respect to y , the horizontal strains in longitudinal directions can be obtained; it yields:

$$\varepsilon_{hy}(y)_{x=0} = -y \cdot \frac{V_L \cdot D^2}{8i^2 z_0} \cdot e^{-\frac{y^2}{2i^2}} \quad (1.11)$$

which describes tension (positive value) ahead the tunnel face ($y < 0$) and compression behind it ($y > 0$).

Because all the above defined displacements and strains strictly depend by the troughs width parameter i and by the Volume Loss V_L , on the next section the attention is going to be focused on them.

1.3.1.3. Volume loss

The volume loss is a measure of total disturbance of the ground caused by tunnelling. In undrained conditions it represents the volume of the settlements trough at the surface.

It can be defined as *“the ratio of the difference between the excavated soil (defined by the outer tunnel diameter) and the tunnel volume, over the tunnel volume”* (cfr. Expression (1.3)).

It is caused by different soil movements due to tunnelling. Attewell (1978) divided the sources of volume loss into four categories:

- **Face loss:** radial soil movements toward the unsupported tunnel face
- **Shield loss:** radial ground loss around the tunnel shield increased by eventual overcutting caused by poor workmanship
- **Ground loss during and subsequent to lining erection:** caused by soil movements towards the tunnel, due to the unsupported soil in between the shield and the last erected lining; to prevent it is common practice to grout any voids between soil and lining
- **Ground loss after grouting:** due to lining deformations after the grouting, caused by the transfer of the overburden pressure.

Several methods have been proposed to estimate the volume loss.

Attewell (1978) proposed a method to determine the four components of V_L based on the ratio between the rate of soil movements into the excavation (determined from laboratory tests) and the rate of tunnel in advance.

Many relations have been proposed to determine V_L on the base of the stability factor N . Broms & Bennermark (1967) defined N as:

$$N = \frac{\sigma_v - \sigma_t}{s_u} \quad (1.12)$$

where σ_v is the total overburden pressure at tunnel axis, σ_t is tunnel support pressure (if present) and s_u is the undrained shear strength of the clay. As greater is N as more plastic zones are going to develop around the tunnel: for $N < 2$ an elastic response is shown with a stable tunnel face (Lake et al., 1992), for $2 < N < 4$ some local plastic zones develop around the tunnel while for $4 < N < 6$ plastic yielding is likely leading to face stability when $N > 6$.

In the past many relations have been suggested relating N with tunnel depth or with V_L ; Mair & Taylor (1993) showed a relation between N and the tunnel depth for unsupported tunnels in London Clay, pointing out a value between 2.5 and 3 for the stability ratio N .

Lake et al. (1992) showed a relation between N and V_L summarizing the relations proposed by many others authors; they showed that a stability ratio $N = 2$ leads to a V_L between 1.5% and 3% (Fig. 1-6).

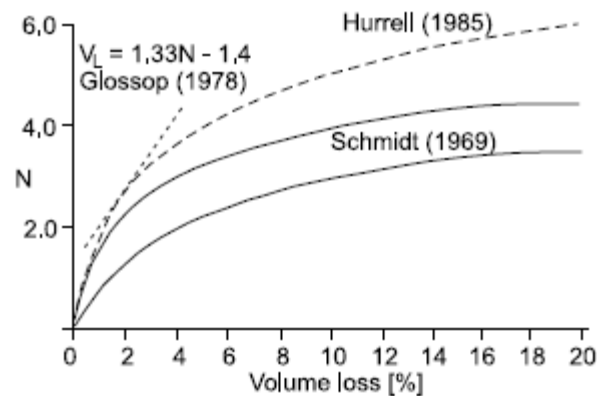


Fig. 1-6. Relations between N and V_L (after Lake et al., 1992)

Davis et al., (1980) presented lower and upper bound analytical solutions for shallow tunnels with support pressure in cohesive soils. They considered the case of plane-strain unlined circular tunnel (radial ground movements), a plane strain heading (face movements) and circular tunnel heading (the full three-dimensional case). They reached the conclusion that in the examined cases, the stability ratio at collapse varies with depth and even showed how for the three-dimensional case the difference between the lower and upper bound collapse load was the greatest, indicating the difficulties in applying analytical solutions for three-dimensional problems. The Authors plotted the results in term of N_{TC} against the cover to diameter ratio C/D . Data from centrifuge tests (Mair, 1979) confirmed the solutions for a plane strain unlined circular heading, with best agreement for C/D less than 3, the value defined as a practical transition between shallow and deep tunnel, the first characterized by a failure mechanism involving the ground surface, the latter by a symmetric failure mechanism with a little influence on the surface.

Mair et al. (1981) introduced the *Load Factor* LF to take account for this effect:

$$LF = \frac{N}{N_{TC}} \quad (1.13)$$

where N is the stability ratio at the working conditions and N_{TC} is the stability ratio at collapse (Fig. 1-7).

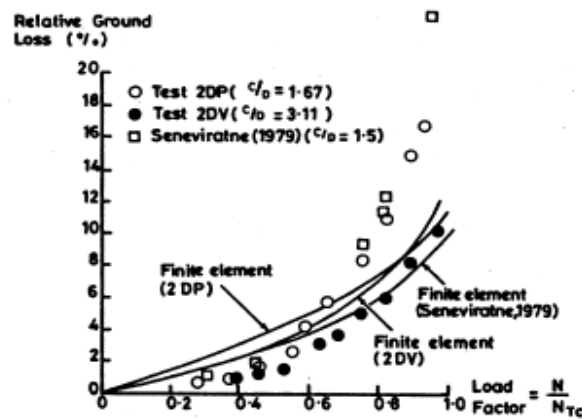


Fig. 1-7. Relations between LF and V_L determined from centrifuge tests and finite element analyses (after Mair et al., 1981)

1.3.1.4. Trough width parameter

Based on 19 case histories for cohesive grounds and on 16 for cohesionless soils (all in the United Kingdom), O'Reilly & New (1982) showed a linear dependence between the trough width parameter i and the tunnel depth z_0 shown in Fig. 1-8, defined by (1.14) and (1.15) and simplified by (1.16) .

$$i = 0.43 \cdot z_0 + 1.1 \quad \text{for cohesive soils} \tag{1.14}$$

$$i = 0.28 \cdot z_0 - 0.1 \quad \text{for non-cohesive soils} \tag{1.15}$$

$$i = K \cdot z_0 \tag{1.16}$$

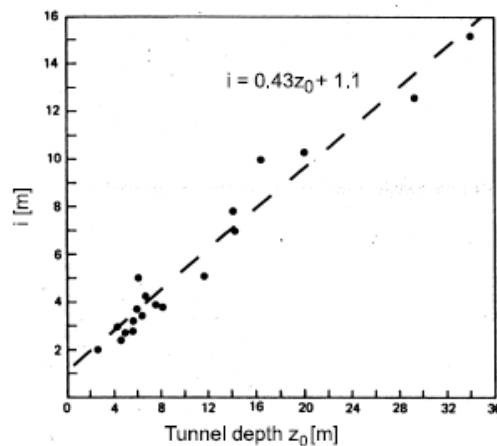


Fig. 1-8. Correlation between i and the tunnel depth z_0 (after O'Reilly & New, 1982)

The Authors pointed that k can vary between $k = 0.4 \div 0.7$, going from stiff to soft clay and concluded that $k = 0.5$ is an appropriate value for clay, for most design purpose. The same result was later confirmed by Rankin (1988) who presented a similar study based on an enlarged data base, so that (1.16) becomes:

$$i = 0.5 \cdot z_0 \quad (1.17)$$

Kimura & Mair (1982) obtained the same results from centrifuge tests and also showed that K value does not depend by the tunnel technique since $k = 0.5$ is obtained independently of the degree of support within the tunnel. Later work by others researchers confirmed that usually $k = 0.4 \div 0.5$ for cohesive soils, while $k = 0.25 \div 0.35$ for cohesionless ground.

1.3.1.5. Subsurface movements

Only the ground surface settlements have been examined in the previous section. Although surface settlements is the most straight forward way to describe ground

deformation, it only gives a limited picture of the real mechanism controlling tunnel-soil and if it is the case, tunnel-soil-building interaction.

Mair & Taylor (1993) described vertical and horizontal subsurface ground movements by applying the plasticity solutions for the unloading of a cylindrical cavity, showing their good agreements with collected field data.

The solution they presented shows a linear relation between ground movements (S_v/R or S_h/R , where S_v and S_h are respectively vertical and horizontal movements while R is the tunnel radius) and the distance from tunnel centre as R/d (where d is the horizontal or vertical distance from tunnel centre). The Authors focused their attention on vertical displacements above the tunnel centre line and on horizontal movements at tunnel axis level. They concluded that the Gaussian curve to describe subsurface settlements troughs is in good agreement with collected field data which means that (1.17) could be straight forward applied by substituting z_0 with $(z_0 - z)$ where z is the required movements 'depth.

$$i = 0.5 \cdot (z_0 - z) \tag{1.18}$$

Presenting field and centrifuge data, Mair et al. (1993) also showed that settlements troughs are wider with depth z . Fig. 1-9 shows the relation between z/z_0 and i/z_0 ; it can be seen how the dashed line, representing (1.18), underestimates i with depth. What better fits the data is the solid line, having equation:

$$\frac{i}{z_0} = 0.175 + 0.325 \cdot \left(1 - \frac{z}{z_0}\right) \tag{1.19}$$

which, substituting $i = k \cdot (z_0 - z)$ becomes:

$$K = 0.325 + \left(\frac{0.175}{1 - \frac{z}{z_0}} \right) \tag{1.20}$$

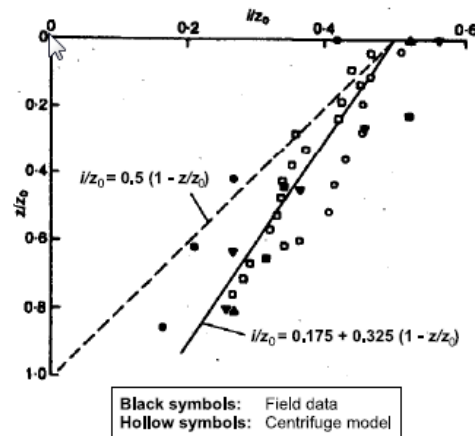


Fig. 1-9. Variation of trough width parameter i of subsurface settlements troughs with depth z (after Mair et al., 1993)

Combining equation (1.3) and (1.4) with (1.19), the maximum settlement of subsurface trough can be expressed as:

$$\frac{S_{v,\max}}{R} = \frac{1.25 \cdot V_L}{0.175 + 0.325 \cdot \left(1 - \frac{z}{z_0}\right)} \cdot \frac{R}{z_0} \quad (1.21)$$

It is represented by curve B and C in Fig. 1-9; it represents lower and upper bound for the range of tunnel depths ($R/z_0 = 0.1 \div 0.6$) and volume losses (1.4%) of field data considered in the graph, and also shows how (1.21) would overpredict subsurface $S_{v,\max}$ settlements troughs. If normalizing $S_{v,\max}$ also against V_L , a good agreement is obtained even with greenfield measurements from the Jubilee Line Extension (St. James's Park) presented by Nyren (1998), having a much higher V_L ($V_L = 3.3\%$).

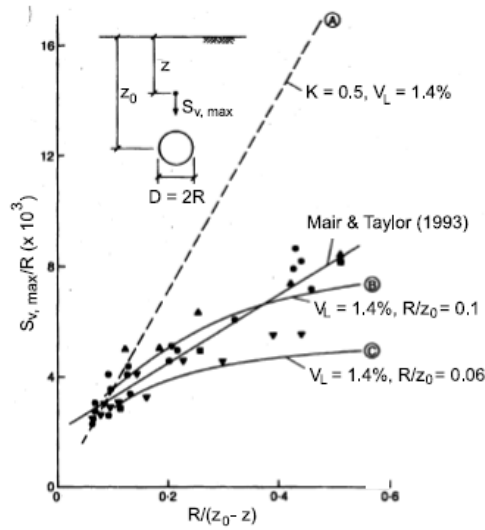


Fig. 1-10. Subsurface settlement above tunnel centre line (after Mair et al., 1993)

A different approach to estimate the trough width and the maximum settlement at surface was proposed by Heath & West (1996). They suggested using a binomial distribution, instead of the Gaussian curve, to describe the settlement trough. Their approach yields to:

$$\frac{i}{i_0} = \sqrt{\frac{z_0 - z}{z_0}} \tag{1.22}$$

where i_0 is the trough width at ground surface level. Equation (1.21) leads to a maximum surface settlement $S_{v,max}$ proportional to $(z_0 - z)^{-1/2}$. Comparing prediction of $S_{v,max}$ obtained from their work with the results given by Mair et al. (1993) it can be seen how the two different approaches give the same results for $0 < \frac{z}{z_0} < 0.8$ while, close to the tunnel, Heath & West (1996) solution predicts larger values of $S_{v,max}$, being in total agreement with field data they collected.

About the horizontal surface movements, derived from the vertical ones, Mair et al. (1993) and Taylor (1995) stated that, in order to achieve a constant volume condition, displacements vectors should point to the point where the line described by (1.17)

intersects the tunnel centre line, located $\frac{0.175 \cdot z_0}{0.325}$ below the tunnel axis level (Fig. 1-10).

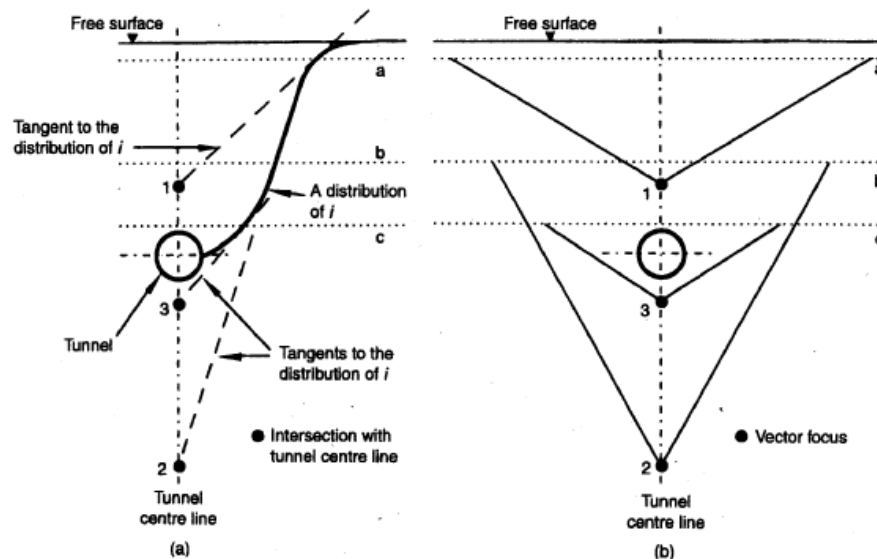


Fig. 1-11. Distribution of i for subsurface settlement troughs with depth (a) and focus of vectors of soil movement (after Grant & Taylor, 2000) (b)

Moreover, New & Bowers (1994) showed how considering the soil particle movement toward a single point at the tunnel axis an overprediction of the soil settlements above the tunnel axis is obtained. They proposed to model the ground loss equally distributed over a horizontal plane at the invert level and showed how this assumption is in good agreement with subsurface field measurements of the Heathrow Express trial tunnel.

Grant & Taylor (2000) proposed different indications about horizontal movements close to the surface, by showing results of a number of centrifuge tests. They showed how their laboratory results were in good agreement with (1.17) apart from a zone in the vicinity of the tunnel where test data show a narrower subsurface trough and close to the surface were wider troughs were measured. They stated that soil displacements vectors point in the direction of the tangent of the distribution of i represented in Fig. 1-11_a; it follows that horizontal displacements at the surface are underestimated by (1.17) while in the vicinity of the tunnel they are overestimated by the same equation.

Finally the influence of different stiffness soil layers overlying clay in which the tunnel has to be constructed, have been investigated by Hagiwara et al. (1999), by performing a number of centrifuge tests. Comparing the results of their tests with a clay-only case, they showed that the settlement troughs become wider as the stiffness of the top layer increases; so they demonstrated how the tunnel induced settlement behaviour is affected by the interaction of stiffness of an overlying material with the soil in which the tunnel is constructed.

1.3.2. Numerical analyses of tunnel construction

Empirical methods are widely used to predict tunnelling induced displacements in greenfield conditions, neglecting building-tunnel interaction. As mostly of tunnel excavations for metro system enlargements take place in urbanized areas, new methods have to be developed and new calculation tools have to be improved to correctly consider buildings presence on the ground. In this regard, numerical modelling provides the possibility to accommodate the different elements of interaction problem in one analysis.

This section gives an overview of how Finite Element Analyses have been applied to predict tunnel induced subsidence mainly in greenfield conditions to demonstrate different approaches to simulate tunnel excavation.

As it can be understood from following pages, despite the tunnel excavation is clearly a 3D problem and three dimensional analyses have to be performed to correctly predict tunnelling induced effects, because of limitations in computational power, 2D analyses are still widely used. Those analyses showed the importance of considering the small strain behaviour of the soil, different values for the lateral coefficient at rest K_0 and the soil anisotropy, which could clearly leads to an improvement in settlement prediction.

With the development in using 3D analyses, the influence of all the parameters above has been investigated. The following points were highlighted:

- about the influence of K_0 , no significant difference in the shape of induced transverse settlement troughs has been noticed between 2D and 3D analyses;

- in longitudinal direction the steady-state conditions should be achieved 2D (Desari et al., 1996) or 5D (Vermeer et al., 2002) behind the tunnel face depending on the used soil model and K_0 values;
- the variety of analyzed problems demonstrates the flexibility of numerical simulation: the used tunnelling technique, the initial stress conditions, the soil anisotropy and the mesh dimension are the observed parameter whose influence on the analyses results is not negligible.

1.3.2.1. Two-dimensional analyses

Despite tunnel excavation is clearly a 3D problems, because of the remarkable computational sources required to perform thorough 3D analyses, tunnel excavation is often modeled two dimensionally. The five methods described below have been proposed to take account of the stress and strain changes ahead the tunnel face when adopting plane strain analyses.

- **GAP Method** (*Rowe at al., 1983*): it prescribes the final tunnel lining position and size smaller than the initial size of the excavation boundary; hence, soil movements are allowed until the soil closes the gap, defined by the difference between the initial excavation boundary and the final tunnel size. This method can be seen as a simulation of radial V_L along tunnel shield, being the GAP parameter representative of the gap between the cutting head and the tunnel lining. However, as the volume loss has a tunnel face component it is difficult to define the gap parameter for different sources of volume loss.
- **Convergence-Confinement Method** (*Panet & Guenot, 1982*): also known as λ -method with λ defining the proportion of unloading before the final lining is installed. For $0 < \lambda < 1$ the remaining radial stress on the lining is $\sigma_r = (1 - \lambda) \cdot \sigma_r^0$.
- **Volume Loss Control Method** (*Swoboda, 1979*): used for modelling tunnel excavation with the *New Austrian Tunnelling Method* (NATM), it lies in reducing soil stiffness within the tunnel boundary before the tunnel excavation is simulated, thus allowing soil to move towards it. Because the Volume Loss is suitable as design parameter, when known, it can be directly adopted in this method.

- **Longitudinal-transverse Method** (*Finno & Clough, 1985*): it follows from plane strain analyses of both longitudinal and transverse sections of the tunnel, leading to account for stress changes and soil movements ahead the tunnel face. In a transverse section stress changes were applied prior to tunnel excavation to obtain soil movements similar to those obtained from longitudinal analyses. Tunnel construction was then simulated adopting the GAP Method. Rowe & Lee (1992) compared the settlements profiles from such a plane strain approach with 3D Finite Element Analyses results, pointing up a significant overestimation of longitudinal settlements and of the plastic zone extension.

Addenbrooke et al. (1997) used the Volume Loss Method to investigate the effects of pre-yield soil models on results, performing a number of plane strain analyses on the tunnel construction of the Jubilee Line Extension beneath St. James's Park in London. They used:

1. Linear elastic Model with Young's modulus increasing with depth
2. Non-linear Elastic Model, based on Jardine et al. (1986) formulation, considering shear stiffness varying with deviatoric strain and mean effective stress while the bulk stiffness depends on volumetric strain and mean effective stress.
3. Non-linear Elastic Model with shear and bulk stiffness depending on deviatoric strain and mean effective stress level, also accounting for loading reversals.

Fig. 1-12 shows how the Authors plotted field data, reported by Standing et al. (1996), together with surface settlements, obtained by using lateral earth pressure coefficient at rest in the clay ($K_0 = 1.5$) within the upper bound of values reported by Hight & Higgins (1995). They demonstrated the necessity of including small strain stiffness into pre-yield model, as the predictions of the linear elastic model are inadequate. Despite the non-linear models responses are quite similar, their settlements troughs are too wide if compared with field data; the maximum settlement is consequently too small, as the analyses were performed under volume loss control. Too wide settlement troughs in a high K_0 -regime has been confirmed even by others authors, such as Gunn, 1993 who presented results from analyses with $K_0 = 1.0$ applying non-linear pre-yield model (Fig. 1-13).

The role of K_0 was highlighted by Gens (1995) and Addenbrooke (1996); they later compared FE predictions for tunnel construction of the Jubilee Line in London for both $K_0 = 1.5$ and $K_0 = 0.5$ with field measurements and demonstrated how the low K_0 cases showed deeper and narrower settlements troughs, consequently closer to field data. Performing axial symmetric analyses the Authors showed a reduction in radial stresses and increase of the hoop stresses around the tunnel boundary. The change in stresses can be consequently represented in plane strain analyses as shown in Fig. 1-14. Analyses adopting such a low K_0 zone together with non-linear elasto-plastic soil model, showed an improved settlement profile compared with the global $K_0 = 1.5$ cases. Similar results were presented by others authors for 2D and 3D analyses (Guedes & Santos Pereira, 2000; Dolezova, 2002; Lee & Ng, 2002).

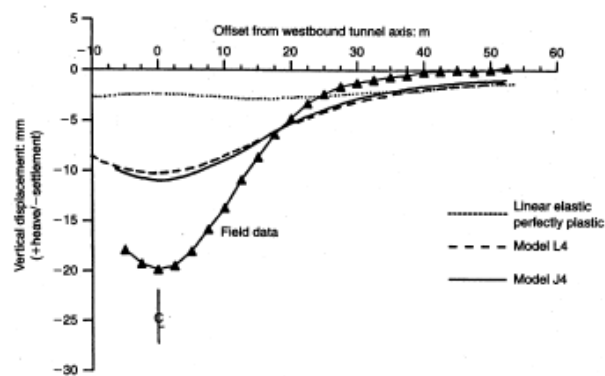


Fig. 1-12. Surface settlements troughs obtained from different isotropic models (non-linear elastic, perfectly plastic, after Addenbrooke et al., 1997)

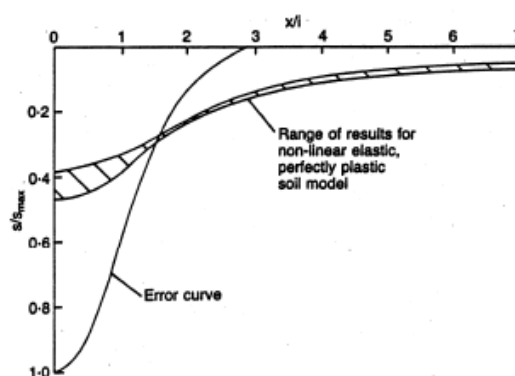


Fig. 1-13. Surface settlements predictions obtained from different input parameters for a non-linear elastic perfectly plastic model (after Gunn, 1993)

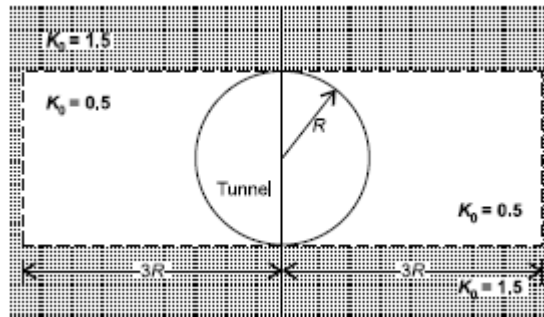


Fig. 1-14. Layout of zone of reduced K_0 (after Potts & Zdravkovic, 2001)

In order to improve FE predicted settlement profile, Lee & Rowe (1989) suggested using anisotropic soil model. By presenting FE results from Heathrow Express trial tunnel Simpson et al. (1996) showed how that anisotropy gives better surface displacements prediction. Addenbrooke et al. (1997) introduced such anisotropy in some of their analyses by deriving the soil parameters from the small strain stiffness formulation of the original isotropic model, defining ratios E'_v/E'_h and G_{vh}/E'_v . They performed two analyses: the first one using anisotropic ratios observed in field measurements reported by Burland & Kalra (1986) (AJ4i: $E'_v/E'_h = 0.625$, $G_{vh}/E'_v = 0.44$), the second one with reduced G_{vh}/E'_v (AJ4ii: $G_{vh}/E'_v = 0.2$) thus making the clay very soft in shear. Results are shown in Fig. 1-15; it is clear how the first parameters set (AJ4i) does not show remarkable improvements in the settlement profile if compared to the linear elastic solution, while the second set of parameters generates a deeper and narrower settlement profile, closer to the field measurements, leading to the conclusion that unrealistic soil stiffness is required to achieve better settlement predictions when modelling tunnel excavation in plane strain with $K_0 > 1.0$.

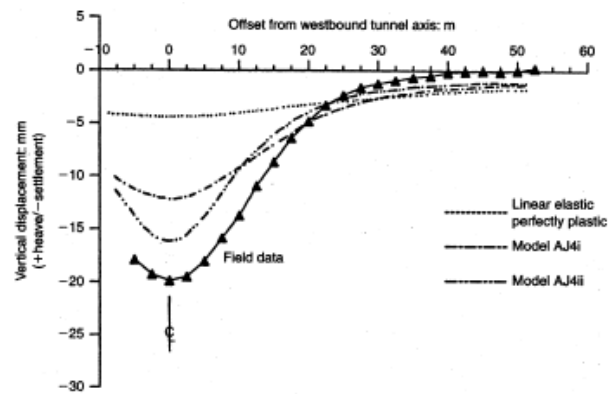


Fig. 1-15. Surface settlement troughs obtained from different anisotropic soil models (AJ4i and AJ4ii: non-linear elastic, perfectly plastic, after Addenbrooke et al., 1997)

1.3.2.2. Three-dimensional analyses

Following pages describe 3D analyses results performed by many authors with different approach, in order to resume the observed influence of some of the analyzed parameters, including the soil behaviour and the machine parameters.

Three main tunnel excavation methods can be defined to perform FE three dimensional analyses:

- **“Step-By-Step”** approach (Katzenbach & Breth, 1981): tunnel excavation is modeled by successive removal of tunnel face elements while installing the final lining behind the tunnel face, at distance equal to excavation length;
- **“Volume Loss Control”** method, as described in *Paragraph 1.3.2.1.*;
- **“Detail Approach”** modelling the excavation machine main features, such as grouting and slurry pressure.

Katzenbach & Breth (1981) and Desari et al. (1996) performed 3D analyses using the “step-by-step” approach of a NATM tunnelling respectively in Frankfurt Clay, with a non-linear elastic soil model and lateral earth pressure at rest $K_0 = 0.8$, and in London Clay with a non-linear elastic perfectly plastic soil model and $K_0 = 1.0$. In the first case the

analyses settlement trough was in good agreement with the field data, in the latter it resulted too wide if compared with the field measurements. Desari et al. (1996) also revealed that the time dependent Young's modulus of the concrete tunnel lining has not great influence on the settlement trough and that the stationary settlement conditions (or "steady-state" conditions, referring to Vermeer et al., 2002) were established 2 diameters behind the tunnel face.

By modelling a similar tunnel construction as Desari et al. (1996), Tang et al. (2000) investigated the excavation length influence on both transverse and longitudinal settlement profile, with two excavation lengths (5 m and 10 m). The London Clay was modeled with a transversely anisotropic linear-elastic perfectly plastic constitutive relationship and with $K_0 = 1.5$, moreover the tunnel construction was modelles as coupled with a coefficient of permeability for the clay $k = 1 * 10^{-9}m/s$ and 2.5 m tunnel advance rate per day. Fig. 1-16 shows for both the excavation lengths the longitudinal settlement profile; it indicates a steady state of settlement approximately 20 m behind the tunnel face and increasing with the increasing excavation length.

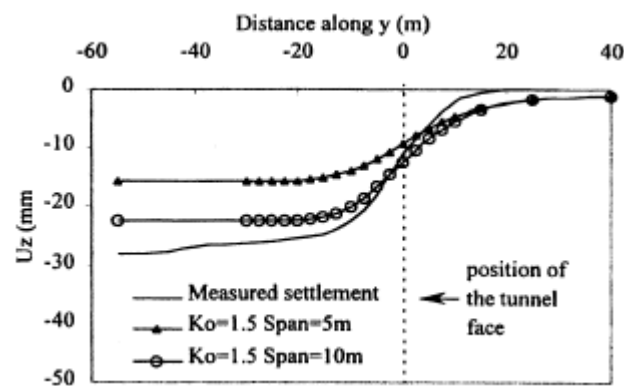


Fig. 1-16. Longitudinal settlement profile obtained for different excavation lengths L_{exc}

Vermeer et al. (2002) highlighted the importance of the first excavation step in 3D step-by-step analyses of an 8 m diameter tunnel, using a linear elastic perfectly plastic soil model with $K_0 = 0.67$ and $L_{exc} = 2 m$ (Fig. 1-17). In the first analysis an unsupported excavation was performed in the first step before the final lining was installed; in the second one lining was installed all over the length of the first excavation step prior to excavation. The Authors concluded that the first excavation step has great influence on

the whole analysis and steady-state conditions develop approximately 40 m (5D) behind the tunnel face. As the obtained settlement profiles were in good agreements with the corresponding plane strain analyses, a *fast settlement analysis*, allowing a significant reduction in calculations time, have been proposed by the same Authors. It consists in defining a two phases step-by-step analysis, and using the obtained volume loss to perform a final plane strain analysis in order to predict the settlement trough. In the first phase of the 3D step-by-step analysis a complete tunnel is constructed up to a distance over which steady-state conditions can develop, then the lining is installed all over the whole length and displacements are set to zero; afterward the second phase is defined performing a single excavation step of L_{exc} without lining installation. The latter phase induces a settlement crater on the surface whose volume loss is used to perform the final 2D analysis using the convergence-confinement method.

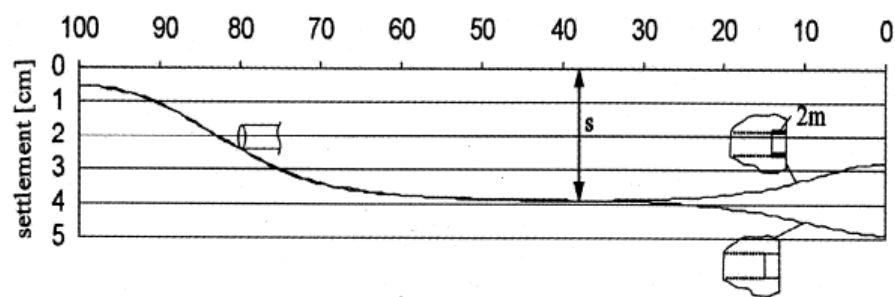


Fig. 1-17. Longitudinal settlement profiles for different excavation methods in the first excavation step (after Vermeer et al., 2002)

In order to reduce the number of steps in a 3D analysis, the excavation technique from plane strain situations were used. Lee & Rowe (1991) performed 3D analyses with the gap method, of a 2.5 m diameter Thunder Bay sewer tunnel in Ontario (Canada), using a transverse anisotropic linear perfectly plastic soil model and lateral earth pressure at rest $K_0 = 0.85$. The radial volume loss was determined from the tunnel machine while the potential face loss was estimated from 3D analysis. The tunnel was excavated over its whole length allowing the full release of axial stress in order to simulate the face loss. The physical gap of the tunnel machine was then applied over the length of the shield, while the total gap (radial and face loss) was applied behind the shield. The lining was installed when the gap was closed. Their prediction were in good agreement with field data and

the transverse settlement trough was slightly too wide with a ratio of settlement trough width $i_{analysis}/i_{data} = 1.1 - 1.2$.

The influence of lateral earth pressure K_0 and of soil anisotropy has been investigated in 3D studies by Guedes & Santos Pereira (2000), Dolezalová (2002), Lee & Ng (2002).

Guedes & Santos Pereira (2000) presented results from 2D and 3D analyses with $K_0 = 0.5$ and $K_0 = 1.0$, concluding that 3D simulation does not change the trend of wider settlement trough with increasing K_0 , as observed in 2D analyses. The same conclusion was stated by Dolezalová (2002) presenting 2D and 3D results of the Mrazovka Exploratory Gallery near Prague; moreover she did not notice any relationship between the type of analysis (2D or 3D) and K_0 .

Lee & Ng (2002) investigated both K_0 and soil anisotropy (expressed as $n' = E'_h/E'_v$) influence on settlement trough. $K_0 = 0.5$ and $K_0 = 1.5$, $n' = 1.0$ (isotropic case) and $n' = 1.6$ were applied in their analyses, while the ratio $G_{vh}/E'_v = 0.44$ was kept as constant. They showed how the transverse settlement trough becomes deeper with decreasing in K_0 and/or increasing in n' , according to Addenbrooke (1996) and Addenbrooke et al. (1997)³. However Lee & Ng (2002) observed the 3D analyses much more affected by changes in n' and K_0 than the 2D ones, in contrast to what has been obtained by Guedes & Santos Pereira (2000) and Dolezalová (2002) who did not find great differences between 3D and plane strain analyses.

Finally the tunnel boring machine features influence was investigated by Komiya et al. (1999) and Dias et al. (2000).

Komiya et al. (1999) performed 3D analyses modelling the excavation machine by a rigid body shield highly stiff and with a self weight modeled by applied body forces. The advance of the tunnel shield was modeled by applying hydraulic jack forces at the back of the shield, so as to reproduce the 3D movements of the machine, accordingly to the excavation practice. As they used records of hydraulic jacks forces, their prediction were quite reasonable in reproducing negligible measured displacements.

³ The n' degree of anisotropy is the inverse of the ratio used by Addenbrooke et al. (1997). $E'_v/E'_h = 0.625$ used by Addenbrooke et al. (1997) is the same as $n' = 1.6$ adopted by Lee & Ng (2002). The degrees of anisotropy are thus equivalent while the tunnel geometry changes.

Conversely, Dias et al. (2000) analyzed the construction of a tunnel in Cairo, modelling the shield machine with its conical shape, with the over cut and by applying pressure at the face and at the circumferential tunnel boundary, in order to simulate slurry and grouting pressure. Their 3D results overestimated the measured settlements by nearly 100%. Comparing the 3D results with plane strain analyses ones, in which grouting pressure and the conical shape of the shield were modeled, the Authors observed the 3D analyses exhibiting a narrower trough than the 2D did.

1.4. Building damage assessment

Since tunnelling excavation in soft ground causes ground movements as described in previous sections, in urban area the ground subsidence can affect existing surface and subsurface structures. As a consequence, predicting tunnel induced deformation of such structures and assessing the risk of damage is an essential part for tunnels planning, designing and building processes (Mair et al., 1996). As it will be shown in the following pages, even if the damage assessment does not account for building characteristics such as building stiffness, detailed strategies have been developed.

1.4.1. Definition of structure deformation parameters

In order to quantify tunnel induced buildings deformation, Burland and Wroth (1974) proposed the following widely accepted in-plane parameters (three-dimensional behaviour such as twisting is not included):

- **Settlements:** the vertical movement of a point, positive if indicating downwards movements (Fig. 1-18_a)
- **Differential or relative settlement (δS_v):** the difference between two settlements values (Fig. 1-18_a)

- **Rotation or slope (θ):** the change in gradient of the straight line defined by two reference points embedded in the structure (Fig. 1-18_a)
- **Angular strain (α):** producing sagging (upward concavity) when positive, hogging (downward concavity) if negative (Fig. 1-18_a)
- **Relative deflection (Δ):** the maximum displacement relative to the straight line connecting two reference points with a distance L , indicating sagging deformation if positive (Fig. 1-18_b)
- **Deflection ratio (DR):** the quotient of relative deflection and the corresponding length: $DR = \Delta/L$ (Fig. 1-18_b)
- **Tilt (ω):** the rigid body rotation of the whole superstructure or a well-defined part of it, difficult to define as the structure normally flexes itself (Fig. 1-18_c)
- **Relative rotation or angular distortion (β):** the rotation of the straight line joining two reference points relative to the tilt (Fig. 1-18_c)
- **Average horizontal strain (ε_h):** $\varepsilon_h = \delta L/L$ defined as change in length δL over the corresponding length L .

To determine the above listed parameters a number of informations, seldom available in engineering practice, are required (Rankine, 1988). However it will be shown that two of them are of significant importance in defining the building damage, such as the deflection ratio (DR) and the horizontal strain (ε_h).

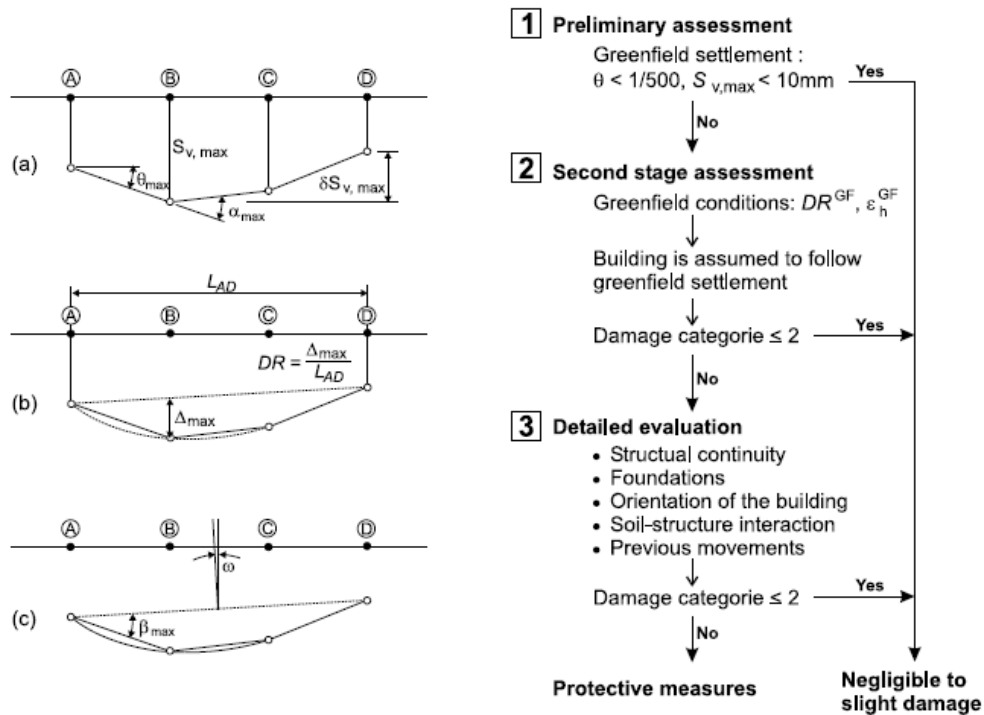


Fig. 1-18. Building deformation parameters (a, b, and c) and schematic diagram of three stage approach for damage risk evaluation

1.4.2. Evaluation of risk of damage

The following pages summarize the “*three stage approach*” widely used to assess the potential building damage for tunnel projects in London (Mair et al., 1996) such as the Jubilee Line Extension, the Channel Tunnel Rail Link and the Cross Rail project. It consists of three stages known as: *preliminary assessments*, *second stage assessment* and *detailed evaluation*.

1.4.2.1. Preliminary assessment

The presence of the building is not considered and the greenfield settlement profile is evaluated.

Rankin (1988) showed that for buildings measuring $\theta < 1/500$ and $S_{v,max} < 10 \text{ mm}$ the risk of damage is negligible, than for such buildings not any more detailed evaluation is carried on; contrariwise in case of exceeding them the second stage assessment has to be carried out. The above values can be reduced with an increasing in buildings sensitivity.

1.4.2.2. Second stage assessment

The building is represented as an elastic beam whose foundation is assumed to follow the settlement profile described by the empirical greenfield trough, not accounting the building's stiffness. The settlement trough is used to calculate the deflection ratio DR (both for sagging and hogging) and the tensile strain ε_h (both for compression and tension) in order to define the strain within the beam and consequently the level of damage, as described in the following sections. Referring to a number of case studies Frischmann et al. (1994) showed that the building's stiffness interacts with the ground such that the deflection ratio and the tensile strain reduce, as a consequence Burland (1995) pointed out that the category of damage obtained by the assumptions underlying this stage, is only a possible degree of damage for the structure, usually higher than the real one.

After the required parameters calculation is performed, the relative category of damage is defined by Tab.1-2 and Tab.1-3. In case of exceeding the second level of damage, corresponding to a damage potentially affecting building serviceability, a more detailed evaluation has to be performed following the next step of the "three stage approach".

1.4.2.3. Detailed evaluation

Details of the building and of the tunnel construction should be taken into account in this approach, including the three-dimensional process of tunnel construction and the building orientation with respect to the tunnel axis. According to Burland (1995), foundations design of the building, its structural continuity and its possible previous movements should also be accounted.

As Fig. 1-19 shows, the soil-structure interaction plays an important role in defining the induced settlement field, since the influence of building's stiffness is likely to reduce the greenfield displacements. However the same Fig. 1-19 shows the measured building settlements significantly differing from the predicted ones according to the effects of building's stiffness, leading to a reduction both of the slope and of the maximum settlement compared to the greenfield situation and moreover of the horizontal strain within the structure (Geddes, 1991). Potts & Addenbrooke (1997) showed that the influence of soil-structure interaction could be incorporated into the second stage assessment in order to reduce the number of cases for which a detailed evaluation has to be carried out; the suggested procedure will be discussed in following pages.

Because of the conservative assumption of the second stage assessment, Burland (1995) pointed out that the category of damage coming out from this evaluation is usually lower than the one obtained from the previous stages. However for buildings remaining in the third or higher category of damage (Tab.1-2) after the detailed evaluation, protective measures have to be considered as necessary.

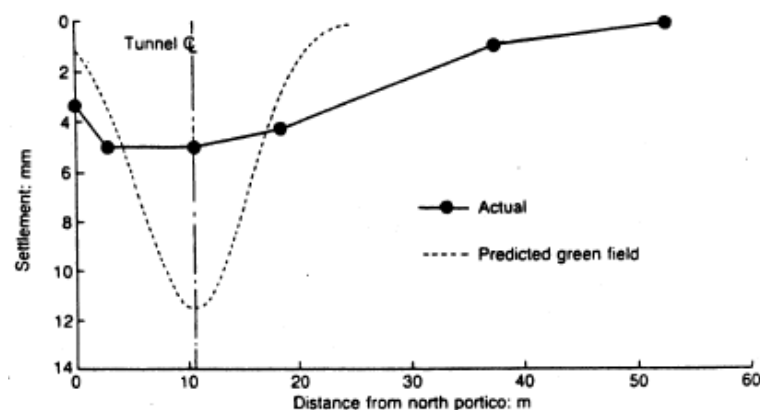


Fig. 1-19. Tunnel induced building settlement of Maison House, London (after Frischmann et al., 1994)

1.4.3. Category of damage

Burland et al. (1977) distinguished between three criteria when considering the building damage: visual appearance, serviceability or function and stability. Since the visual damage is difficult to quantify as it depends on subjective criteria, they proposed a system to identify and classify the level of damage, based on the ease of repair, resumed in Tab.1-2. Such a table was developed for brickwork or stone masonry and the relative degree of severity only concerns to standard domestic or office buildings; the same Authors pointed out that more stringent criteria has to be defined when initial cracks can lead to corrosion, penetration etc.

The 6 categories of damage resumed in Tab.1-2 can be subdivided into the group of damage levels indicated in Tab.1-3 categories 0 up to 2 correspond to aesthetical damage, categories 3 and 4 to serviceability damage and category 5 to damage affecting the stability of the structure. As mentioned in the previous pages, the division between category 2 and 3 represents an important threshold since Burland (1995) pointed out that damage related to categories 0 to 2 can result from several causes within the structure (such as thermal effects), however damage of category 3 or higher is frequently associated with ground movements.

Category of damage	Normal degree of severity	Description of typical damage (Ease of repair is printed <i>italic</i>)
		Note: Crack width is only one factor in assessing category of damage and should not be used on its own as a direct measure of it
0	Negligible	Hairline cracks less than about 0.1 mm
1	Very Slight	<i>Fine cracks which are easily treated during normal decoration.</i> Damage generally restricted to internal wall finishes. Close inspection may reveal some cracks in external brickworks or masonry. Typical crack widths up to 1 mm.
2	Slight	<i>Cracks easily filled. Re-decoration probably required. Recurrent cracks can be masked by suitable linings.</i> Cracks may be visible externally and <i>some repointing may be required to ensure weathertightness.</i> Doors and windows may stick slightly. Typical crack width up to 5 mm.
3	Moderate	<i>The cracks require some opening up and can be patched by mason. Repointing of external brickwork and possibly a small amount of brickwork to be replaced.</i> Doors and windows sticking. Service pipes may fracture. Weathertightness often impaired. Typical crack widths are 5 to 15 mm or several up to 3 mm.
4	Severe	<i>Extensive repair work involving breaking-out and replacing sections of walls, especially over doors and windows.</i> Windows and door frames distorted, floor sloping noticeably ¹ . Walls leaning ¹ or bulging noticeably, some loss of bearing in beams. Service pipes disrupted. Typical crack widths are 15 to 25 mm but also depends on the number of cracks.
5	Very severe	<i>This requires a major repair job involving partial or complete rebuilding.</i> Beams lose bearing, walls lean badly and require shoring. Windows broken with distortion. Danger of instability. Typical crack widths are greater than 25 mm but depends on the number of cracks.

¹ **Note:** Local deviation of slope, from the horizontal or vertical, of more than 1/100 will normally be clearly visible. Overall deviations in excess of 1/150 are undesirable.

Tab.1-2. Classification of visible damage to walls with particular reference to ease of repair of plaster and brickwork masonry (after Burland, 1995)

Category of damage	Normal degree of severity	Limiting Tensile strain [%]
0	Negligible	0 - 0.05
1	Very slight	0.05 - 0.075
2	Slight	0.075 - 0.15
3	Moderate*	0.15 - 0.3
4 to 5	Severe to Very Severe	>0.3

*Note: Boscardin & Cording (1989) describe the damage corresponding to the tensile strain in the range 0.015 - 0.3% as 'moderate to severe'. However, none of the cases quoted by them exhibit severe damage for this range of strains. There is therefore no evidence to suggest that tensile strains up to 0.3% will result in severe damage.

Tab.1-3. Relation between category of damage and limiting tensile strain (after Boscardin & Cording, 1989 and Burland, 1995)

1.4.4. Calculation of building strain

Basing on results of a number of large scale tests on masonry panels and walls, Burland & Wroth (1974) showed that the onset of cracking is usually associated to a well defined value of average tensile strain, defined as critical strain ϵ_{crit} , measured over a length of 1 m or more. It results to be unrelated to the mode of deformation and its values are $\epsilon_{crit} = 0.05\% - 0.1\%$ for brick works, $\epsilon_{crit} = 0.03\% - 0.05\%$ for concrete. Burland and Wroth (1974) noted that these values are usually larger than the local strain corresponding with tensile failure.

In 1977 Burland et al. replaced the notation of ϵ_{crit} by the ϵ_{lim} , referred to as the limiting tensile strain in order to take account of different materials and serviceability limit states.

Boscardin & Cording (1989) linked values of limiting strains to the categories of damage resumed Tab.1-2, as reported in Tab.1-3.

Burland & Wroth (1974) and Burland (1977) applied the concept of limiting tensile strain to elastic beam theory. In such a way they could demonstrate the mechanism controlling the onset of cracking within a structure.

The elastic beam used in their model is described by a width B and high H. Two possible deformations can occur: bending deformation (Fig. 1-20_c), leading to a cracking

mechanism caused by direct tensile strain, and shear deformation, leading to diagonal cracks caused by diagonal tensile strains (Fig. 1-20_d).

Basing on Timoshenko theory for an elastic beam under particular load conditions, for a centrally loaded beam subjected both to shear and bending deformation, the total deflection is given by:

$$\Delta = \frac{PB^3}{48EI} \cdot \left(1 + \frac{18EI}{B^2HG}\right) \quad (1.23)$$

where E is Young's modulus, G is the shear modulus and P the point load applied in the middle of the beam. For an isotropic elastic material $E/G = 2 \cdot (1 + \nu) = 2.6$ (assuming $\nu = 0.3$).

The maximum values for the tensile strain within the beam depends by the deformation mode and by the neutral axis position. For neutral axis in the middle of the beam, Burland & Wroth expressed equation (1.23) in terms of deflection ratio Δ/L , maximum extreme fibre strain $\varepsilon_{b,max}$ and maximum diagonal strain $\varepsilon_{d,max}$ as reported below:

$$\frac{\Delta}{B} = \left(0.167 \cdot \frac{B}{H} + 0.65 \cdot \frac{H}{B}\right) \cdot \varepsilon_{b,max} \quad (1.24)$$

$$\frac{\Delta}{B} = \left(0.25 \cdot \frac{B^2}{H^2} + 1\right) \cdot \varepsilon_{d,max} \quad (1.25)$$

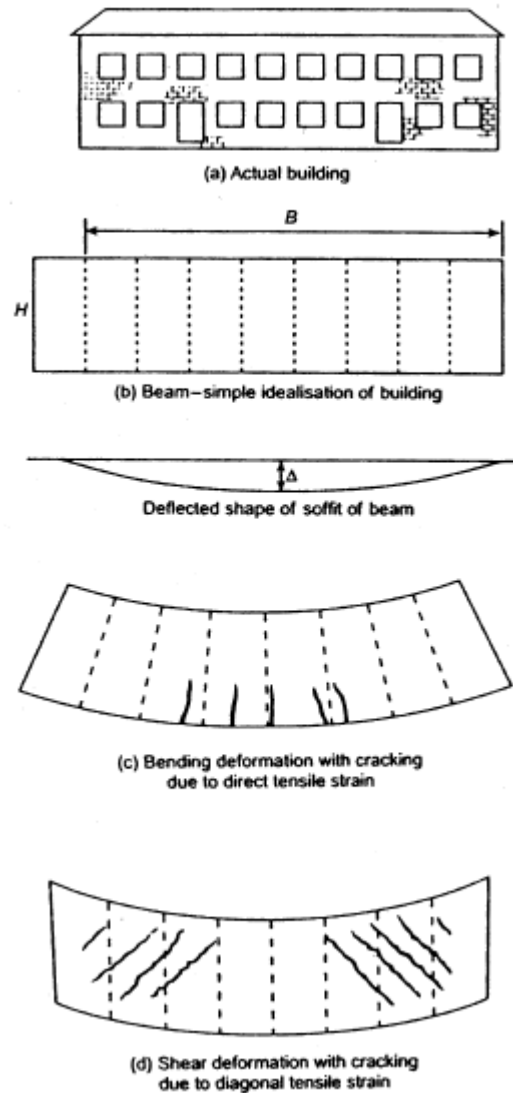


Fig. 1-20. Cracking of a simple beam in different modes of deformation (after Burland & Wroth, 1974)

Both the equations are plotted in Fig. 1-21_a for $\epsilon_{lim} = \epsilon_{max}$; it shows for $B/H < 0.5$ the diagonal strain being more critical and for B/H increasing above this value, bending becoming the most critical mode of deformation. Despite for the equations above the neutral axis was assumed to be in the middle of the beam, since foundations offer significant restraint to their deformations, it can be more realistic to consider the neutral axis at the lower extreme fiber. It leads equations (1.23) and (1.25) changing in (1.26) and (1.27) .

$$(1.26)$$

$$\frac{\Delta}{B} = \left(0.083 \cdot \frac{B}{H} + 1.3 \cdot \frac{H}{B} \right) \cdot \varepsilon_{b,max}$$

(1.27)

$$\frac{\Delta}{B} = \left(0.064 \cdot \frac{B^2}{H^2} + 1 \right) \cdot \varepsilon_{d,max}$$

As the neutral axis is assumed to be at the lower extreme fiber, equations (1.26) only applies for hogging deformation mode; indeed, in the case of sagging there are no tensile strains. Equations (1.26) and (1.27) are plotted in Fig. 1-21_b. Comparing Fig. 1-21_a with Fig. 1-21_b it is clear how for a given value of $\Delta/(B\varepsilon_{lim})$ the value of B/H in the second figure is twice that in first one.

Whereas the building weight induced displacements mainly develop in vertical direction leading to sagging and/or hogging deformations (Burland & Wroth, 1974 and Burland, 1977), the tunnelling induced ground movements leads as well to horizontal strains. Geddes (1978) highlighted that the horizontal strains can have a significant influence on existing building. Boscardin & Cording (1989) included them in the above mentioned framework by superimposing building strain due to deflection deformation with the horizontal ground strain ε_h . The resultant extreme fiber strain and the resultant diagonal tensile strain are respectively given by:

(1.28)

$$\varepsilon_{b,r} = \varepsilon_{b,max} + \varepsilon_h$$

(1.29)

$$\varepsilon_{dr} = \varepsilon_h \cdot \frac{1 - \nu}{2} + \sqrt{\varepsilon_h^2 \cdot \left(\frac{1 - \nu}{2} \right)^2 + \varepsilon_{d,max}^2}$$

where ν is the Poisson's ratio of the beam.

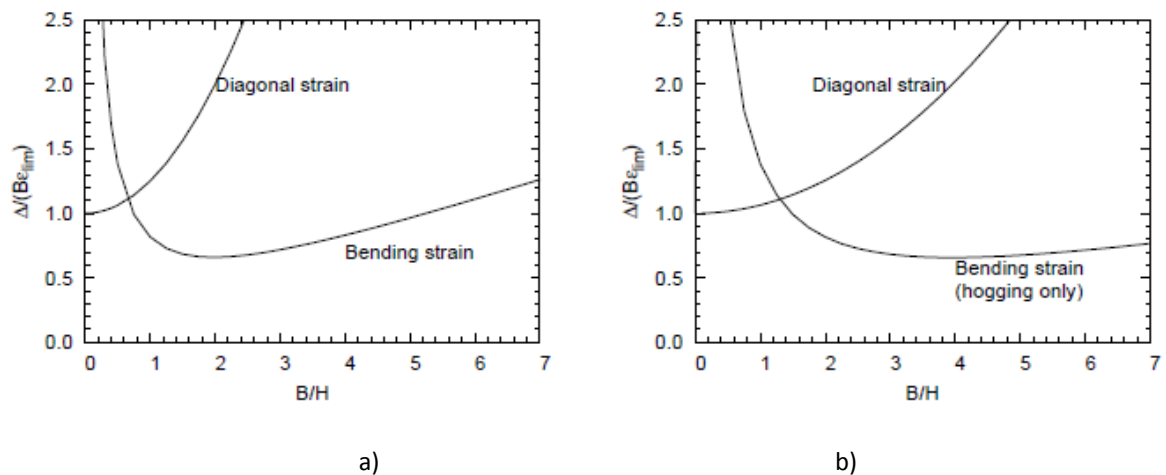


Fig. 1-21. Relationship between $\Delta/(B\epsilon_{crit})$ and B/H for rectangular beam deflecting due to combined bending and shear: a) neutral axis in the middle, b) neutral axis at the bottom (after Burland & Wroth, 1974)

By referring to Boscardin & Cording (1989), Geddes (1991) pointed out that the shear strains develop at the structure-ground interface and then that the strain in the structure may differ considerably from the ground strain, as a consequence the approach proposed by Boscardin & Cording (1989) generally overestimates a structure horizontal's strain. The same Authors related the limiting strain to angular distortion β and horizontal strain as shown in Fig. 1-21 where a number of case studies subjected to tunnel construction and shallow mines are reported. Boscardin & Cording (1989) concluded that the level of recorded damage for most cases fell within the boundaries by the curves of limiting strains.

Burland (1995) presented similar plots for horizontal strain and deflection ratio, developing diagrams showing the relationship between DR and ϵ_h for particular B/H values (Fig. 1-23). Each contour line in the plot represents a value of limiting strain listed in Tab.1-3; for $DR = 0$ the limiting values of horizontal strain are the same as ϵ_{lim} given in the same table.

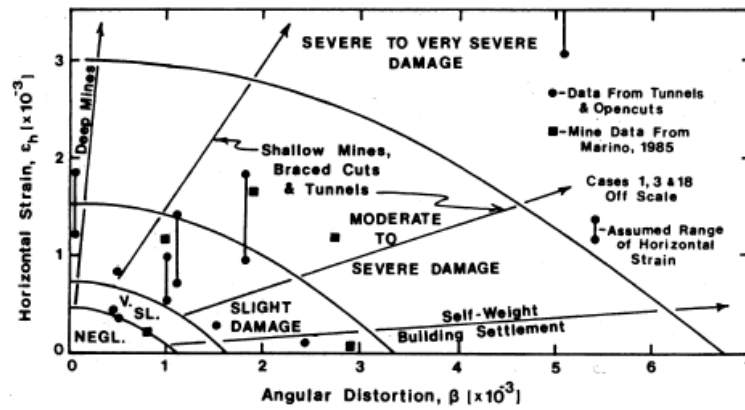


Fig. 1-22. Relation of damage to angular distortion and horizontal extension (after Boscardin & Cording, 1989)

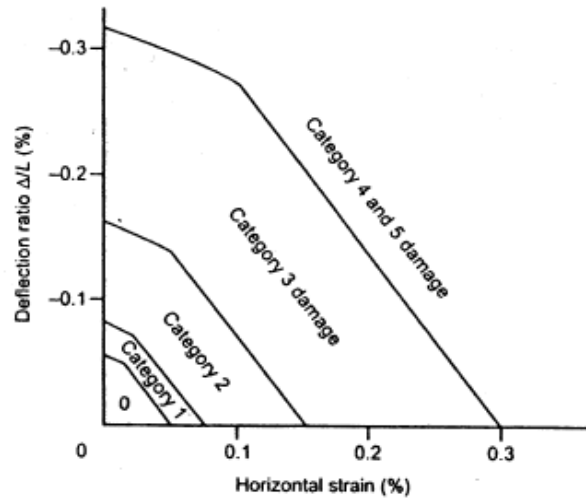


Fig. 1-23. Relation of damage category to deflection ratio and horizontal tensile strain for hogging ($B/H = 1$) (after Burland, 1995)

Apart from the *Cumana*, the railway line connecting the old town to the Western Flegrea area, going from *Montesanto* to *Pozzuoli*, working since 1889, what is actually known as Line 2, opened in 1925, has been the first Neapolitan metro line to be built. It initially was an ordinary railway line, later adapted to a metropolitan line, connecting the Western suburb of *Bagnoli* to the Eastern area of the city center in *Piazza Garibaldi* (where the central train station is located), passing through what in that period were considered the most important places of the city, *Fuorigrotta*, *Mergellina*, *Chiaia* and *Montesanto*. The line was named as Line 2 around 1990, after the Line 1 started to be built.

The first part of Line 1 to be realized was the stretch from *Vanvitelli* to *Colli Aminei*, in the Northern area of the city.

Line 1 actually consists of a 13 km tunnel and 14 stations shafts (*Dante*, *Museo*, *Materdei*, *Salvator Rosa*, *Cilea/Quattro Giornate*, *Medaglie d'Oro*, *Vanvitelli*, *Montedonzelli*, *Rione Alto*, *Policlinico*, *Colli Aminei*, *Frullone/San Rocco*, *Chiaiano/(Marianella, Piscinola/Scampia)*, all excavated in what is the most urbanized area of Neapolitan environment. Despite the segment connecting *Piazza Dante*, in the old town, to *Piscinola*, in the North-Eastern part of the city, is already working, the building process of the Line is still in progress; the completion of the operations is planned for 2013. Once the building process will be totally finished, the line will form a circular ring connecting all the strategical parts of the city, the old town (*Toledo*, *Piazza Dante*, *Piazza Cavour*, *Museo*, *Materdei*), the university area (*Università*), the hospital area (*Policlinico*), the central train station (*Piazza Garibaldi*), the seaport (*Piazza Municipio*) and the airport (*Capodichino*) to the Northern suburbs of the Neapolitan environment (*Piscinola*, *Scampia*). Moreover thanks to some strategical interchanges with Line 2 (in *Museo* and *Piazza Garibaldi*) and Line 6 (in *Piazza Municipio*), the mentioned areas will be easily reached even from the Eastern and the Western parts of the city.

In order to obtain an efficient and well classified Neapolitan metro system, after the Line 1 excavation process started, and after the old train line was identified as Line 2, the preexisting Eastern train lines of *Circumvesuviana*, *Circumflegrea* and *Cumana* (working respectively since 1891, 1962 and 1889) have been named as Line 3, Line 4, Line 5 and Line 7.

At the moment, a part of the Southern part of Line 1 (from *Piazza Garibaldi* to *Piazza Dante*) to be accomplished, Line 6 is the last line to be built.

The building process of the line is actually in progress. Once completed, the line will connect the University suburb of *Fuorigrotta*, in the Western area of the City, to the old town (*Piazza Municipio*).

The design of the line is dated back to the 80s when the idea was to create a “*metrotramvia*”, something in between an underground Metro line and a superficial Tramline, crossing from West to East the Neapolitan territory.

Although the construction process was supposed to be finished within 1990, because of technical and administrative problems it was interrupted and suspended for more than 10 years. The building operations restarted in 2002.

Since January 2007 the first part of the Line, from *Fuorigrotta* to *Mergellina* station, is working while the stretch between *Mergellina* and *Piazza Municipio* is going to be finished in the next months. At the moment the last 3 km tunnel excavation is underway.

2.2. LINE 6: the design

The original design of Line 6 counts about an 8 km long tunnel going from *Mostra Station* in Fuorigrotta suburb, to *Piazza Municipio* station in the old town, where the seaport is located. Once completed, Line 6 will count 8 station shafts, up to 45 m depth: *Mostra, Augusto, Lala, Mergellina, Arco Mirelli, San Pasquale, Chiaia e Municipio* (Fig.2-2).

The beginning part of the line (*Mostra – Mergellina*) has already been realized and it is working since 2007. The excavation process of the line restarted 2009 from Via Piedigrotta, nearby *Mergellina* station, where the old TBM was stuck for more than 10 years.

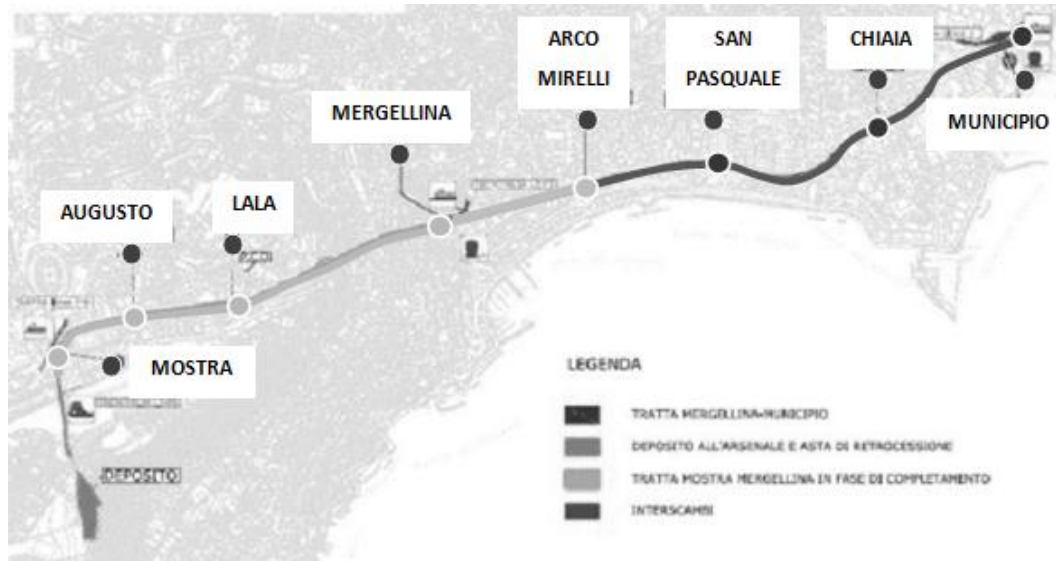


Fig.2-2. Line 6 plan

According to the design, the tunnel is located beneath Via Piedigrotta and it follows its route in the whole stretch between *Mergellina* and *Piazza Vittoria*. It crosses one of the most densely urbanized areas of the city (Riviera di Chiaia), and it has to be excavated in what is the typical Neapolitan ground succession, made by *Pozzolane* (volcanic loose sand) and *Yellow Neapolitan Tuff* (YNT).

The tunnel is always located below the groundwater level, mainly crossing the *Pozzolone* layer. As a matter of fact about 1.2 km (from *Mergellina* to *Piazza Vittoria*) of the 3.3 km missing tunnel of the line, have to be excavated in the *Pozzolane* ground layer, saving a small 200 m long stretch, between *Arco Mirelli* and *Via S. M. in Portico*, where a 10 m YNT cover has been measured; in that area the tunnel is 12 m to 20 m deep. Conversely from *Piazza Vittoria* up to *Piazza Municipio*, the tunnel is located up to 44 m deep and crosses the YNT layer, with an extreme 33 m thick YNT cover layer.

An EPB (*Earth Pressure Balance*) machine has been chosen to carry on the tunnel digging operations.

The sandy ground and the high groundwater level led to prefer an EPB machine rather than a Hydroshield TBM. The possibility in applying a face pressure using the excavated material, preserved and constantly checked in the excavation chamber, and the change to straight install the final lining few meters behind the shield, allow to better control the induced displacements and consequently to reduce the effects on preexisting buildings.

Moreover, because of the opportunity to dig and simultaneously assembling the final lining, the chosen digging technique leads to a shortening of the tunnel construction process.

The new machine is an 8.10 m diameter EPB. Because it has to replace the old Hydroschild TBM machine stuck into the ground at the beginning of Via Piedigrotta, nearby *Mergellina* station, the EPB diameter is smaller than the TBM one, so that it can be easily put into the previously excavated portion of tunnel, after the old TBM have been disassembled and pulled out.

The final lining is made by (8+1) precast concrete segments (0.30 x 1.70 x 1.50) m. The inner diameter is 7.20 m and the outer is 7.85 m, from this it follows about 150 mm interspace between the machine and the final lining to be filled. The lining used materials are an R_{ck} 45 MPa concrete and a FeB 44 K steel reinforcement. The main material properties are described below.

Concrete	R_{ck} 45 MPa
f_{ck}	$0.83 \cdot R_{ck} = 37.4$ MPa
f_{ctk}	$0.7 \cdot 0.269 \cdot (R_{ck})^{2/3} = 2.4$ MPa
E_c	$5700 \cdot (R_{ck})^{0.5} = 38250$ MPa
Steel reinforcement	FeB 44 K
f_{yk}	440 MPa
E_s	210000 MPa

Tab.2-1. Material properties

Since the tunnel has to be excavated in a densely urbanized area, the surrounding buildings defense from the induced tunnel displacements is required; hence many ground reinforcement have been implemented, before the tunnel digging operations started. In detail, a number of jet grouting columns have been realized sideways along Via Piedigrotta, where two micropiles lines were previously realized to protect the preexisting buildings.

Being the tunnel line always below the groundwater level a possible water flow toward the machine is possible when the old shield is removed; hence a number of jet grouting injections from the ground level, together with concrete and chemical columns (from the

tunnel to the area below the shield), have been realized in front of and all around the old TBM, so as to prevent excessive displacements when the machine is removed and the digging operations restart. The purpose is to obtain a less permeable and more stable ground layer around the machine.

The main jet grouting columns properties are described in the table below.

JET GROUTING COLOUMNS	
Diameter	ϕ 900
Geometry (triangular grid)	0.75 m x 0.75 m x 0.75 m
Injecting pressure	≥ 40 MPa
Expected treated soil resistance	≥ 6 MPa

Tab.2-2. Jet grouting columns properties

2.2.1. Ground conditions

The whole Line 6 route is located in a volcanic area named as “*Distretto Vulcanico Flegreo-Napoletano*”, including Naples, the islands Procida and Ischia and the North-Western area of the Neapolitan bay.

From site investigations campaigns performed all over the years, since the first stretch of the line started to be built, many kind of soils have been identified as Fig.2-8 shows. Because of the similarity in physical and mechanical properties between the upper sandy layers found all along the line track, it is possible to consider the whole stratigraphy mainly affected by two kind of soils: disturbed and undisturbed superficial loose Piroclastiti deposits and *Yellow Neapolitan Tuff* (YNT).

The upper loose Piroclastiti deposit is made by three different stratifications: the deepest (10 m thick) made by Piroclastiti deposits, the middle one (from 16 m to 18 m thick) made by undisturbed Piroclastiti and the most superficial one (10 m thick) made by Piroclastiti reworked by flood. Because of the Piroclastiti deposits high variability in grain size and lithology a complex groundwater flow takes place and a number of

interconnected and overlapping groundwater levels are formed. However the measured piezometric level in that area is varying among 1 and 2 m a.m.s.l.

The Tuff layer has highly variable thickness across the whole tunnel line: 110 m in the Posillipo area, from 60 m to 90 m between Piazza Vittoria and Piazza Plebiscito. Its upper limit increases going from Mergellina (15 m deep) to Piazza Vittoria (60 m deep) and decreases going to Piazza Municipio (15 m deep) (Fig.2-7).

In between Mergellina and Piazza dei Martiri the tunnel is always located in the Piroclastiti deposit below 11 m up to 16 m thick ground cover, except for a 200 m long stretch straddle Arco Mirelli station. However from Piazza dei Martiri to Piazza Municipio the tunnel affects the YNT with a 33 m up to 15 m thick ground cover. Because of a number of geological faults affecting the YNT, its permeability is comparable to the upper sandy layers one ($k = 10^{-4} \div 10^{-5}$).

The main physical and geotechnical characteristics of soils affected by the tunnel excavation have been obtained by numerous site investigations and laboratory tests carried out in between 1990 and 2005. Tab.2-3 summarizes the number of boreholes and the tests performed all over the years. Details of performed site investigations are reported in the *Appendix II*.

INVESTIGATION CAMPAIGNS	BOREHOLES	CPT	SPT	PERMEABILITY TESTS	LABORATORY TESTS
1990	45	5	-	-	On loose soils
1998 - 2000	24	6	60	Lefranc	On Tuff
2005	10 (Arco Mirelli Station)	-	10	Lugeon x 2	-
	10 (San Pasquale Station)	-	10	Lugeon x 2	-
	10 (Chiaia Station)	-	7	-	-

Tab.2-3. General informations about site and laboratory investigation campaign performed from 1990 up to 2005

2.2.1.1. Site and laboratory investigations

On the basis of informations collected during the first site investigation campaign in 1990, performed to realize the first Line 6 stretch (Fuorigrotta – Mergellina), a number of further site and laboratory investigations were planned in order to have a global view about the soil affected by the Mergellina – Municipio tunnel excavation.

Appendix II reports informations about the performed investigations and the results from in situ (CPT, SPT, Lefranc and /or Lugeon permeability tests) and laboratory tests. From the collected informations the main physical and mechanical parameters for each soil layer were extracted (Fig.2-3 - Fig.2-6). Informations from CPT and SPT investigations have been processed using Durgunoglu e Mitchell (1975) and De Mello (1971) relations, while results of laboratory tests have been depicted in the Mohr plane (t, s') imposing $c' = 0$, as figures below show. CPT tests have been used for strain parameters calculation too, by means of empirical correlation:

$$E = \beta \cdot q_c$$

with $\beta = 2.5$ as suggested by Meyerhof e Fellenius (1985).

Figures and tables below report the informations obtained for each soil layer and Tab.2-4 resumes the main physical and mechanical parameters.

SAND	Average value
γ [kN/m ³]	16
γ_{sat} [kN/m ³]	18
γ' [kN/m ³]	8
k [cm/s]	$10^{-04} - 10^{-05}$
Uniaxial compression strength [MPa]	0
c' [kPa]	37°
ϕ' [°]	50000
E' [MPa]	0.3
ν'	0.5
k_o	16

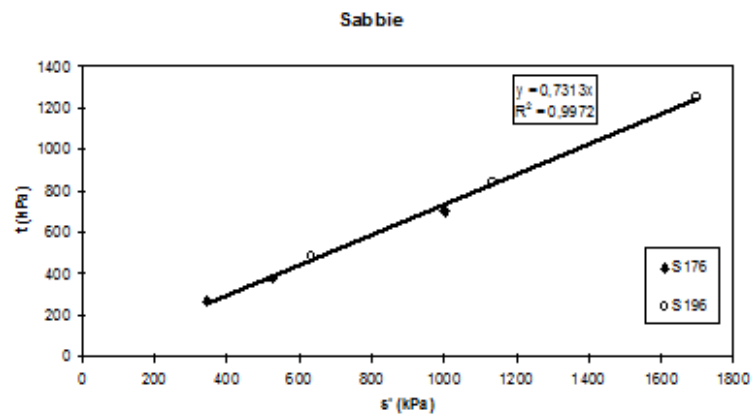
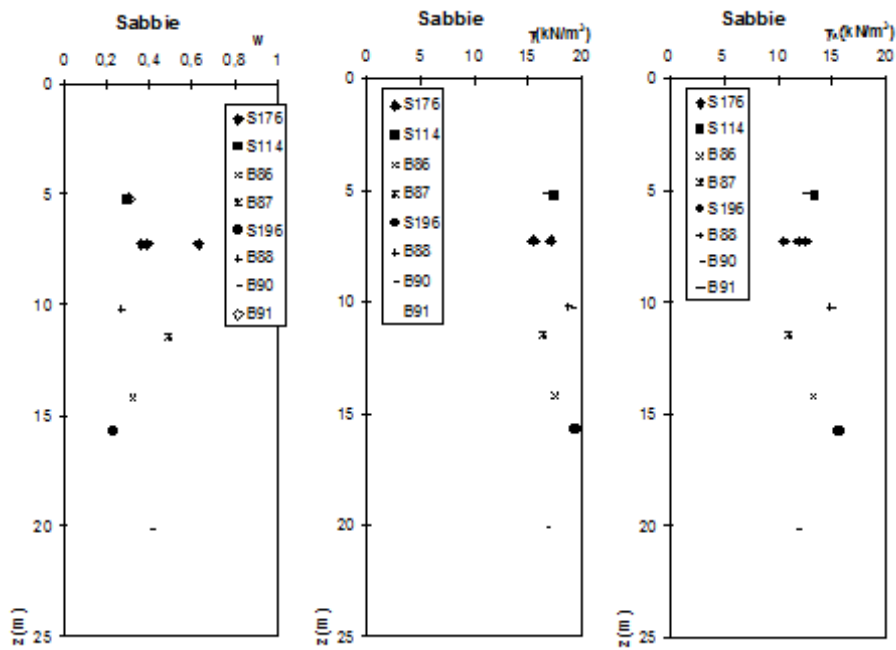


Fig.2-3. Sand physical-mechanical properties

PIROCLASTITI	Average value
γ [kN/m ³]	14
γ_{sat} [kN/m ³]	16
γ' [kN/m ³]	6
k [cm/s]	$10^{-04} - 10^{-05}$
Uniaxial compression strength [MPa]	0
c' [kPa]	36°
ϕ' [°]	40000
E' [MPa]	0.3
ν'	0.5
k_o	14

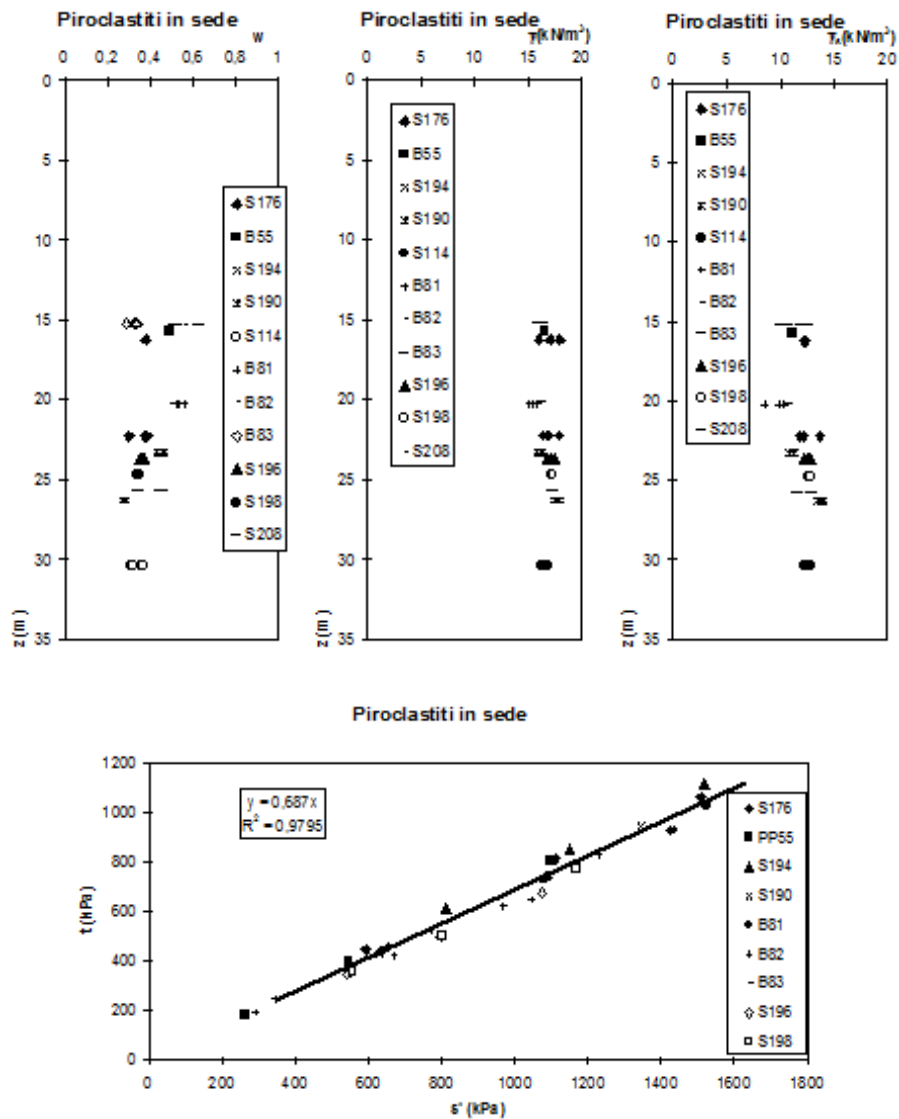


Fig.2-4. Piroclastiti physical-mechanical properties

CINERITI	Average value
γ [kN/m ³]	14
γ_{sat} [kN/m ³]	16
γ' [kN/m ³]	6
k [cm/s]	$10^{-04} - 10^{-05}$
Uniaxial compression strength [MPa]	0
c' [kPa]	37°
ϕ' [°]	50000
E' [MPa]	0.3
ν'	0.5
k_o	

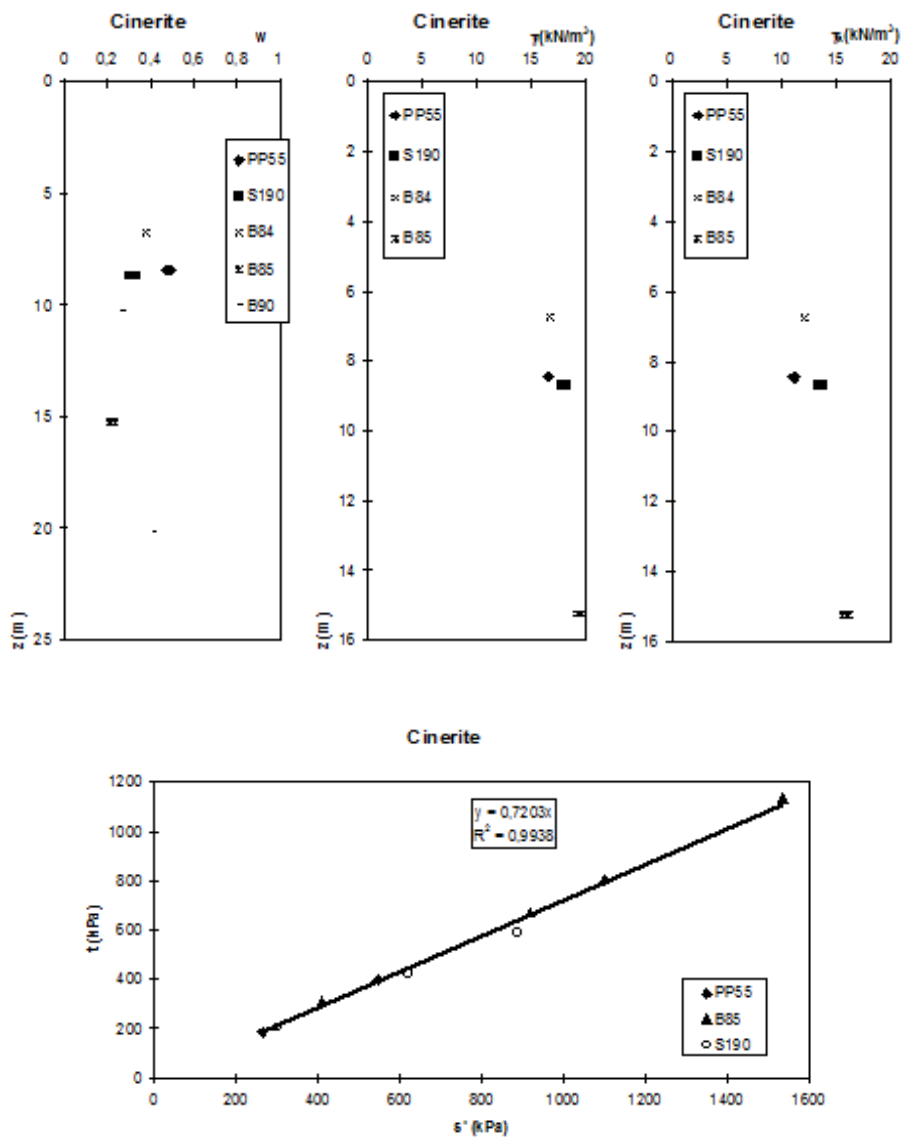


Fig.2-5. Cinerite physical-mechanical properties

TUFF	Average value
γ [kN/m ³]	14
γ_{sat} [kN/m ³]	16
γ' [kN/m ³]	6
k [cm/s]	10^{-4} - 10^{-3}
Uniaxial compression strength [MPa]	2.5
c' [kPa]	500
ϕ' [°]	27°
E' [MPa]	1000
ν'	0.3
k_o	0.5

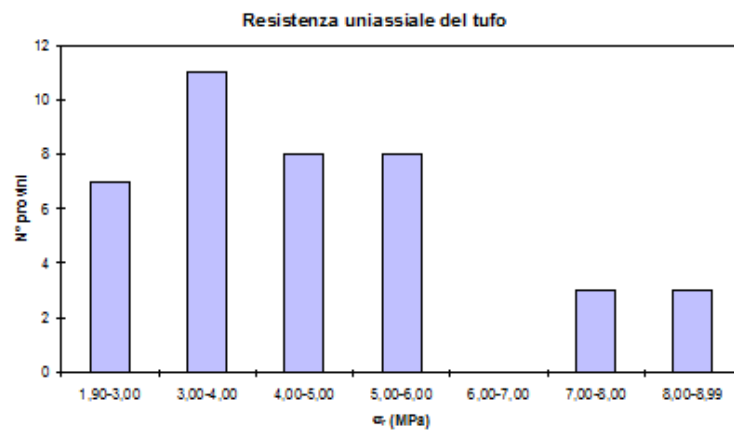
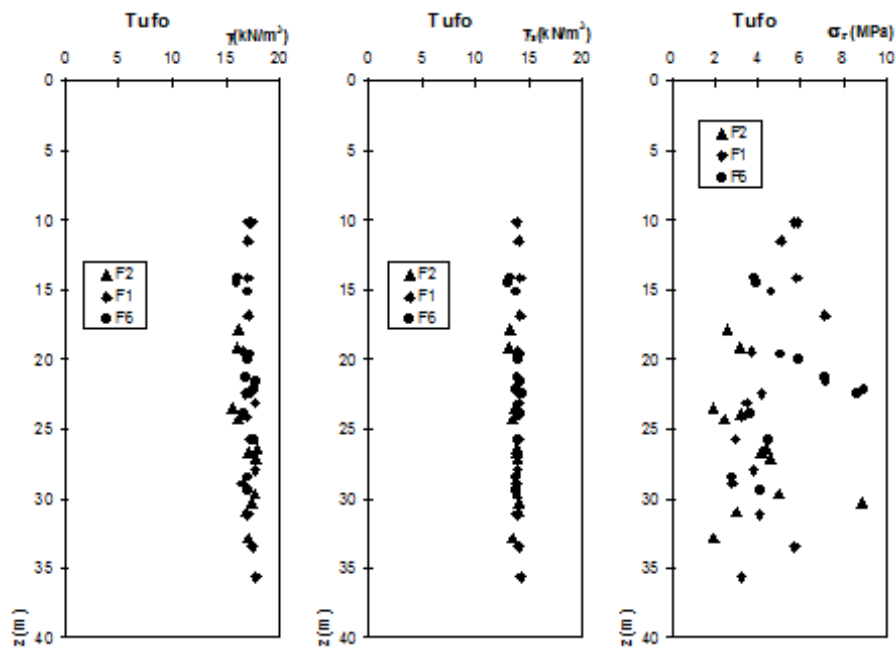


Fig.2-6. Tuff physical-mechanical properties

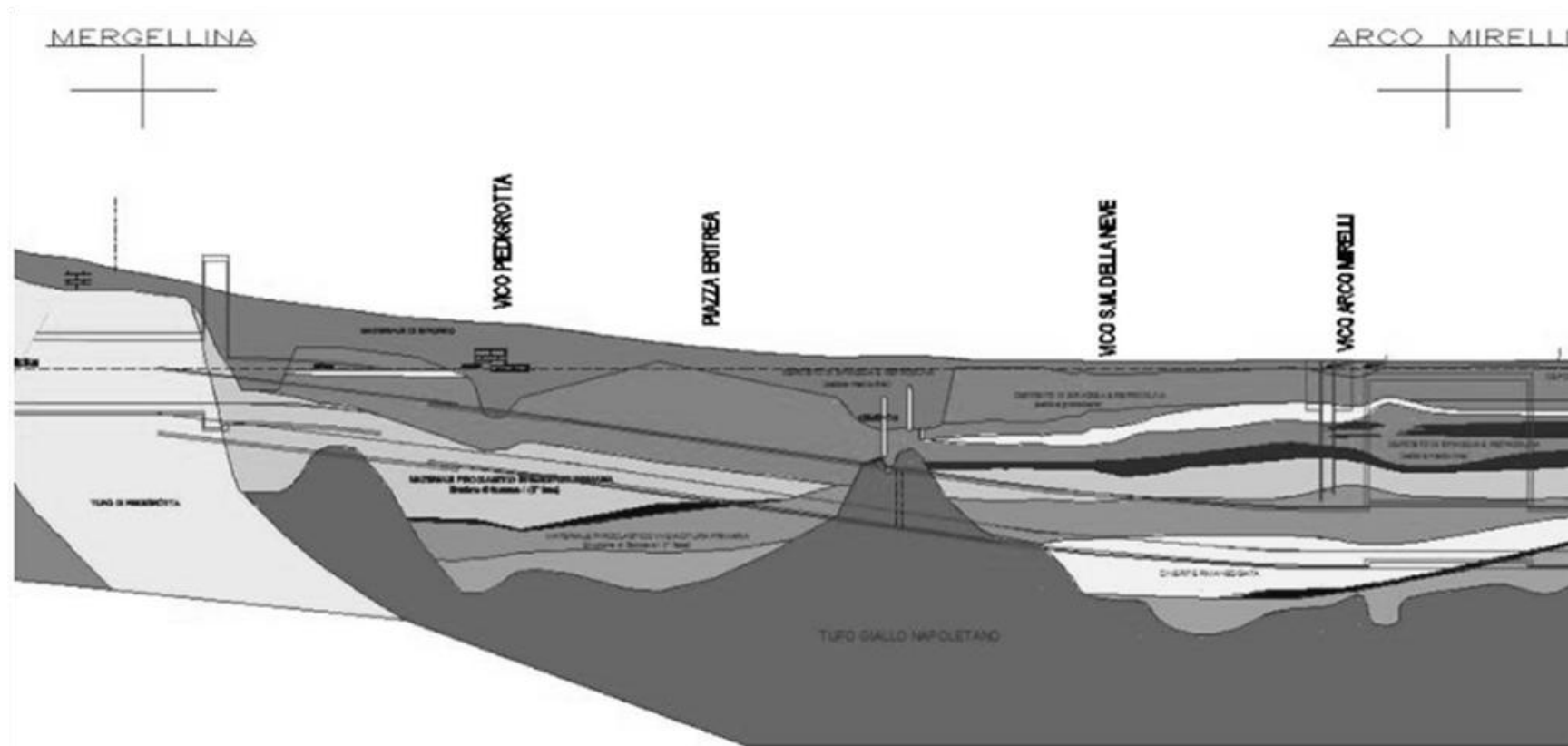


Fig.2-8. Stratigraphic profile within Mergellina and Arco Mirelli stations

2.2.2. The used excavation technique

The loose sandy soil and the high groundwater level (-1 m a.m.s.l.), led to choose and EPB machine rather than a TBM, to carry on the tunnel digging operations. As a matter of fact, the operating system of the machine leads to solve many problems related among the others to the supporting face pressure, the presence of water in the machine and the volume loss, to be maintained below 0.5%.

Using an EPB machine not any supporting function is assigned to the cutterhead. The front stability is ensured by the pressure that a plastic ground mixture applies on the ground face.

Once the excavation ground have been loosened, the “cake” (fluid ground and smoothing-agents mixture) in front of the machine falls through the the cutting wheel openings into the excavation chamber; uncontrolled penetrations of the soil in it are prevented thanks to the thrust cylinders forces transmitted from the pressure bulkhead onto the soil. A state of equilibrium is reached when the soil in the excavation chamber cannot be compacted any further by the native earth and water pressure. Thus the face stability is always guaranteed only by the thrust cylinders pressure, transferred through the bulkhead on the mixed ground into the excavation chamber. Therefore this is only responsible for mixing the excavated ground inside and outside the excavation chamber.

The excavated material is removed from the excavation chamber by an auger conveyor. The amount of removed material is controlled by the speed of the auger and the cross-section of the opening of the upper auger conveyor driver. The excavated material is conveyed on some belts to the so called reversible conveyor from which the transportation gantries in the backup areas are loaded when the conveyor belt is put into reverse.

The lining segments of the tunnel are located by means of erectors behind the pressure bulkhead and then temporarily bolted in place. Mortar is continuously forced into the remaining gap between the segments ‘outer side and the soil, through injection openings in the tailskin or openings in the segments.

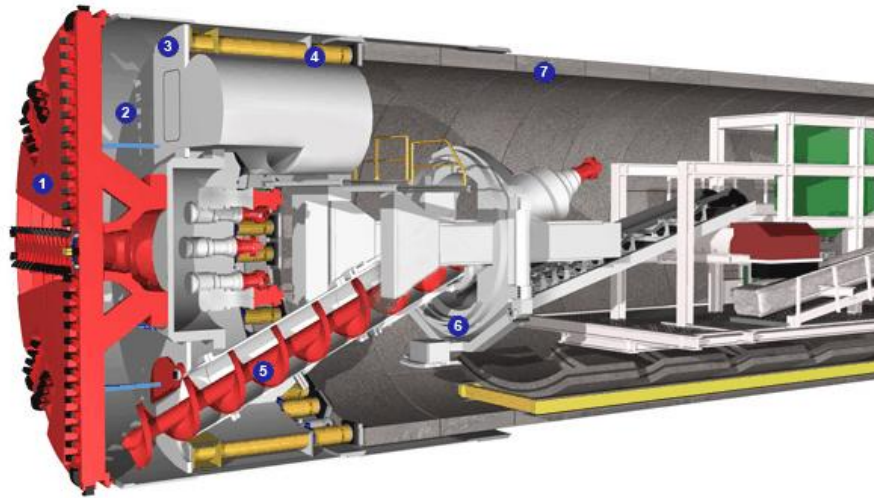


Fig.2-9. 1) Cutting wheel; 2) Excavation chamber; 3) Pressure bulkhead; 4) Thrust cylinder; 5) Auger conveyor; 6) Erectors; 7) Lining segments

As the tunnel excavation occurs in sandy loose soil, with no any self-sufficiency ability, the used machine is equipped of particular system to realize mortar injections (maximum 4-6 bar) in between the final lining outer line and the soil.

Though a Slurry TBM machine using bentonite should be appropriate for the soil in point, an EPB machine has been preferred for the reasons below:

1. less material to be injected in the excavation chamber and to pull out
2. lower pressure to guarantee the front stability
3. better performance in the loose soil
4. less environmental impact
5. less expensive

Among the others, some more reasons strictly related to the use of bentonite rather than tenso-active products, led to choose the EPB instead of the Slurry TBM:

1. because of the high specific gravity the bentonite could easily penetrate in the grains of the sand, thus a lower shield pressure on the face and higher surface displacements occur
2. to mix the bentonite mud to the ground a large amount of water is required, thus a less safe working environment

3. the bentonite makes the excavated ground fluid for so long to complicate its transport to the landfill
4. using bentonite a more complex and cumbersome system is required.

Concluding, the main properties of the used machine are described below:

EPB	
Cutter weal diameter	8.10 m
Total length	8.00 m
Maximum pressure in the excavation chamber	3 bar
Maximum thrust cylinder lengthening	2.00 m
Auger conveyor diameter	900 mm

Tab.2-6. Excavation machine properties

2.2.3. The monitoring plan

As the tunnel excavation affects a very urbanized area, a complete monitoring plan development has been required.

In order to achieve a global view of the tunnelling induced effects in the surrounding environment, a number of monitoring instruments have been installed on preexisting buildings, into and on the ground surface and inside the final tunnel lining.

Ground and buildings deformations have been constantly controlled by mean of topographic instruments installed into and on the ground surface and on the buildings faces overlooking Via Piedigrotta.

To obtain a comprehensive view of the tunneling induced effects in the surrounding environment, since the tunnel line always located below the

groundwater level, some piezometers have been installed nearby the tunnel operating area as to monitor the induced groundwater variations.

Moreover, some strain-gages have been installed in some of the tunnel lining segments to control the induced deformations and the internal stress variations.

According to the monitoring scheduled instruments, three different monitoring sections have been defined along the whole tunnel line:

1. topographic sections: with mainly topographic instruments
2. main geotechnical section: with both topographic instruments, inclinometers, piezometers and strain-gages in the tunnel lining
3. secondary geotechnical section: the same as the previous one, with no monitored tunnel lining segments.

For each installed instrument, the frequency of the measurements is differently defined according to the operations site in progress and to the front machine position in respect to the measuring section.

In the pages and in the tables below the monitoring sections are fully described together with the scheduled frequency for each monitoring instrument (Tab.2-7-Tab.2-11).

TOPOGRAPHIC SECTIONS

They are made only by topographic instruments such as:

- n° 7 topographic landmarks on the ground surface orthogonal to the tunnel.

The sections are about 50 m apart and the central landmark has to be installed on the tunnel axis. If necessary, n° 5 landmarks can be installed when the section interferes with preexisting structures.

MAIN GEOTECHNICAL SECTIONS

They are made by monitoring instruments installed both in the ground surface surrounding the tunnel and in the tunnel lining segments. The used instruments:

- n° 7 topographic landmarks on the ground surface orthogonal to the tunnel axis
- n° 2 inclinometers out of the tunnel excavation area, from 2 to 5 m faraway from the outer tunnel lining, up to 10 m below the invert
- n° 1 piezometer
- n° 8 instrumented segments per lining ring

SECONDARY GEOTECHNICAL SECTIONS

The instruments for this section are the same as the main geotechnical sections' ones except for the lining segments monitoring instruments.

WORK IN PROGRESS	TUNNEL FACE RESPECT TO THE SECTION	MEASURES FREQUENCY
SETTING UP	<ul style="list-style-type: none"> • Zero reading • 2 measures/month (until the tunneling operations start) 	
TUNNEL EXCAVATION	<ul style="list-style-type: none"> • $-5Z_0 < TF < -2Z_0$ • $-2Z_0 < TF < 2Z_0$ • $2Z_0 < TF < 5Z_0$ • $TF > 5Z_0$ • 3 months after the tunnel face passed the measuring section 	<ul style="list-style-type: none"> • 1-2 measures/week • 1-2 measures/day • 1-2 measures/week • 1-2 measures/month • 1-2 measures/month

Tab.2-7. Scheduled measurements frequency for the topographic instruments on the ground surface

WORK IN PROGRESS	TUNNEL FACE RESPECT TO THE SECTION	MEASURES FREQUENCY
SETTING UP	<ul style="list-style-type: none"> • Zero reading • 2 measures/month (until the tunneling operations start) 	
TUNNEL EXCAVATION	<ul style="list-style-type: none"> • $-5Z_0 < TF < -2Z_0$ • $-2Z_0 < TF < 2Z_0$ • $2Z_0 < TF < 5Z_0$ • $TF > 5Z_0$ • 3 months after the tunnel face passed the measuring section 	<ul style="list-style-type: none"> • 2 measures/week • 2 measures/day • 2 measures/week • 1 measures/month • 1 measures/month

Tab.2-8. Scheduled measurements frequency for landmarks on buildings

WORK IN PROGRESS	TUNNEL FACE RESPECT TO THE SECTION	MEASURES FREQUENCY
SETTING UP	<ul style="list-style-type: none"> • Zero reading • 1 measures/month (until the tunneling operations start) 	
TUNNEL EXCAVATION	<ul style="list-style-type: none"> • $-5Z_0 < TF < -2Z_0$ • $-2Z_0 < TF < 2Z_0$ • $2Z_0 < TF < 5Z_0$ • $TF > 5Z_0$ • until the excavation ends 	<ul style="list-style-type: none"> • 1-2 measures/week • 1-2 measures/day • 1-2 measures/week • 1-2 measures/month • 1-2 measures/month

Tab.2-9. Fig. Scheduled piezometric measurements frequency

WORK IN PROGRESS	TUNNEL FACE RESPECT TO THE SECTION	MEASURES FREQUENCY
SETTING UP	<ul style="list-style-type: none"> • Zero reading • 1 measures/month (until the tunneling operations start) 	
TUNNEL EXCAVATION	<ul style="list-style-type: none"> • $-5Z_0 < TF < -2Z_0$ • $-2Z_0 < TF < 2Z_0$ • $2Z_0 < TF < 5Z_0$ • $TF > 5Z_0$ • 3 months after the tunnel face passed the measuring section 	<ul style="list-style-type: none"> • 1-2 measures/week • 1-2 measures/day • 1-2 measures/week • 1-2 measures/month • 1-2 measures/month

Tab.2-10. Fig. Scheduled extensometer and inclinometers measurements frequency

WORK IN PROGRESS	TUNNEL FACE RESPECT TO THE SECTION	MEASURES FREQUENCY
SETTING UP	<ul style="list-style-type: none"> • Instruments testing • Zero reading 	
AGING OF CONCRETE	<ul style="list-style-type: none"> • 1 measure/6 hours • 2 measures/day 	<ul style="list-style-type: none"> • during the first 20 days • until the concrete aging is finished
SEGMENTS INSTALLATION	<ul style="list-style-type: none"> • 1 measure/6 hours • 2 measures/day • 1 measure/day 	<ul style="list-style-type: none"> • for the first 60 m next to the installed ring • until the measured deformation is stabilized • until the line is completed

Tab.2-11. Fig. Scheduled tunnel lining stress measurements frequency

2.2.3.1. Installed monitoring instruments

LANDMARKS ON THE GROUND SURFACE

N° 45 topographic sections, on average 10 m spaced, were installed on the ground surface along Via Piedigrotta, perpendicular to the tunnel axis. Each section is made at least by 5 landmarks, 5 m spaced, with the central one located at the tunnel axis.

Fig.2-10 show an example of the topographic landmarks sections location along Via Piedigrotta while in Tab.2-12 their exact position is indicated.

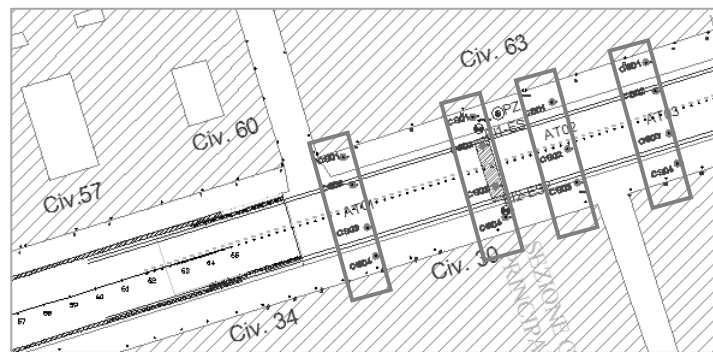


Fig.2-10. Fig. Example of installed ground landmarks

ID	Z ₀ [m]	ID	Z ₀ [m]	ID	Z ₀ [m]	ID	Z ₀ [m]	ID	Z ₀ [m]	ID	Z ₀ [m]	ID	Z ₀ [m]
AT01	299.80	AT06	385.90	AT13	443.92	AT19	503.93	AT26	554.47	AT33	623.80	SP02	694.00
SP01	316.67	AT07	399.58	AT14	451.31	AT20	511.24	AT27	563.02	AT34	639.35	AT40	701.64
AT02	326.50	AT08	407.70	AT15	458.70	AT21	518.83	AT28	578.20	AT35	646.56	AT41	708.31
AT03	339.30	AT09	414.93	AT16	466.01	AT22	525.80	AT29	584.98	AT36	654.35	AT42	727.71
AT04	355.83	AT10	421.94	AT17	473.38	AT23	533.02	AT30	591.69	AT37	668.28		
AT04bis	356.00	AT11	429.19	SC01	485.58	AT24	542.09	AT31	608.77	AT38	685.81		
AT05	372.31	AT12	436.44	AT18	496.02	AT25	545.67	AT32	616.90	AT39	683.30		

Tab.2-12. Fig. Landmarks on the ground surface

LANDMARKS ON BUILDINGS

To control the preexisting buildings tunneling induced deformations a number of landmarks have been installed on their facades.

29 buildings have been instrumented nearby the tunnel track, along Via Piedigrotta and Riviera di Chiaia.

The monitoring plan provided a landmark each 6/8 m for masonry and landmarks next to the pillars for the concrete buildings, depending on the accessibility of the structure.

In Tab.2-13 below, the monitored buildings together with the number of installed landmarks on them, are resumed.

Address	Building n°	Number of installed landmarks	Building n°	Number of installed landmarks
Via Piedigrotta	7	5	57	3
	11	10	60	10
	16	4	63	14
	19	6	65	5
	23	9	67	3
	30	6	93	6
	34	12	96	3
	54	5	98	3
Riviera di Chiaia	23	10	50	2
	33	5	53	3
	36	5	57	2
	44	4	61	3
	48	2	66	8
Largo Torretta	19	9	-	-
P.za della Repubblica	2	5	-	-
Via C. Cucca	3	5	-	-

Tab.2-13. Landmarks on buildings

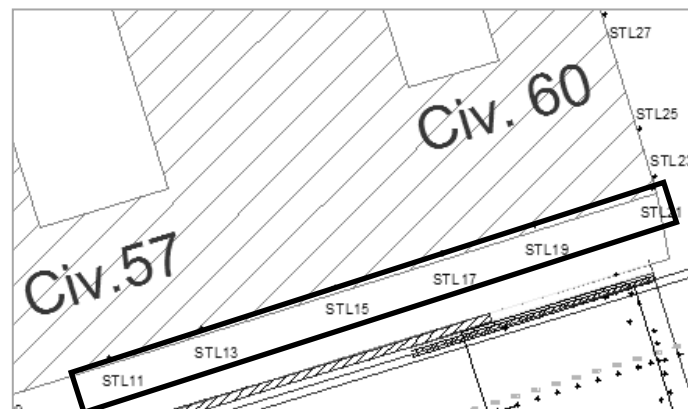


Fig.2-11. Example of landmarks on buildings

2.3. The empirical methods for prediction of tunnelling induced displacements

In this section empirical formula will be used to predict tunnel induced displacements along Via Piedigrotta and Riviera di Chiaia, where the worst combinations of factors, such as cover layer thickness and buildings to tunnel distance appear. The analyzed stretch ends in Arco Mirelli station.

As the cover layer thickness varies from 12 m to 18 m, empirical formula have been applied for 7 different tunnel depths and buildings damage analysis has been carried on for 23 buildings.

As better explained in the *Background* section of this work, transversal and longitudinal displacements curves result from K and V_L , depending by cohesive or cohesionless soils and by the used excavation technique. For the case in question the chosen values for the parameters above are respectively 0.30 and 0.5%. Horizontal and vertical displacements in transversal and longitudinal directions are plotted in Fig.2-12 to Fig.2-15 for 12m up to 18 m cover layers thickness; Tab.2-14 resumes obtained results.

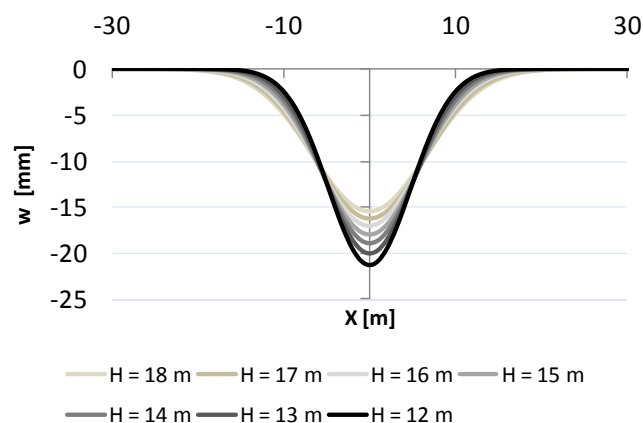


Fig.2-12. Transversal section: predicted vertical displacements ($K = 0.30 - V_L = 0.5\%$)

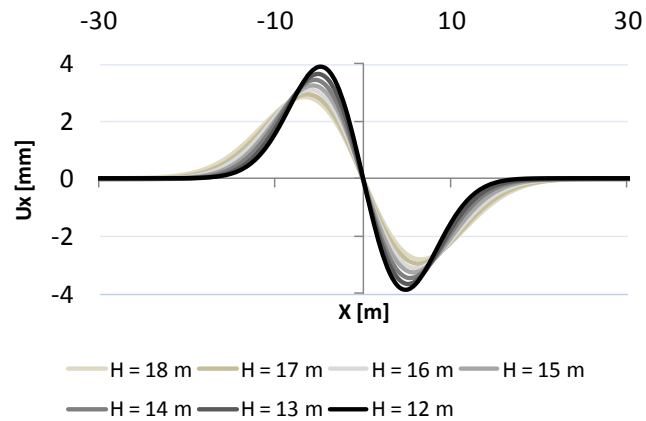


Fig.2-13. Transversal section: predicted horizontal displacements ($K = 0.30 - V_L = 0.5\%$)

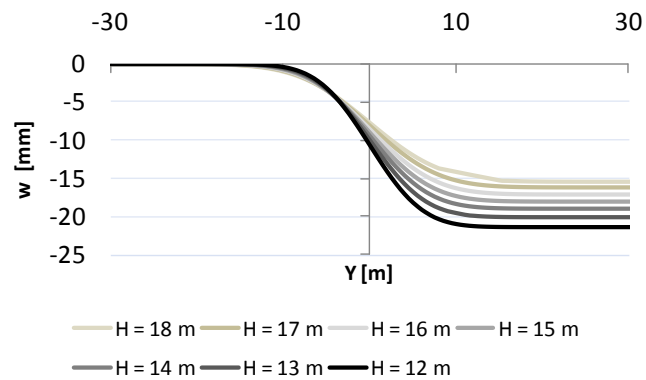


Fig.2-14. Longitudinal section: predicted vertical displacements ($K = 0.30 - V_L = 0.5\%$)

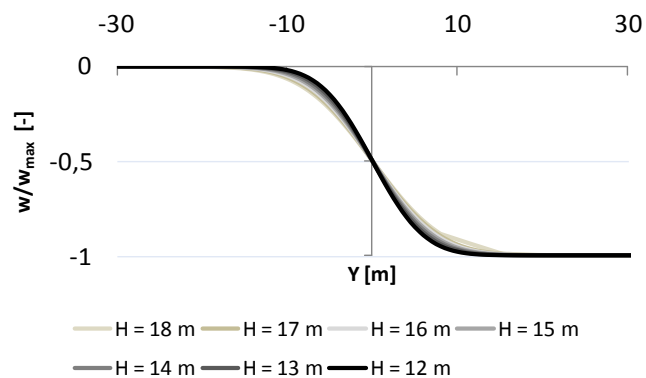


Fig.2-15. Longitudinal section: vertical displacements on maximum vertical settlements ($K = 0.30 - V_L = 0.5\%$)

K = 0.3 - $V_L = 0.5\%$					
H [m]	Z ₀ [m]	BUILDINGS	i [m]	w _{max} [mm]	U _{x,max} [mm]
18	22	RC.50 - RC.53 - RC.57 - RC.61	6.6	15.52	2.82
17	21	RC.40 - RC.48	6.3	16.26	2.95
16	20	RC.22 - RC.36	6.0	17.07	3.11
15	19	PG.19 - PG.2 - RC.23	5.7	17.97	3.26
14	18	PG.11 - PG.7 - PG.93 - PG.96 - PG.98	5.4	18.96	3.43
13	17	PG.23 - PG.65 - PG.67 - PG.16	5.1	20.07	3.65
12	16	PG.63 - PG.30	4.8	21.32	3.87

Tab.2-14. Main indications about displacements curves for different cover layers thickness

On the base of calculated displacements, buildings damage analysis has been done to define the level of damage caused by predicted displacements all along the analyzed tunnel stretch. Figures below show results in the damage abacus; in most of the cases buildings belong to the 0 category of damage, with the exception of buildings 93, 96 and 98 along Via Piedigrotta belonging to the 1st one respectively corresponding to the “Negligible” and “Very slight” class on the damage abacus (after Boscardin & Cording, 1989 and Burland, 1995). Fig.2-18 represents the plan of tunnelling induced damage.

BUILDINGS			L/H	ε_h	Δ/L	CLASS OF DAMAGE (after Boscardin & Cording, 1989) and Burland, 1995)		
VIA PIEDIGROTTA	1	PG.63	Masonry	1.7	0.013	0.020	0	Negligible
				2.2	0.011	0.018		
				4.0	0.013	0.012		
	2	PG.30	Masonry	0.8	0.013	0.023	0	Negligible
	3	PG.23	Masonry	0.5	0.029	0.022	0	Negligible
				0.9	0.016	0.022		
				1.2	0.011	0.019		
	4	PG.65	Masonry	0.9	0.026	0.022	0	Negligible
	5	PG.67	Concrete	1.4	0.026	0.014	0	Negligible
	6	PG.16	Masonry	0.4	0.025	0.020	0	Negligible
				0.7	0.026	0.023		
0.8				0.026	0.022			
7	PG.11	Concrete	0.3	0.033	0.017	0	Negligible	
8	PG.7	Masonry	0.7	0.037	0.014	0	Negligible	
9	PG.93	Masonry	1.0	0.045	0.022	1	Very slight	
10	PG.96	Masonry	1.2	0.045	0.022	1	Negligible	
11	PG.98	Masonry	1.2	0.045	0.022	1	Very slight	
LARGO TORRETTA	12	LT.19	Masonry	1.2	0.029	0.017	0	Negligible
VIA C. CUCCA	13	CC.3	Masonry	1.4	0.013	0.020	0	Negligible

Tab.2-15. Via Piedigrotta, Largo Torretta and Via C. Cucca: analysed buildings and related level of damage

BUILDINGS			L/H	ε_h	Δ/L	Δ/L CLASS OF DAMAGE (after Boscardin & Cording, 1989) and Burland, 1995)		
RIVIERA DI CHIAIA	1	RC.23	Masonry	0.7	0.031	0.014	0	Negligible
	2	RC.33	Masonry	2.3	0.015	0.020	0	Negligible
				3.5	0.015	0.018		
				4.0	0.015	0.017		
	3	RC.36	Masonry	2.1	0.012	0.019	0	Negligible
	4	RC.48	Concrete	0.5	0.021	0.016	0	Negligible
				0.8	0.023	0.019		
				1.1	0.023	0.018		
	5	RC.40-44	Masonry	2.9	0.008	0.016	0	Negligible
				0.0	0.008	0.026		
				0.0	0.008	0.081		
	6	RC.50	Masonry	2.4	0.010	0.017	0	Negligible
				2.7	0.010	0.016		
				3.0	0.010	0.016		
	7	RC.53	Masonry	2.7	0.007	0.015	0	Negligible
				3.0	0.010	0.014		
				3.4	0.010	0.013		
	8	RC.57	Masonry	0.9	0.020	0.014	0	Negligible
1.6				0.010	0.017			
9	RC.61	Masonry	2.2	0.010	0.016	0	Negligible	
			2.4	0.010	0.016			
			2.6	0.010	0.015			

Tab.2-16. Riviera di Chiaia: analysed buildings and related level of damage

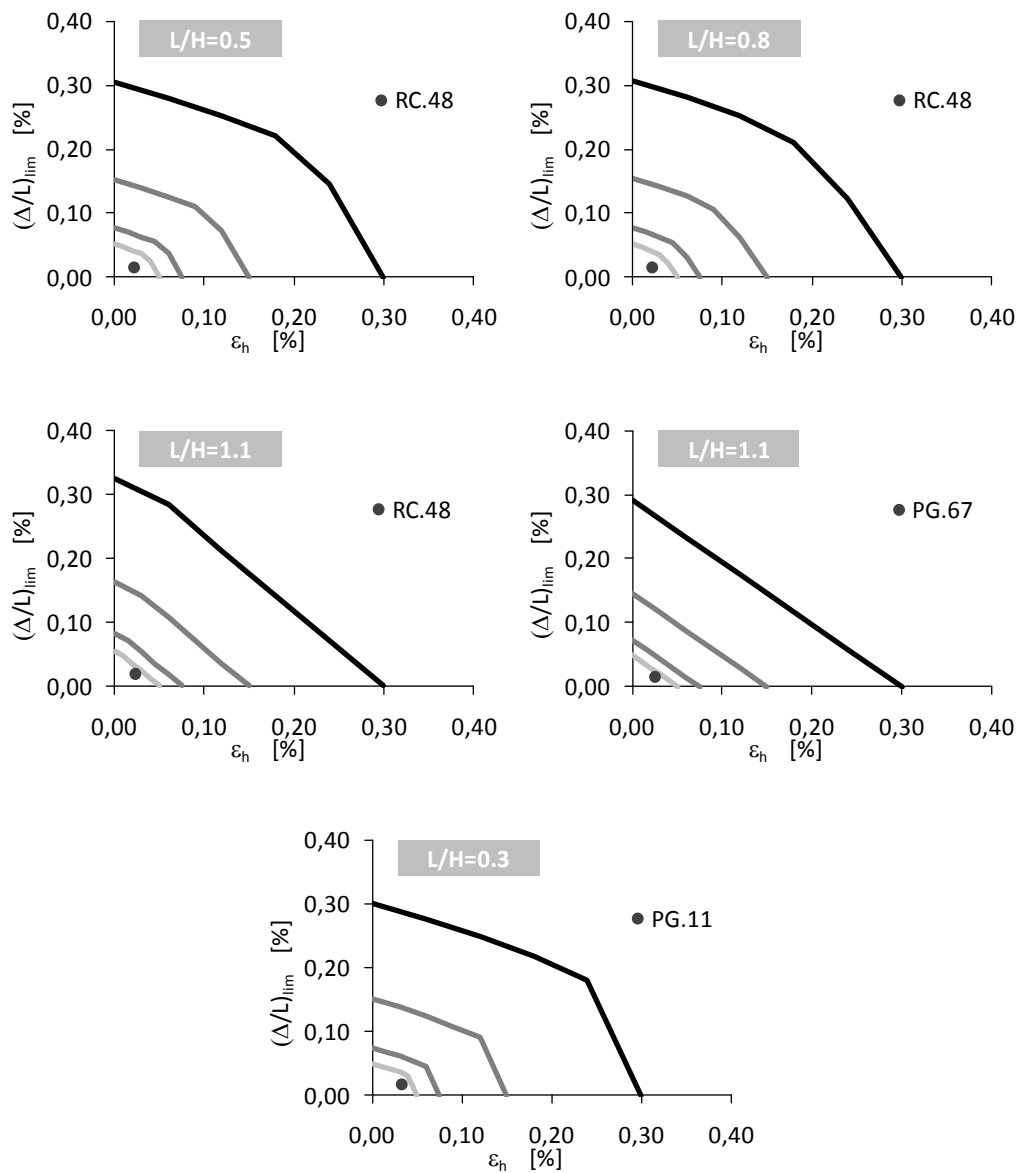
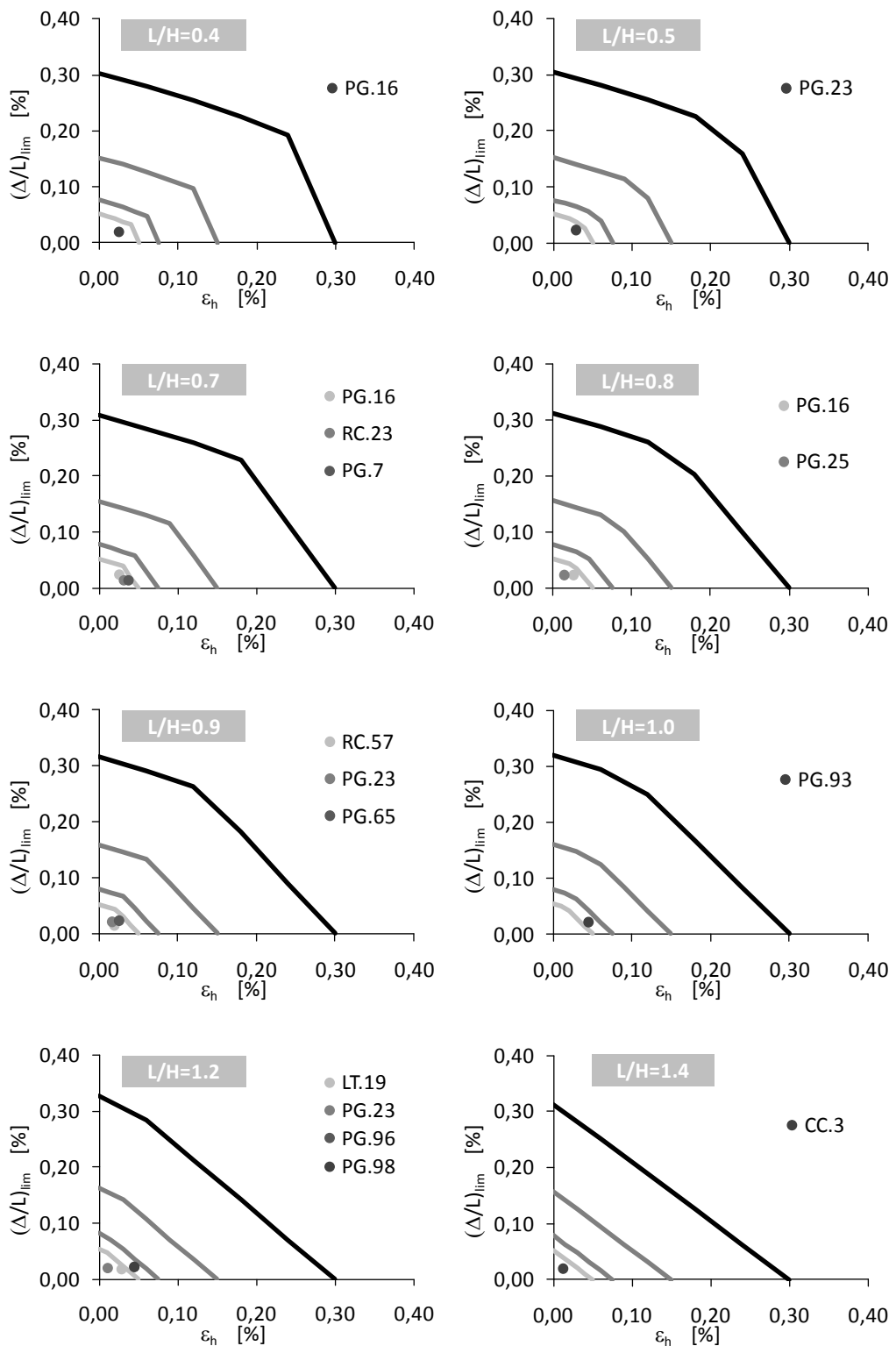
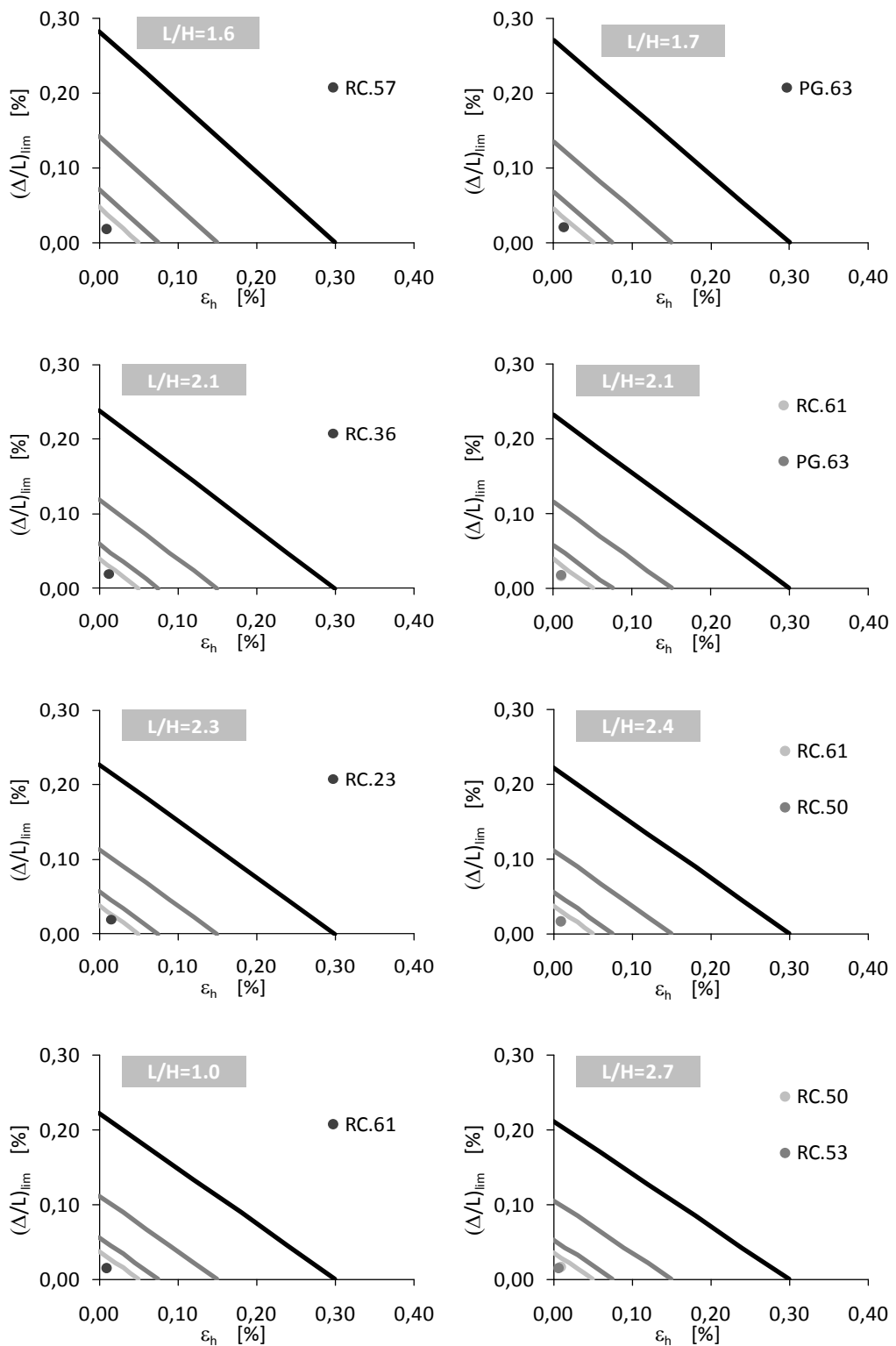


Fig.2-16. Damage abacus for concrete buildings (PG.11 and PG.67 along Via Piedigrotta and RC.48 along Riviera di Chiaia)





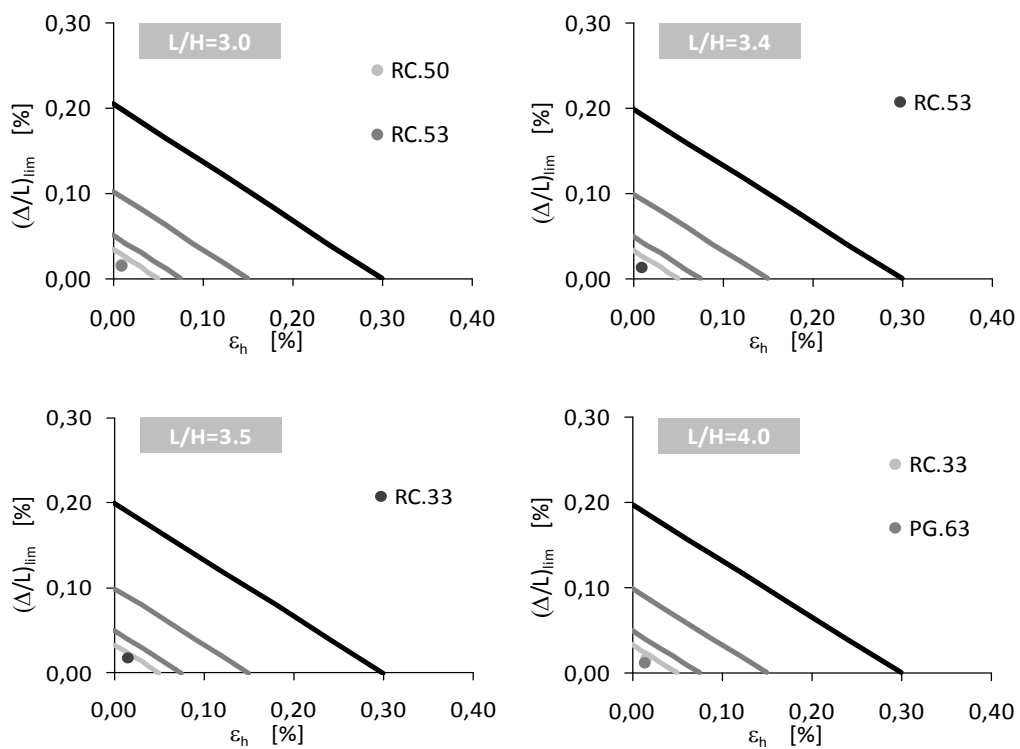


Fig.2-17. Damage abacus for brick buildings



Fig.2-18. Damage plan

Chapter 3. LINE 6: ANALYSIS OF MONITORING DATA

3.1. Introduction

As explained in Chapter 2, a number of monitoring instruments have been installed all along the Line 6 track, to control the tunnelling induced effects (buildings and ground displacements, groundwater variations and lining stresses); it follows that several data, from topographic landmarks on the ground surface and on preexisting buildings, piezometers, extensometers-inclinometers and strain-gages in the tunnel lining segments, have been collected.

In the following pages the data coming from the installed topographic instruments will be discuss with the aim of overseeing the tunnelling effects on preexisting buildings and consequently their induced level of damage.

3.2. Tunnel excavation

Before the Line 6 tunnelling operations started, several yard operations took place: the old stuck TBM machine was disassembled and pulled out and the new EPB machine was carried to the yard and then assembled. These operations took about three months; they started in July 2009, when the old TBM started to be disassembled and finished in September 2009 when the new EPB was assembled.

The pictures below show the above mentioned operations, preparatory to the tunnel excavation process.



Fig.3-1. Disassembly the old TBM machine



Fig.3-2. New front with spritz-beton



Fig.3-3. Carrying and casting the frontal piece of the cutting head



Fig.3-4. Carrying and casting the cutting weal



Fig.3-5. Assembled cutting head and cutting wheel

Once the above mentioned operations finished, on the April 7th, 2009 the tunnelling operations started from km (0 + 292.90). Basing on the last update on August the 31st 2010, the machine is at km (0 + 716.13): 423 m of tunnel have been excavated and 250 lining segments have been installed.

The detailed tunnel production day by day is resumed in the *Appendix* and it is represented in Fig.3-6, Fig.3-7 and Fig.3-8.

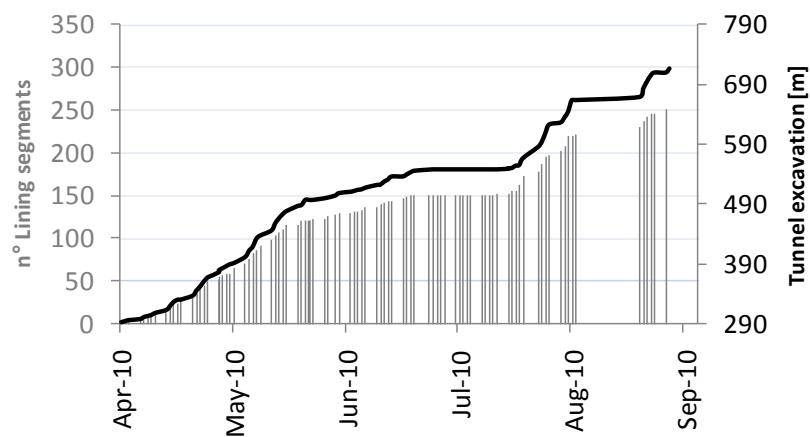


Fig.3-6. Progressive tunnel production

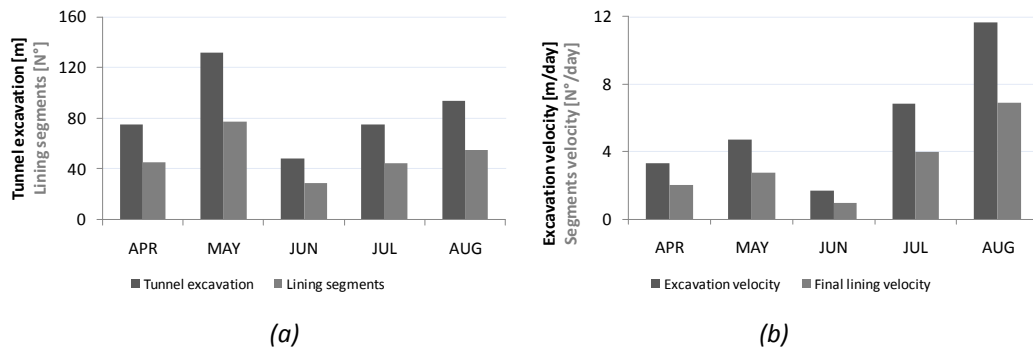


Fig.3-7. Tunnel production (a) and tunnel production velocity (b)

From the graphs in Fig.3-7 an average of 85 m/month for the excavated tunnel and of 50 segments/month for the installed final lining can be determined, with respective velocities of 3 m/day and 2 segments/day.

In terms of excavated distance, the best production has been recorded in May, when 132 m of tunnel were excavated and 78 lining segments were installed. On the opposite side, the worst production was realized in June because of several technical problems which slowed down the excavation procedure; among these a remarkable water inflow from the front observed between May the 31st and June the 18th and the opening of a hole on June the 28th in the ground nearby Largo Torretta, probably related to the next discovery of gas pipes in that area and immediately filled with 140 mc of grout.

As the graph in Fig.3-6 shows, the tunnel production in July stopped for about 20 days because of the need to repair the roadway and the leakage of mud in the road. Nevertheless since the machine restarted to excavate, the recorded production has been quite significant, as the tunnel velocity shows in Fig.3-7. However the best production was in August when of 93 m of tunnel were excavated and 55 lining segments were installed with respective velocity of 12 m/day and 7 segments/day.

In Fig.3-8 the detailed tunnel excavation velocity (m/day) is separately represented per month.

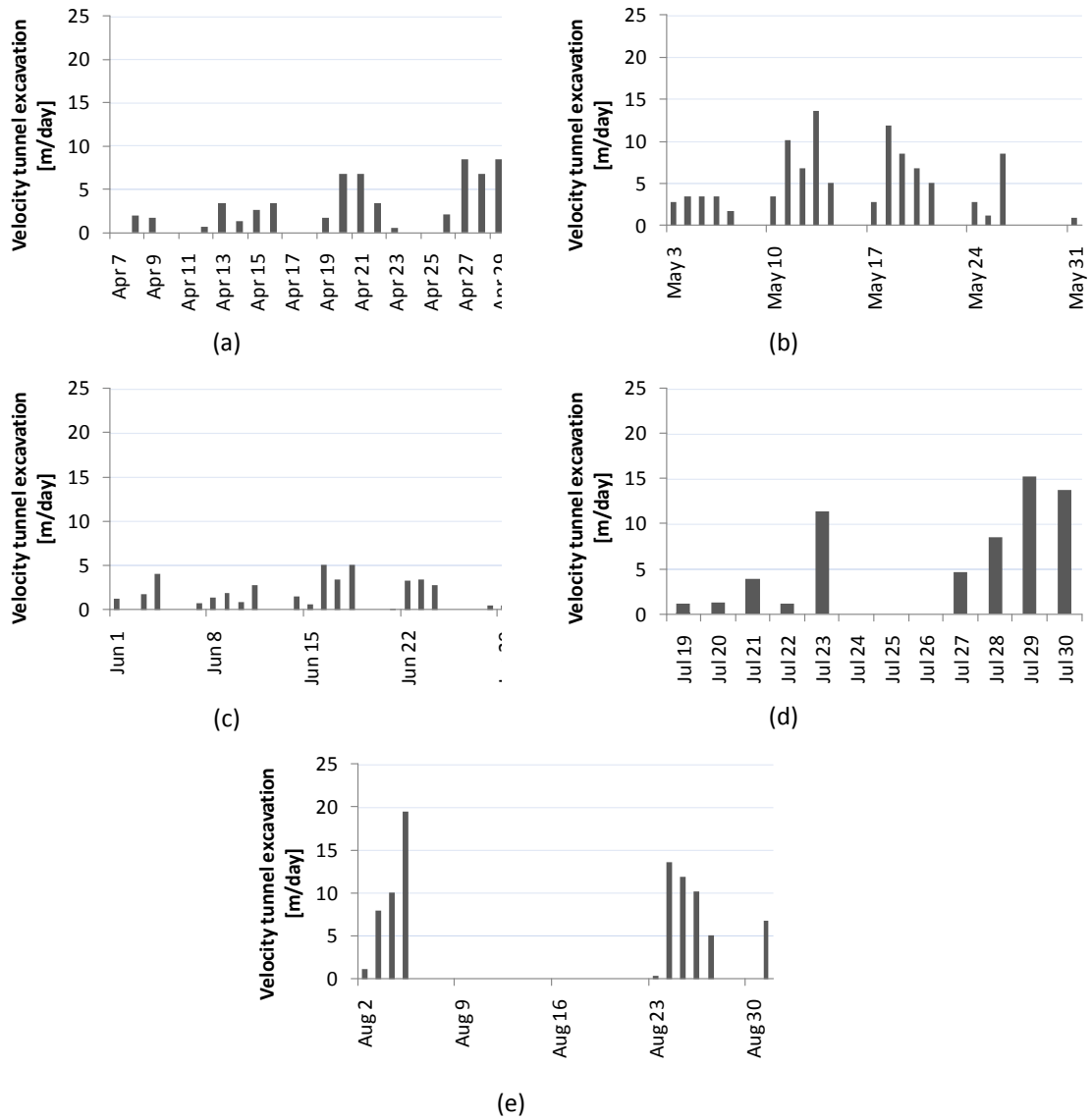


Fig.3-8. Excavation velocity: (a) April, (b) May, (c) June, (d) July, (e) August

3.3. Field monitoring data

In the following pages, collected data from monitoring instruments installed both on the ground surface and on preexisting buildings 'facades will be discuss.

The observed effects in terms of measured displacements are strictly related to the EPB performance (excavation velocity and/or applied pressures and forces); in this way the machine parameters have been continually supervised checking the applied pressures and torque moment required for the machine advance.

3.3.1. Excavation machine performances

Thanks to a number of sensors on the EPB machine, measurements of front pressure (FP), grouting pressure (GP) and torque moments (TM) applied for advancing with the tunnel excavation were collected. Tab.3-1 resumes the measured minimum and maximum values for each parameter while Fig.3-9 shows their trend versus the tunnel advance production. As the figure depicts, the front pressure is linearly increasing with the tunnel advance, whereas both the grouting pressure and the torque moments have a non uniform trend. For the grouting pressure peak values have been recorded between June the 18th and July the 28th when electrical problems with the cutterhead and water inflow from the front have been noticed. In the same interval an instantaneous 50% reduction of the torque moments has been measured.

EPB parameters	Minimum value	Maximum value
Front Pressure (FP)	110 kPa	295 kPa
Grouting Pressure (GP)	56 kPa	574 kPa
Torque Moments (TM)	2824 kNm	9631 kNm

Tab.3-1. Minimum and maximum values for applied front pressure, grouting pressure and torque moments

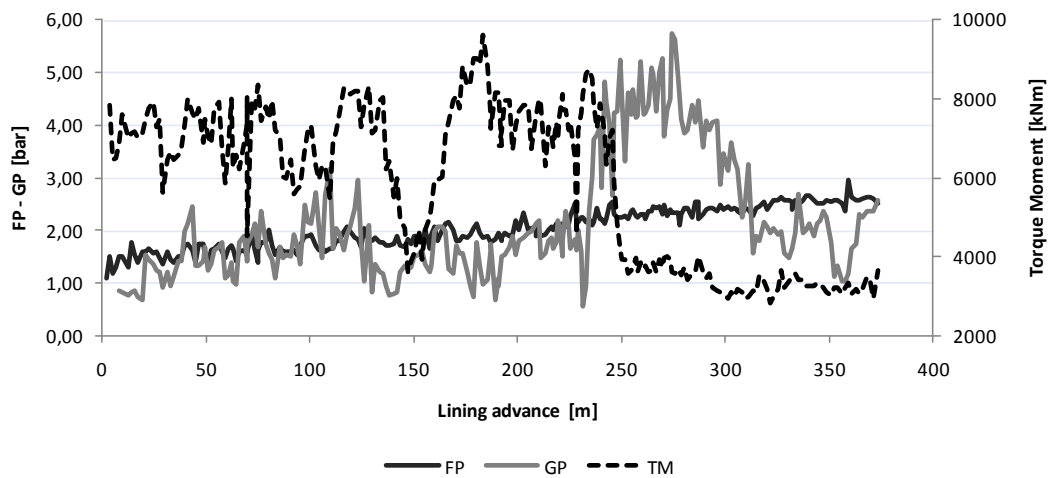


Fig.3-9. EPB performances: front pressure (FP), grouting pressure (GP) and torque moments (TM)

3.3.2. Landmarks on the ground surface

Basing on the monitoring data updated up to August the 31st, 45 landmarks sections have been installed on the roadway, above the tunnel track.

Each section is made by 3 to 5 landmarks with the central one installed at the tunnel axis. Detailed indications about the identification name, the position and the number of landmarks for each monitoring sections are resumed in Tab.2-12 (Chapter 2).

In the monitoring plan the landmarks sections are represented together with the tunnel track.

In Tab.3-2 informations about the zero and the last reading of each measuring sections are resumed. The table shows that for landmarks sections AT01 to AT30, in the first 300 m from the tunnel starting point, measuring data have been collected for more than one month; the zero readings have been recorded between April/May and the last readings at the end of July, when 330 m of tunnel were

excavated and the tunnel face was at km (0 + 622.73). Contrariwise for sections AT30 up to AT42 less than one month of recorded measures was observed: zero readings were recorded between the end of July and August and the last measures at the end of August (saving sections AT31 and AT32 for which only few data were collected being the last measures dated at August the 4th).

ID	ZERO reading	LAST reading	ID	ZERO reading	LAST reading	ID	ZERO reading	LAST reading
AT01	30-Mar-10	27-Jul-10	AT09	11-May-10	27-Jul-10	SC01	24-May-10	27-Jul-10
SP01	7-Apr-10	27-Jul-10	AT10	12-May-10	27-Jul-10	AT18	25-May-10	27-Jul-10
AT02	9-Apr-10	27-Jul-10	AT11	14-May-10	27-Jul-10	AT19	26-May-10	27-Jul-10
AT03	15-Apr-10	27-Jul-10	AT12	14-May-10	27-Jul-10	AT20	26-May-10	27-Jul-10
AT04	3-May-10	27-Jul-10	AT13	17-May-10	27-Jul-10	AT21	26-May-10	27-Jul-10
AT05	30-Apr-10	27-Jul-10	AT14	17-May-10	27-Jul-10	AT22	31-May-10	27-Jul-10
AT06	5-May-10	27-Jul-10	AT15	19-May-10	27-Jul-10	AT23	31-May-10	27-Jul-10
AT07	5-May-10	27-Jul-10	AT16	19-May-10	27-Jul-10	AT24	11-Jun-10	27-Jul-10
AT08	11-May-10	27-Jul-10	AT17	19-May-10	27-Jul-10	AT25	15-Jun-10	27-Jul-10

ID	ZERO reading	LAST reading	ID	ZERO reading	LAST reading
AT26	17-Jun-10	28-Jul-10	AT35	30-Jul-10	24-Aug-10
AT27	21-Jun-10	29-Jul-10	AT36	2-Aug-10	26-Aug-10
AT28	21-Jun-10	30-Jul-10	AT37	6-Aug-10	26-Aug-10
AT29	21-Jun-10	30-Jul-10	AT38	23-Aug-10	27-Aug-10
AT30	21-Jun-10	2-Aug-10	AT39	23-Aug-10	31-Aug-10
AT31	28-Jul-10	4-Aug-10	SP01	24-Aug-10	31-Aug-10
AT32	29-Jul-10	4-Aug-10	AT40	25-Aug-10	31-Aug-10
AT33	29-Jul-10	23-Aug-10	AT41	27-Aug-10	31-Aug-10
AT34	29-Jul-10	24-Aug-10	AT42	30-Aug-10	31-Aug-10

Tab.3-2. Measures zero and last readings

Referring to the design measurements frequency for the roadway landmarks, it has been observed that not for all the landmark sections the scheduled frequency has been respected. In many cases the landmarks readings started just before the tunnel face crossed the measuring section, preventing to record data when the tunnel face is at distance $2Z_0$ before the section (when the recording frequency was supposed to be equal to 1-2 measures/day – *cfr.* Tab. 2-7) and so to completely

observe the advancing tunnel effects. In some cases, similar problems in respecting the designed measures frequency have been observed even in the range ($2Z_0 - 5Z_0$) of tunnel-section distance, when 1-2 measures/week have been planned to be recorded. As matter of fact, after the tunnel passed distance $2Z_0$ from the sections, for sections AT01 up to AT21 the measures frequency has been respected whereas for AT22 up to AT30 sections not any data was collected. Observing how for the first 24 sections (AT01 – AT22) the maximum settlements have been measured even beyond the distance $2Z_0$ between the tunnel face and the sections, doubts about the settlements reached their maximum value for sections AT22 to AT30 are then reasonable.

Fig.3-10 and Fig.3-11 show informations about the maximum measured displacements measured for each section, the related distance between the sections and the tunnel face location and the time, as number of days after the tunnel underpassed the sections. The same informations are resumed in Tab.3-3.

Looking at the graphs of Fig.3-10, three different zones can be indentified:

- zone A: sections from AT01 (km 0 + 299.8) to AT09 (km 0 + 414.9)
- zone B: sections from AT10 (km 0 + 429.2) to AT30 (km 0 + 591.7)
- zone C: sections from AT31 (km 0 + 608.8) to AT42 (km 0 + 727.7).

Zone A includes sections from AT01 to AT09 installed along Via Piedigrotta between the tunnel starting point and Piazza Eritrea. They measured the maximum settlements, reached at the maximum distance (compared to the other two zones) between the tunnel face and the sections (Fig.3-10_b). All sections measured from 10 mm up to 15 mm settlements saving section AT04 unreasonably measuring 42 mm displacements, sections AT01 and SP01 respectively 6 and 23 m away from the tunnel starting point, which probably did not experience their maximum displacements since they didn't suffer the tunnelling effects for the whole $2Z_0$ meters before them. A part of these three sections the average displacement in zone A is about 13 mm while the maximum is 15 mm measured by section AT08 (Fig.3-10_a). As Fig.3-10_b and Fig.3-10_c show, the maximum displacements have been measured mostly within the first 20 days (except for sections AT01 and AT04 whose displacements increased until 66 and 46 days after tunnel underpassed

them) and between 50 m and 100 m after the tunnel face crossed the sections (saving section AT01 which measured the maximum displacement 236 m after the tunnel underpassed it), farther than distance $2Z_0$ inside which, basing on the design monitoring plan, the maximum settlement was supposed to be reached.

Zone B including sections from AT10 to AT30 features lower maximum displacements (on average 6 mm) reached on average 13 days after the tunnel underpassed the sections, and shorter distances between the tunnel face and the sections related to the measured maximum displacements (about 38 m, similar to the expected $2Z_0$).

Zone C including sections from AT31 to AT42, features the smallest maximum displacements (on average 3 mm) reached 4 days and 18 m after the tunnel underpassed them. Basing on the last update on August the 31st when the tunnel face was at km (0 + 709.00), it could be reasonable to think that the maximum displacements didn't have time to totally develop for some of those sections, because of the short distance between some measuring sections and the last updated tunnel face location: as matter of fact, the tunnel face on August the 31st is located not more than 7 m beyond sections SC01, AT40, AT41 and AT42.

Synthesizing, looking at the face locations related to the maximum displacements than the measuring sections locations (Fig.3-10_b), in zones B and C, for sections AT10 up to AT42, the measured maximum displacements is always reached within 50 m after the tunnel face underpassed the sections (on average 30 m), saving section AT17 measuring the maximum displacements 112 m away the tunnel face (Fig.3-11_a). Moreover, looking at Fig.3-10_c it is clear how the maximum displacements are always reached within 30 days (on average 10 days) after the tunnel face underpassed the sections, saving sections AT01 and AT04 (zone A) and AT17 (zone B) whose displacements increased until 66, 46 and 67 days after the tunnel underpassed them. The same information is represented in Fig.3-11_b showing how in most of the cases the maximum displacements are reached within 20 days after the tunnel passed the sections.

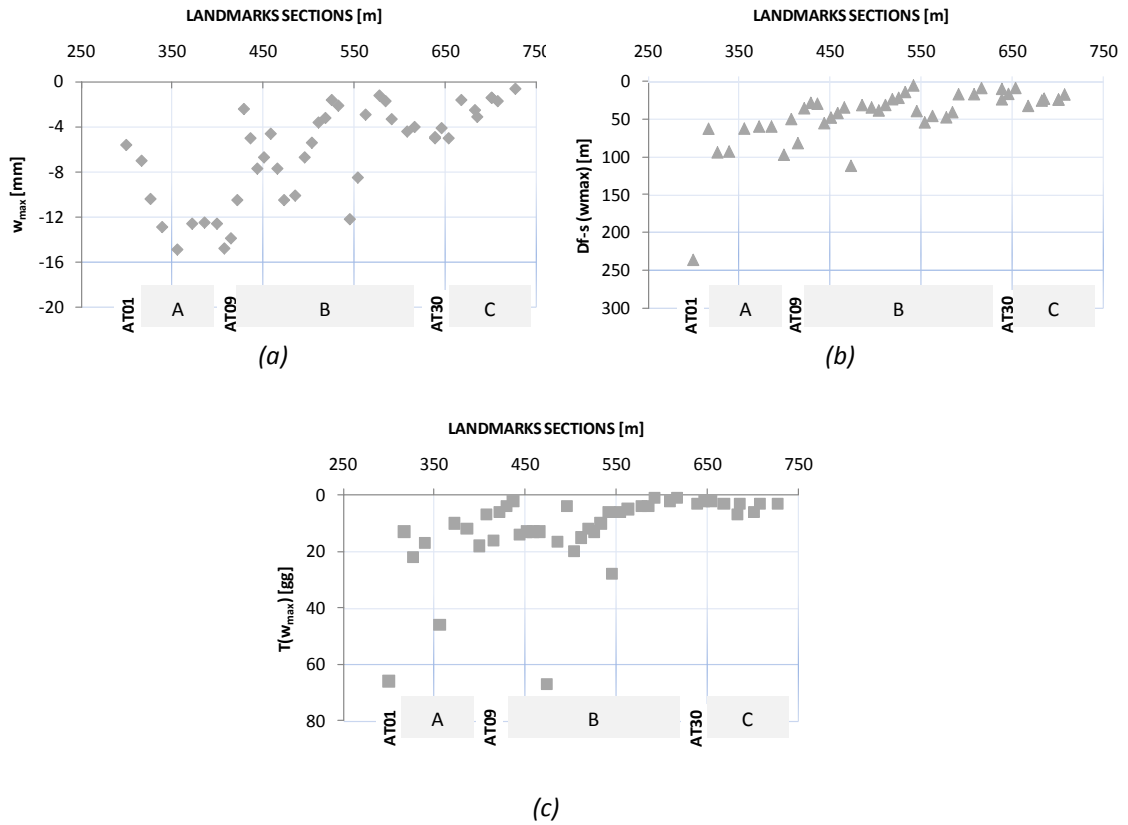


Fig.3-10. Landmarks w_{max} (a), Landmarks $T(w_{max})$ (b), Landmarks $D_{f-s}(w_{max})$ (c)

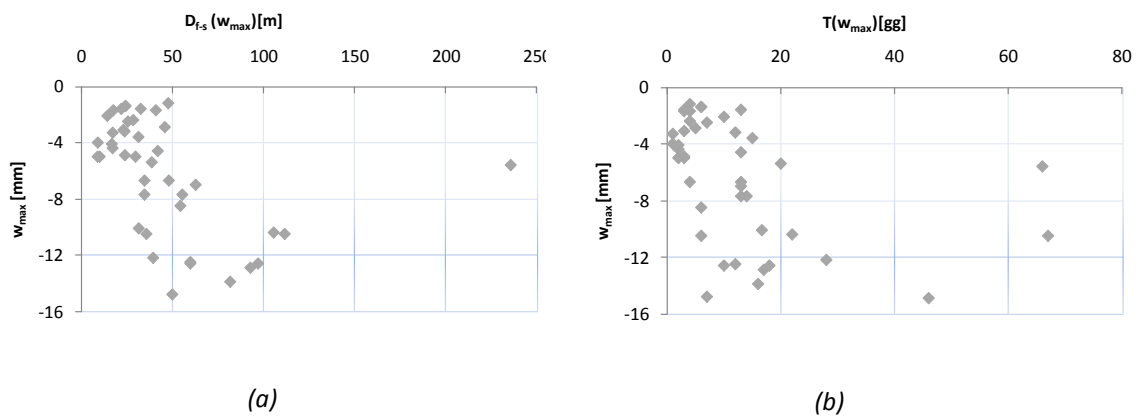


Fig.3-11. Landmarks w_{max} - $D_{f-s}(w_{max})$ (a), Landmarks w_{max} - $T(w_{max})$ (b)

In Fig.3-10 displacement measured by section AT24 was deleted since it can be easily related to a particular event occurred on June the 28th when a hole in Largo

Torretta appeared. This singular event leads to about 62 mm settlements measured on the ground surface as Tab.3-3 reports and Fig.3-12 shows.

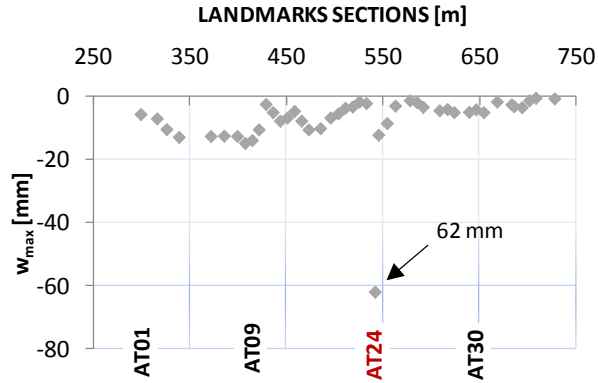


Fig.3-12. Vertical displacements measure by landmarks sections

ID	w_{max} [mm]	$D_{f-s}(w_{max})$ [m]	$T(w_{max})$ [days]	ID	w_{max} [mm]	$D_{f-s}(w_{max})$ [m]	$T(w_{max})$ [days]	ID	w_{max} [mm]	$D_{f-s}(w_{max})$ [m]	$T(w_{max})$ [days]
AT01	-5.60	236	66	AT09	-13.90	82	16	SC01	-10.10	32	17
SP01	-7.00	63	13	AT10	-10.50	36	6	AT18	-6.70	35	4
AT02	-10.40	106	22	AT11	-2.40	29	4	AT19	-5.40	39	20
AT03	-12.90	93	17	AT12	-5.00	30	2	AT20	-3.60	31	15
AT04	-42.40	180	46	AT13	-7.70	56	14	AT21	-3.20	24	12
AT05	-12.60	60	10	AT14	-6.70	48	13	AT22	-1.60	22	13
AT06	-12.50	60	12	AT15	-4.60	42	13	AT23	-2.10	14	10
AT07	-12.60	97	18	AT16	-7.70	35	13	AT24	-62.30	6	6
AT08	-14.80	50	7	AT17	-10.50	112	67	AT25	-12.20	40	28

ID	w_{max} [mm]	$D_{f-s}(w_{max})$ [m]	$T(w_{max})$ [days]	ID	w_{max} [mm]	$D_{f-s}(w_{max})$ [m]	$T(w_{max})$ [days]
AT26	-8.50	55	6	AT35	-4.10	17	2
AT27	-2.90	46	5	AT36	-5.00	9	2
AT28	-1.20	48	4	AT37	-1.60	33	3
AT29	-1.70	41	4	AT38	-3.10	23	3
AT30	-3.30	17	1	AT39	-2.50	26	7
AT31	-4.40	17	2	SP02	-3.40	15	3
AT32	-4.00	9	1	AT40	-1.20	7	6
AT33	-5.00	10	3	AT41	-0.80	-1	3
AT34	-4.90	24	3	AT42	-0.60	-19	3

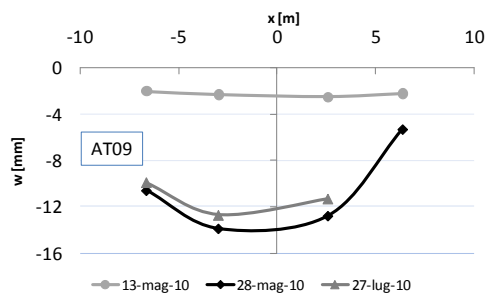
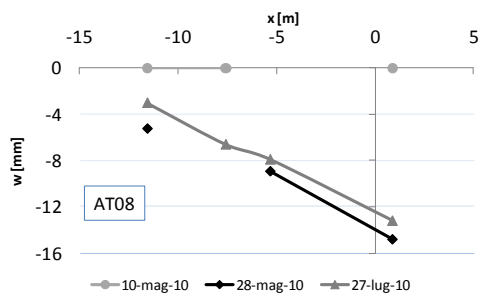
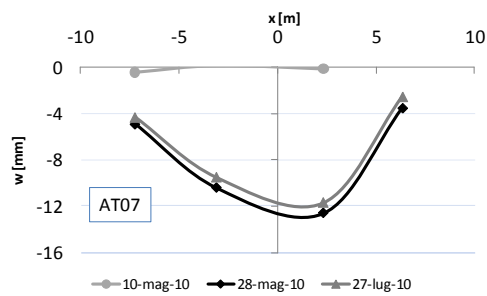
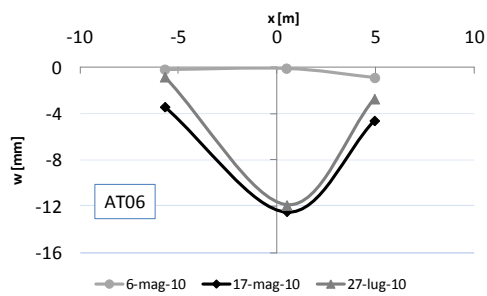
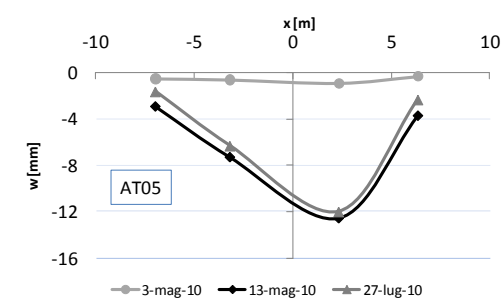
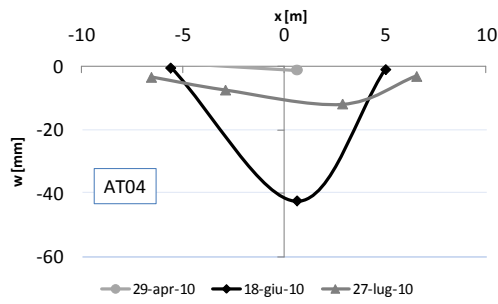
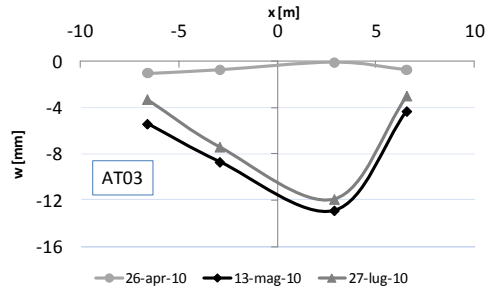
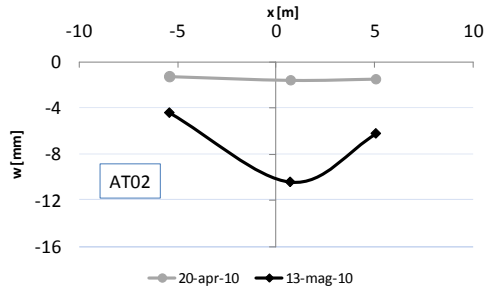
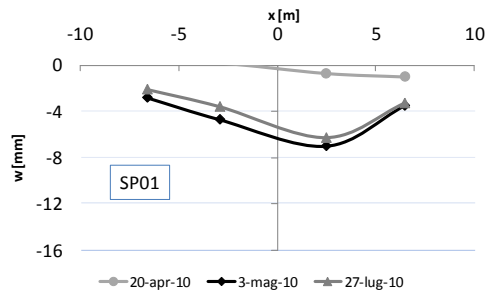
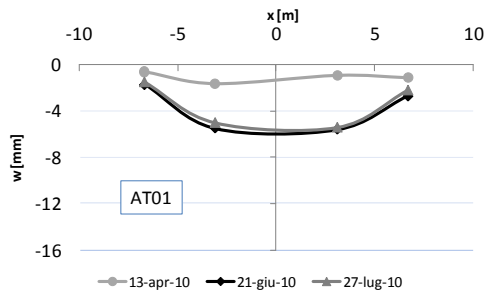
Tab.3-3. Maximum displacements of monitoring sections

Graphs in Fig.3-13 show the transversal deformed shapes obtained by ground landmarks measurements concerning the initial reading (referred to the tunnelling starting operations on April the 7th), the maximum settlement and last recorded measure. Looking at the maximum measured settlement, the measuring sections can be collected into three main groups (Tab.3-4), together with two different singular special cases (sections AT04 and AT24, measuring remarkable settlement if compared with the others sections). Looking at the collected data of face and grouting pressure the decreasing maximum settlements along Via Piedigrotta, going to Municipio Station, could be easily related to the increasing applied pressures (Fig.3-18 and Fig.3-19).

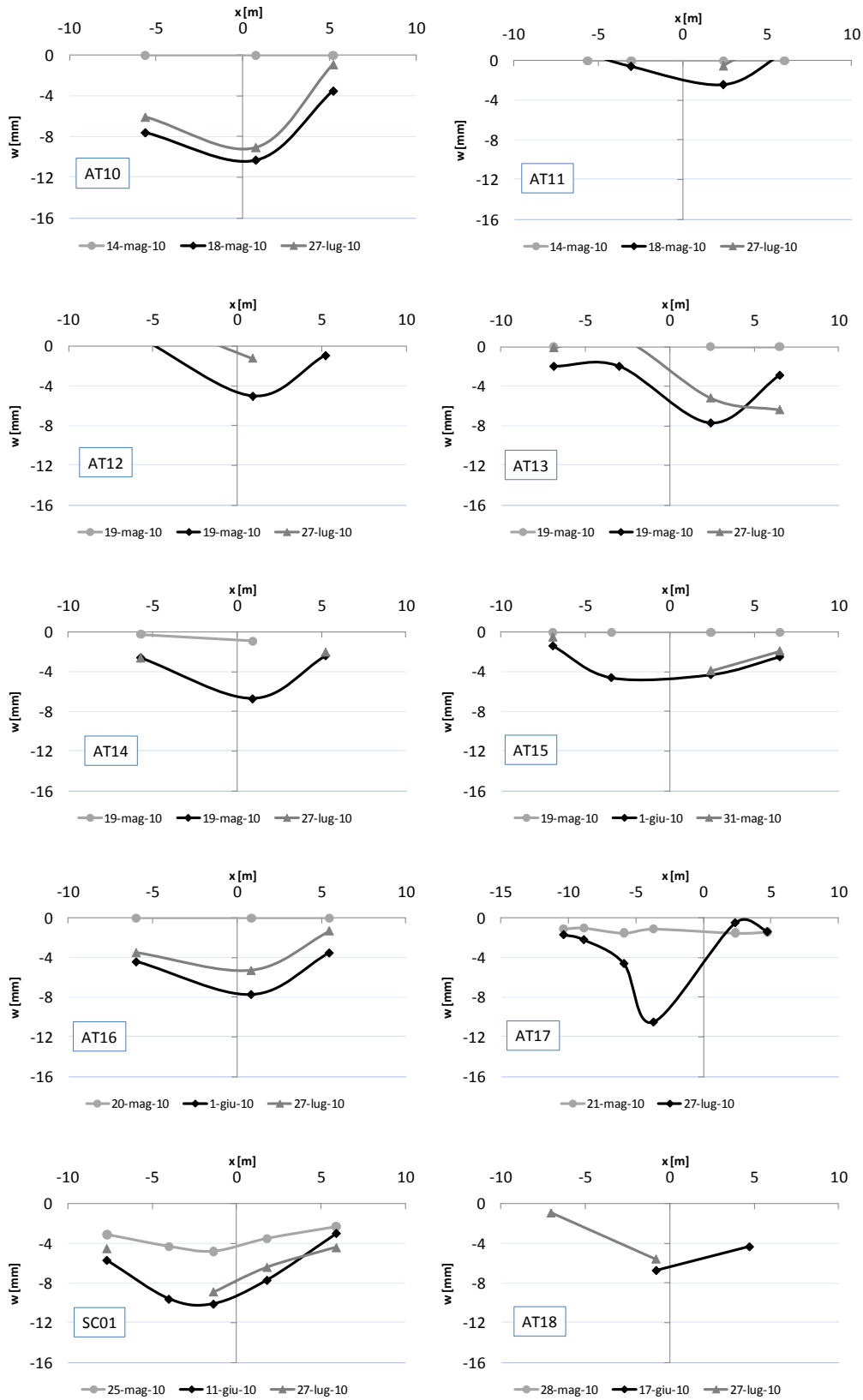
Fig.3-14 and Fig.3-15 show the transversal and longitudinal displacements curves for the three identified groups whereas Fig.3-17 shows the maximum longitudinal settlements contour.

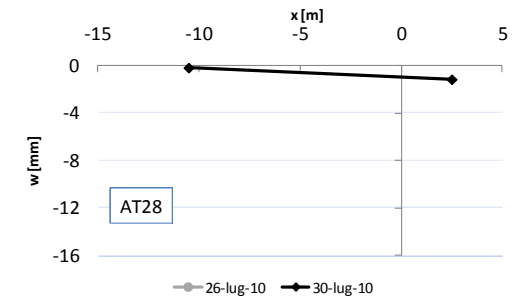
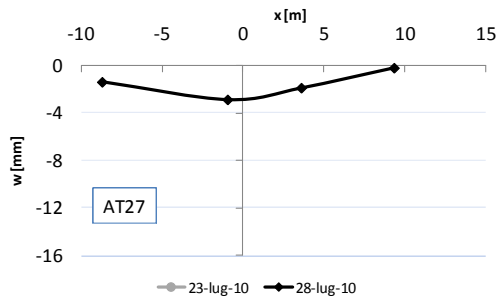
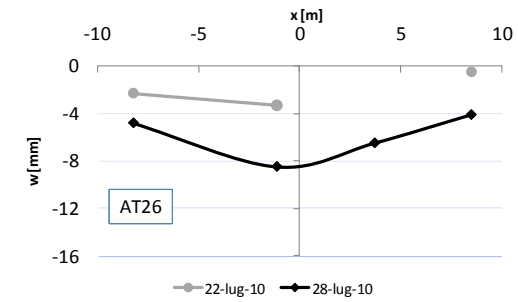
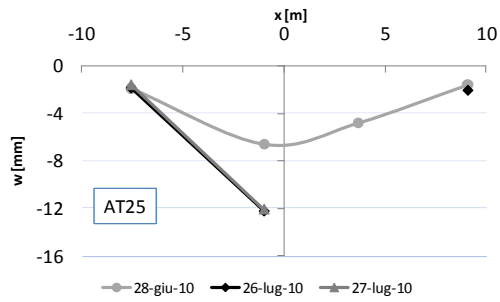
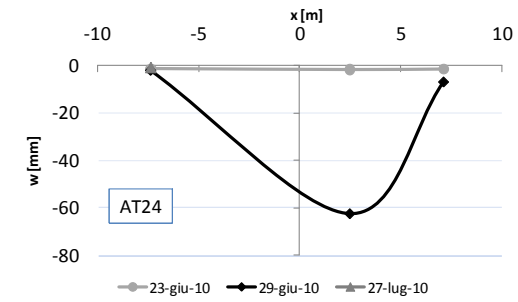
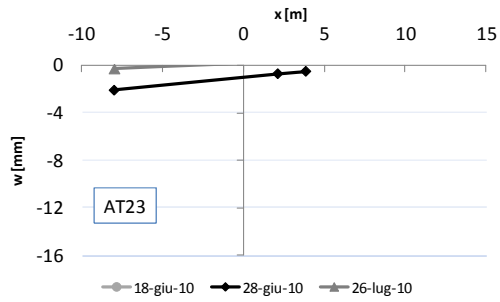
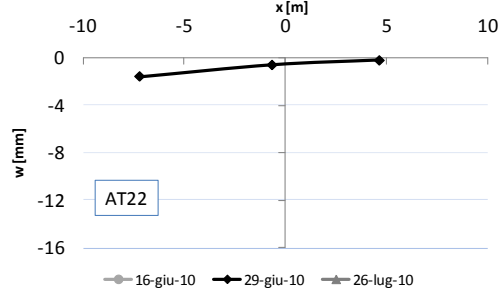
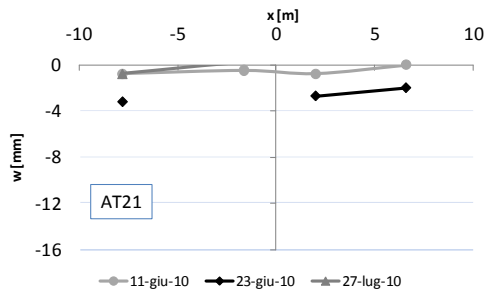
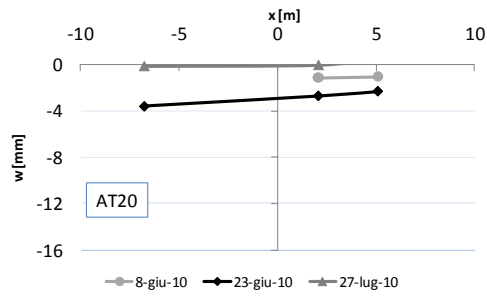
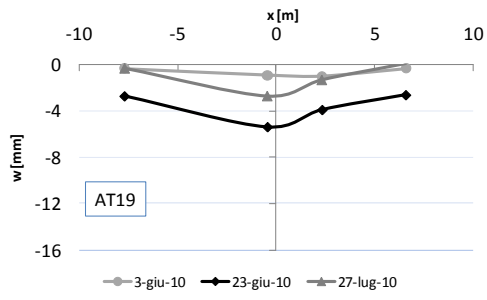
GROUP	ID	w_{max} [mm]
1	AT01 – SP01 (zone A)	5 ÷ 8
	AT12 – AT16 (zone B)	
	AT18 – AT19 (zone B)	
	AT26 (zone B)	
2	AT02 – AT10 (zone A)	8 ÷ 14
	AT17 (zone B)	
	AT25 (zone B)	
	SC01 (zone B)	
3	AT11 (zone B)	≤ 5
	AT20 – AT23 (zone B)	
	AT27 – AT42 (zone B - C)	
SINGULAR CASES	AT04 (zone A)	42.40
	AT24 (zone B)	62.30

Tab.3-4. Maximum displacements of monitoring sections

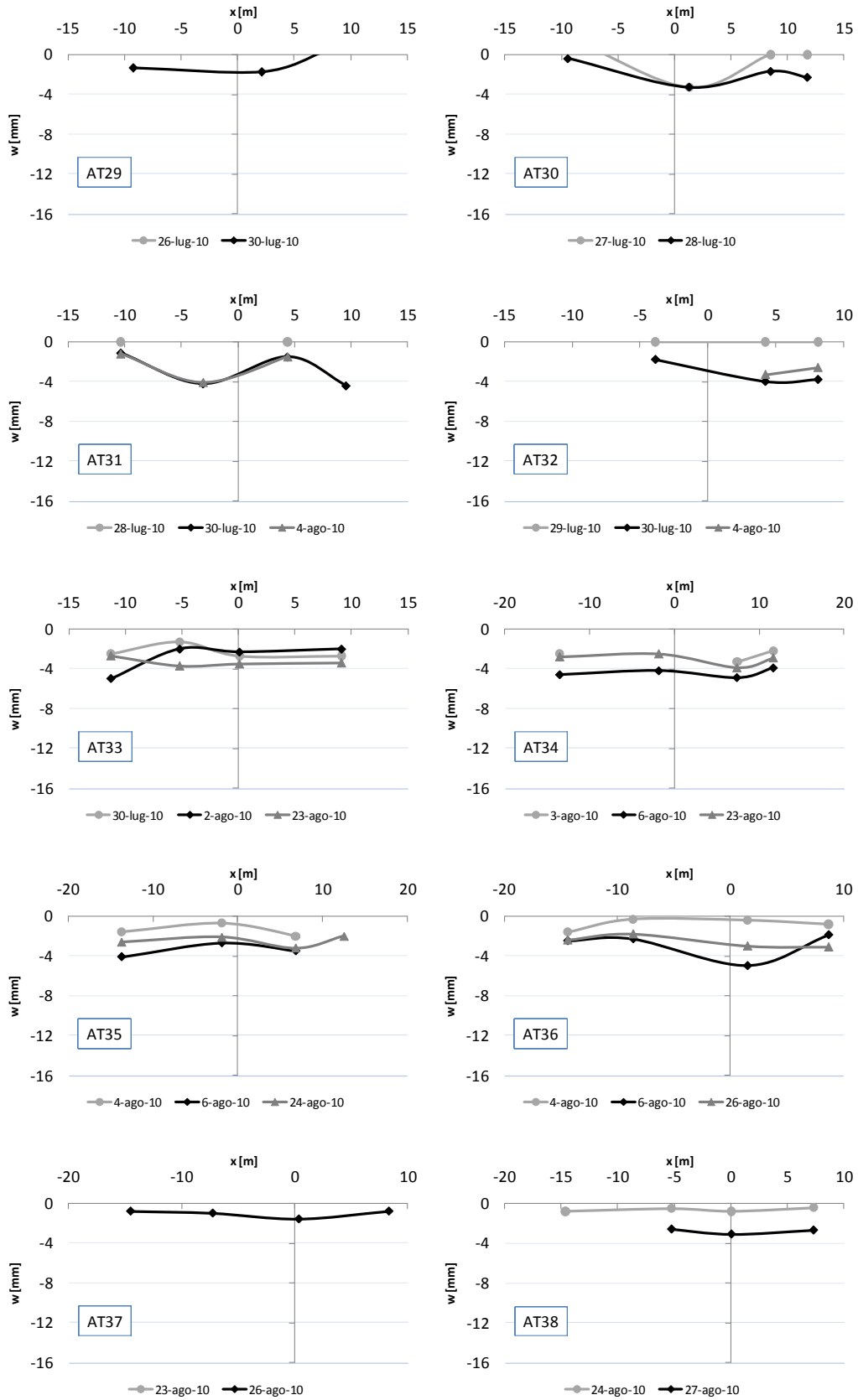


LINE 6: ANALYSIS OF MONITORING DATA





LINE 6: ANALYSIS OF MONITORING DATA



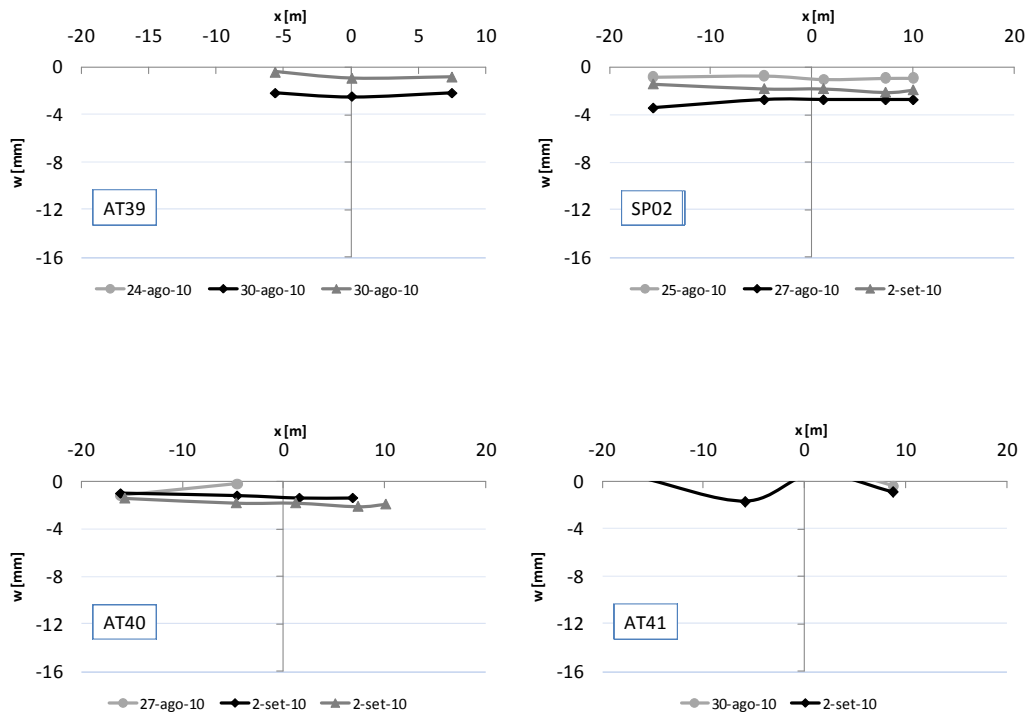


Fig.3-13. Topographic landmarks on the ground surface: measured deformed shapes

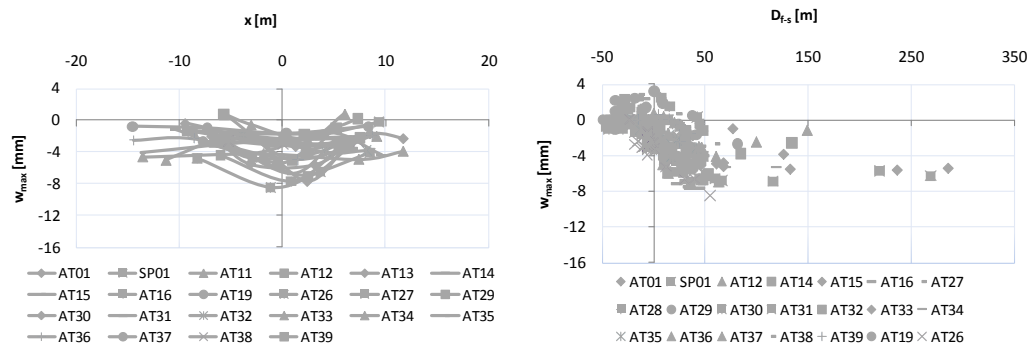


Fig.3-14. Group 1: Transversal (a) and longitudinal (b) displacements curves: $w_{max} = 5 \div 8$ m

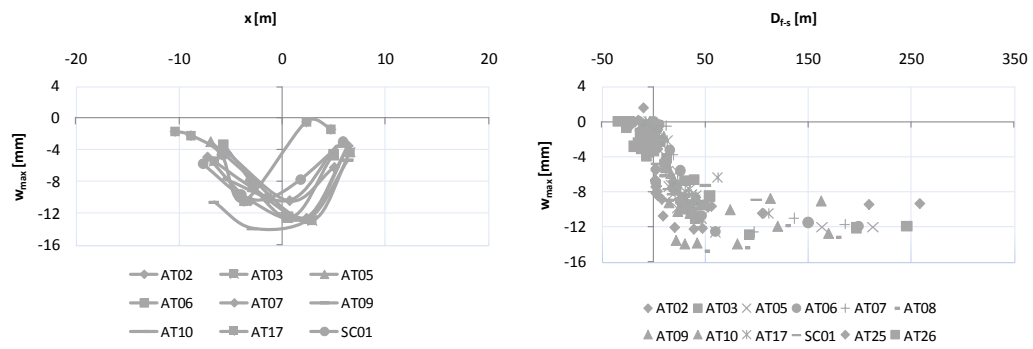


Fig.3-15. Group 2: Transversal (a) and longitudinal (b) displacements curves: $w_{max} = 8 \div 14$ mm

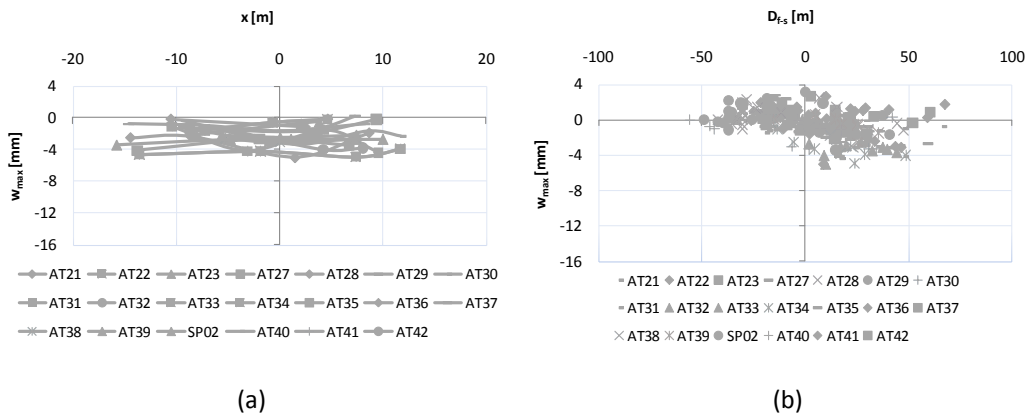


Fig.3-16. Group 3: Transversal (a) and longitudinal (b) displacements curves: $w_{max} \leq 5 \text{ mm}$

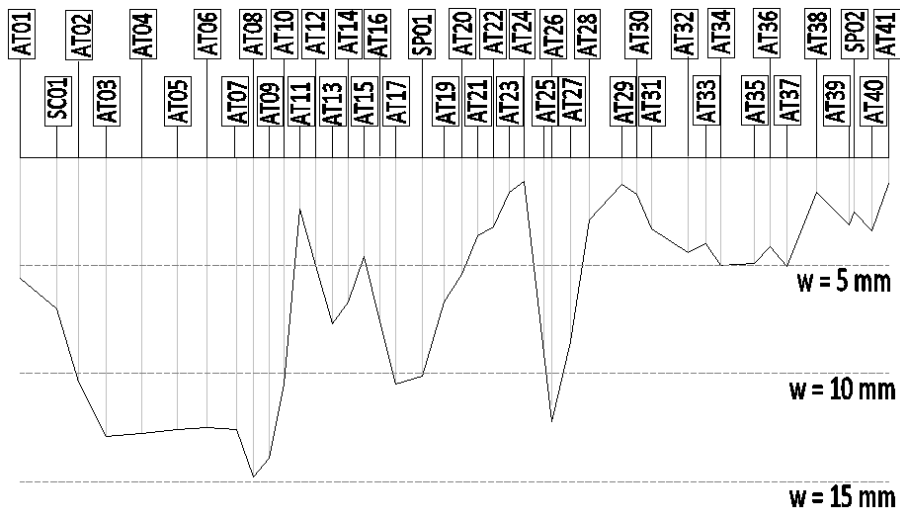


Fig.3-17. Ground surface maximum settlements longitudinal contour

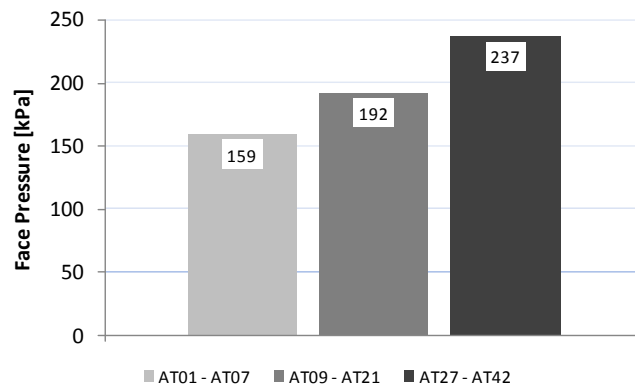


Fig.3-18. Measured front pressure

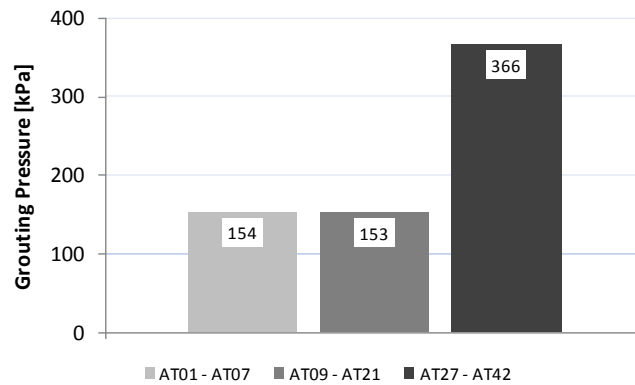


Fig.3-19. Measured grouting pressure

Looking at the measured displacements in the longitudinal direction at the tunnel axis, Fig.3-20 shows their trend with the tunnel-section distance. Excluding sections not reaching the maximum displacements because too close to the tunnel face (zone C), Fig.3-21 shows the percentage of maximum displacements reached at the tunnel front and at the passage of the shield tail (two times the tunnel depth from the sections). The average values are respectively 22% and 80%, according to the Craig & Muir Wood (1978) indications for sand below the water table (Chapter 1_Tab.1.1).

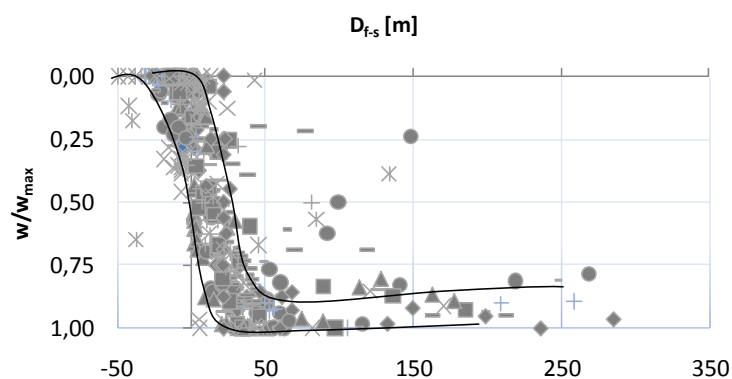


Fig.3-20. Settlements trend with the tunnel-section distance

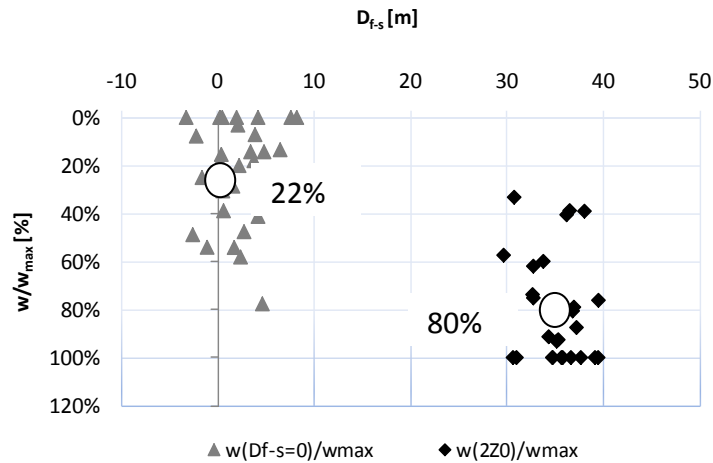


Fig.3-21. Percentage of maximum settlements reached at the tunnel face and $2Z_0$ away from it

3.3.3. Landmarks on buildings

As described in Chapter 2, 29 buildings to the tunnel track side all along Via Piedigrotta, Riviera di Chiaia, Largo Torretta, Piazza Repubblica and Via C. Cucca, have been instrumented with landmarks on their facades. In the table below the number of landmarks for each building are related and in the following pages, collected monitoring data up the August the 31st will be discuss.

Tab.3-6 resumes monitored buildings main features (when available) such as brick work or concrete building, length, height, number of floors and foundations depth.

Basing on the last monitoring update on August the 31st, Tab.3-7 and Tab.3-8 relate informations about the zero and the last reading for each building and their maximum measured settlements.

Address	Building n°	Number of Installed landmarks	Building n°	Number of Installed landmarks
Via Piedigrotta	7	5	57	3
	11	10	60	10
	16	4	63	14
	19	6	65	5
	23	9	67	3
	30	6	93	6
	34	12	96	3
	54	5	98	3
Riviera di Chiaia	23	10	50	2
	33	5	53	3
	36	5	57	2
	44	4	61	3
	48	2	66	8
Largo Torretta	19	9	-	-
P.za della Repubblica	2	5	-	-
Via C. Cucca	3	5	-	-

Tab.3-5. Landmarks on buildings

In Fig.3-22 the buildings 'maximum settlements are related to the distance between the tunnel face and the building landmark measuring it; the maximum measured displacements is about 8 mm for building n°23 in Riviera di Chiaia, reached when the tunnel was about 46 m beyond it (Tab.3-7 and Tab.3-8). The same figure shows the maximum settlements reached mostly within 100 meters between the tunnel face and the buildings, saving building civ.60 along Via Piedigrotta reaching its maximum displacement 145 m after the tunnel underpassed it. Fig.3-23 and Fig.3-24 show the landmarks displacements with the relative tunnel section distance (the black line concerns the landmark measuring the maximum settlement for each building) and the buildings deformed shape when the maximum displacements was reached, as indicated in Tab.3-7 and Tab.3-8.

Fig.3-25 shows monitored buildings maximum displacements longitudinal contour. The measured settlements are approximately 5 mm, always lower than the ground surface ones and almost uniform all along the tunnel track, but with the same settlements decrease as shown by landmarks on ground surface, nearness buildings 93, 96, 98, 11 and 7 next to Piazza Eritrea (Fig.3-26).

BUILDINGS ID	FLOORS [N°]	MATERIAL	FOUDATION	FOUDATION DEPTH [m]	LENGTH [m]	HEIGHT [m]	
VIA PIEDIGROTTA	34	9+2	Concrete	Piles	-7	36.6	32.5
	30	6	Masonry	Masonry	-5	30	25
	23-26	5	Masonry	Masonry	-6	43	25
	16	6	Masonry	Masonry	-2	15	25
	11	8	Concrete	Piles	-3	38	32
	10	1	Masonry	Masonry	-	9	8
	7	2	Masonry	Masonry	-5	20	10.5
	19	3	Masonry	-	-	22	14
	60	3	Masonry	Masonry	-5	16	15
	63	3	Masonry	Masonry	-	51	16
	65	4	Masonry	Masonry	-	20	15
	67	11	Concrete	Piles	-	31	37
	90 - 93	4	Masonry	Masonry	-2	13	19
	96 - 101	4	Masonry	Arch – Wood Steel	-2	26	12
RIVIERA DI CHIAIA	23	4	Masonry	Masonry	-	32.6	12
	33	3	Masonry	Masonry	-2	27.7	9
	36	4	Masonry	Masonry	-2	33	12
	40 - 44	4	Masonry	Masonry	-2	31.5	12
	48	8	Concrete	Piles	-4	18.8	24
	50	4	Masonry	Masonry	-5	11.6	12
	53	5	Masonry	Masonry	-3.5	16.2	15
	57	5	Masonry	Masonry	-3.5	19	15
	61	5	Masonry	Masonry	-3.5	18.6	15
	66	3	Masonry	Masonry	-3.5	50	9
P.za REPUBBLICA	57	5	Masonry	Arch – Wood Steel	-3	32.6	9
L.go TORRETTA	61	5	Masonry	Masonry	-3	27.7	18
Via C. CUCCA	66	3	Masonry	Masonry	-	8.8	9

Tab.3-6. Buildings main features

ID	Zero reading	Last reading	w _{max} [mm]	D _{f-s} [m]	Date (w _{max})	
VIA PIEDIGROTTA	57	30-Mar-10	17-May-10	-3.80	21.6	12-apr-10
	60	30-Mar-10	17-May-10	-2.90	145.3	13-mag-10
	63	30-Mar-10	17-May-10	-4.80	113.9	13-mag-10
	65	30-Mar-10	17-May-10	-6.60	83.6	14-mag-10
	67	30-Mar-10	17-May-10	-3.90	62.7	17-mag-10
	93	30-Mar-10	17-May-10	-4.90	12.9	14-mag-10
	96	30-Mar-10	17-May-10	-1.20	45.5	26-mag-10
	98	30-Mar-10	17-May-10	-1.20	41.4	26-mag-10
	34	30-Mar-10	26-May-10	-3.70	20.6	12-apr-10
	30	30-Mar-10	13-May-10	-5.70	45.2	29-apr-10
	23	30-Mar-10	17-May-10	-5.20	75.7	14-mag-10
	16	30-Mar-10	17-May-10	-5.40	56.5	17-mag-10
	11	30-Mar-10	26-May-10	-5.80	47.3	18-mag-10
	7	30-Mar-10	26-May-10	-1.60	50.2	24-mag-10
	19	30-Mar-10	26-May-10	-2.80	26.1	25-mag-10

Tab.3-7. Buildings along Via Piedigrotta: zero and last reading and maximum measured settlements

ID	Zero reading	Last reading	w _{max} [mm]	D _{f-s} [m]	Date	
RIVIERA DI CHIAIA	23	19-May-10	27-Jul-10	-7.70	45.60	14-Jun-10
	33	27-Jul-10	26-May-10	-4.80	31.8	28-Jun-10
	36	26-May-10	26-May-10	-5.40	36.11	28-Jul-10
	44	17-Jun-10	05-Aug-10	-4.60	63.5	03-Aug-10
	48	23-Jul-10	31-Aug-10	-4.80	98.6	31-Aug-10
	50	29-Jul-10	23-Aug-10	-3.50	35.3	06-Aug-10
	53	29-Jul-10	31-Aug-10	-3.60	37.1	24-Aug-10
	57	29-Jul-10	31-Aug-10	-5.20	57.6	30-Aug-10
	61	06-Aug-10	31-Aug-10	-2.40	15.5	27-Aug-10
	66	24-Aug-10	31-Aug-10	-2.80	11.8	27-Aug-10
P.za REPUBBLICA	2	25-Aug-10	30-Jul-10	-2.20	54.1	25-Aug-10
Via C. CUCCA	3	17-Jun-10	17-May-10	-5.30	49.6	14-Jun-10
Largo TORRETTA	19	27-Jul-10	18-May-10	-4.60	41.6	16-Jun-10

Tab.3-8. Buildings along Riviera di Chiaia: zero and last reading and maximum measured settlements

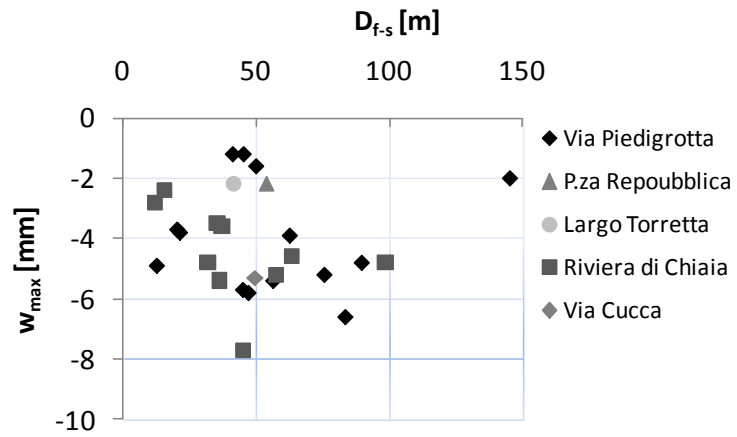
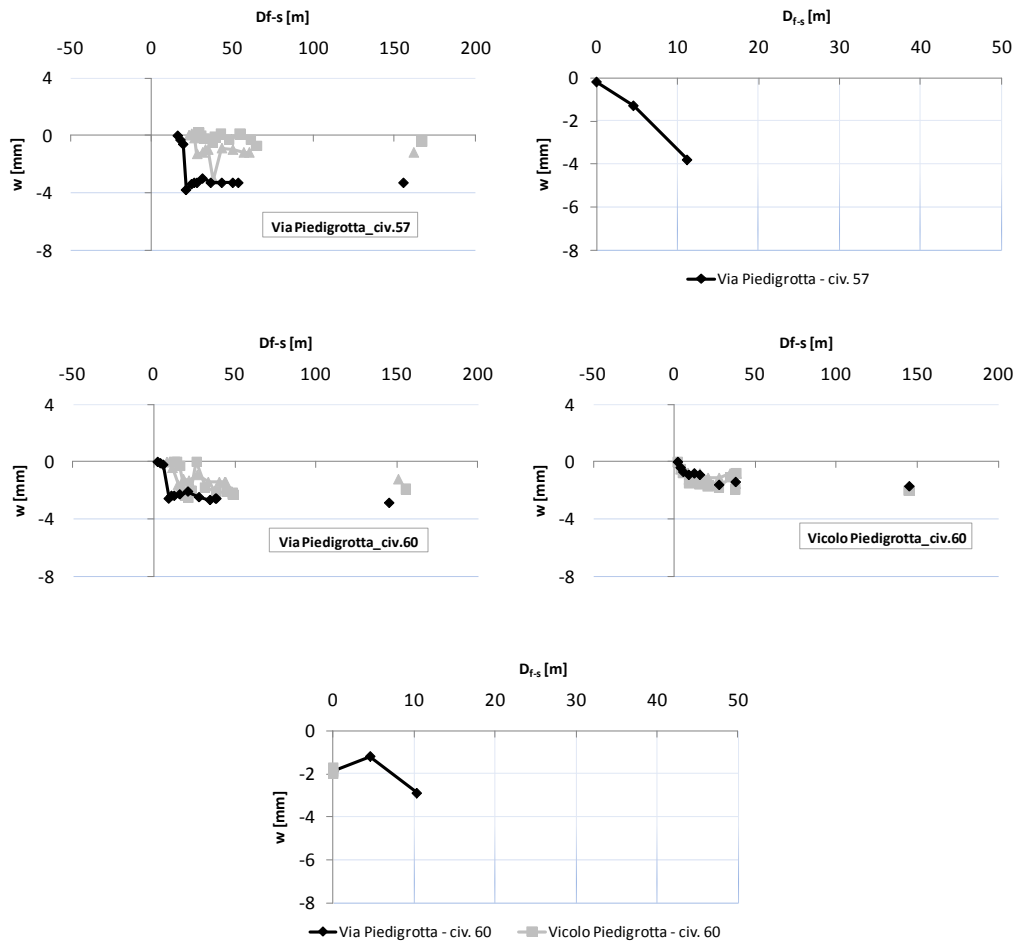
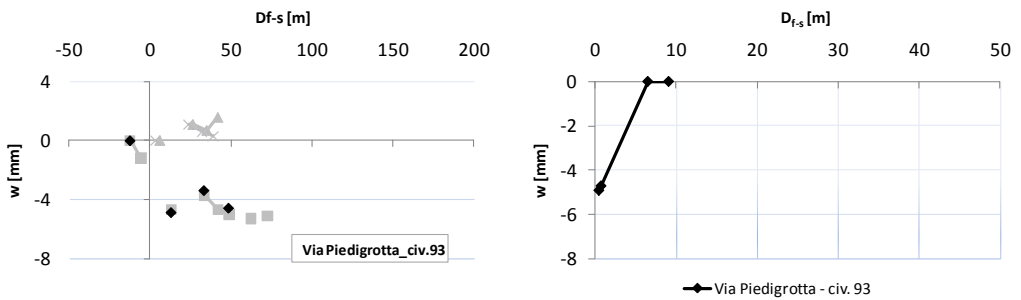
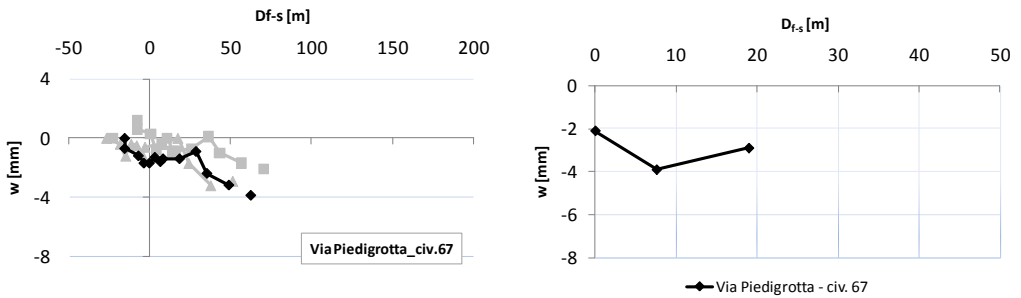
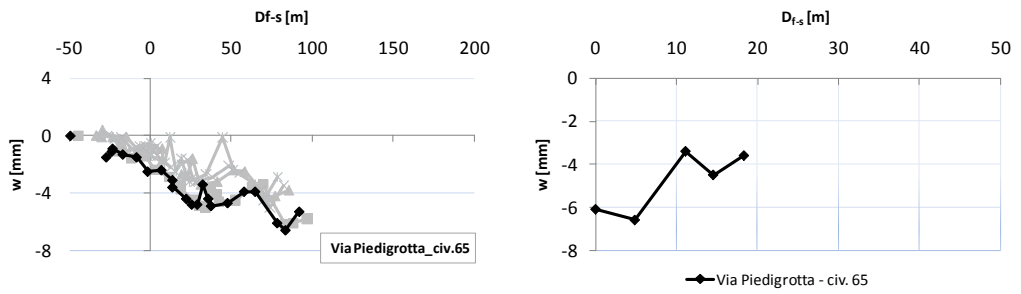
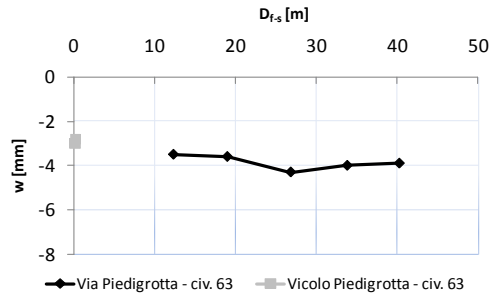
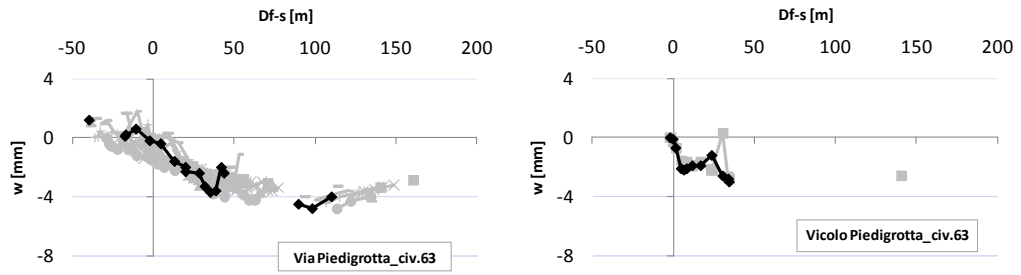
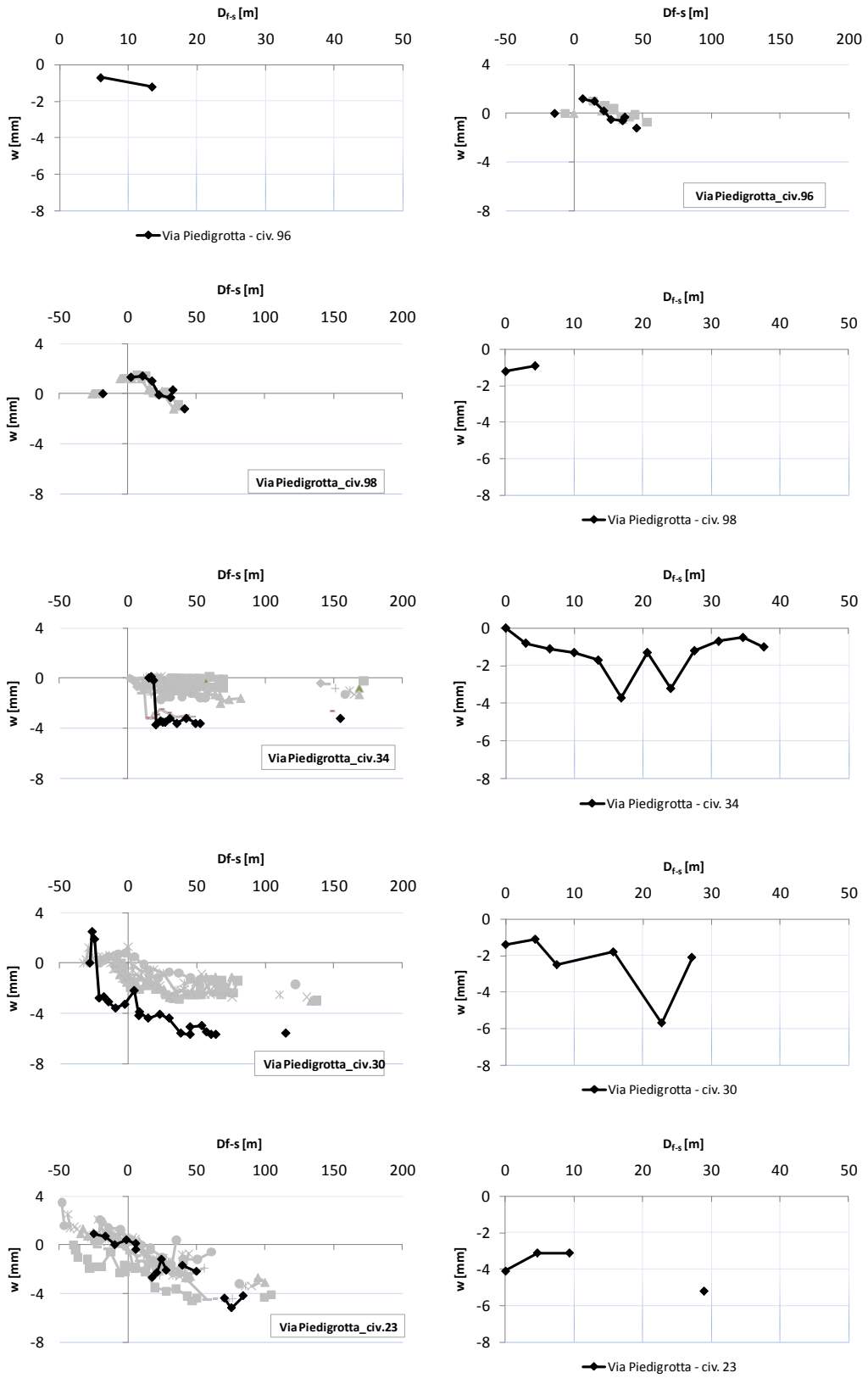


Fig.3-22. Via Piedigrotta: maximum buildings settlements



LINE 6: ANALYSIS OF MONITORING DATA





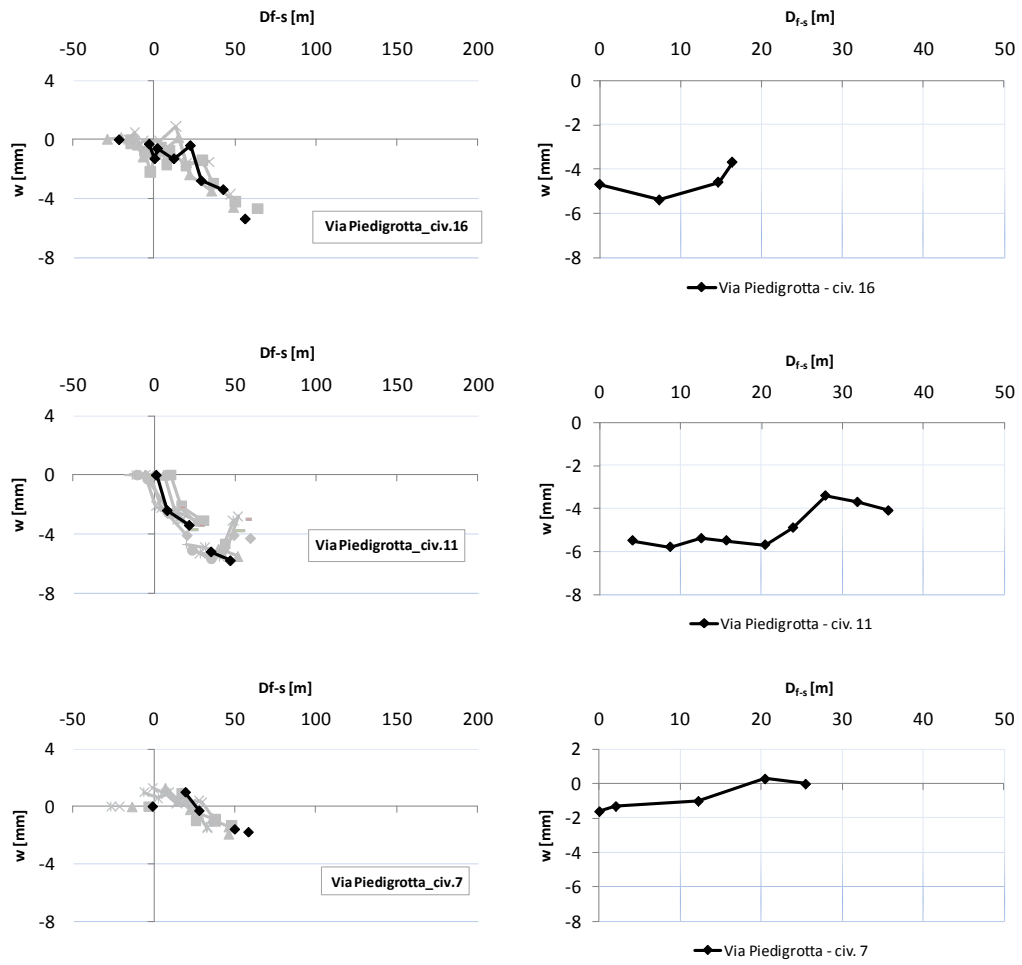
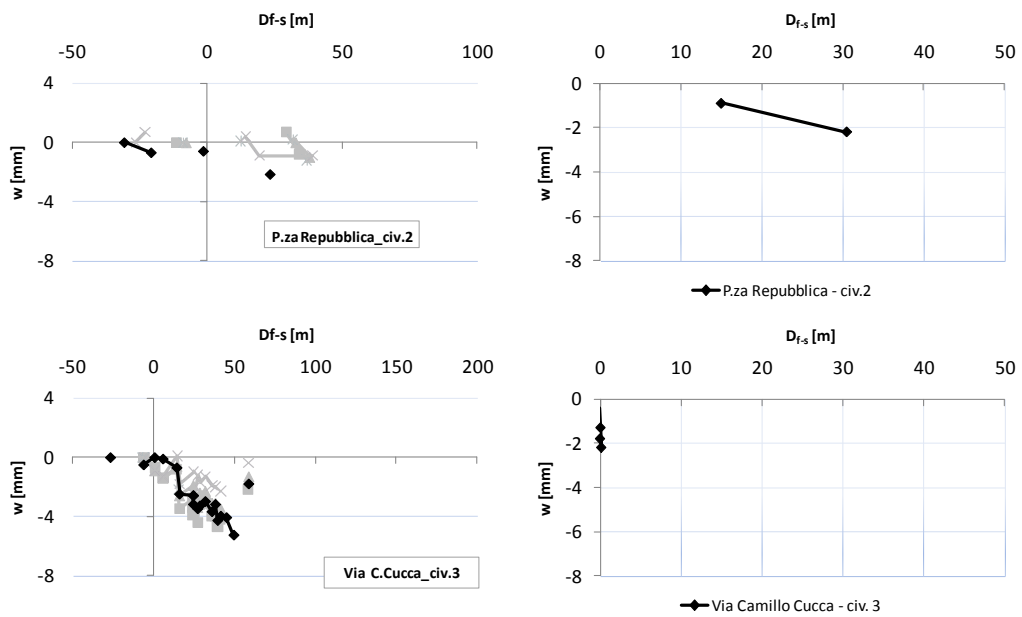
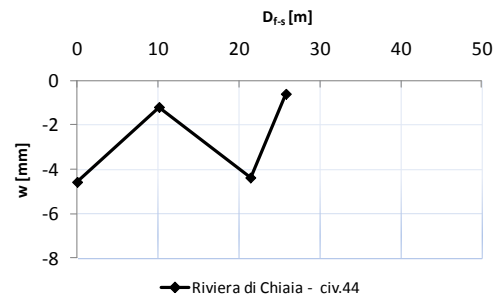
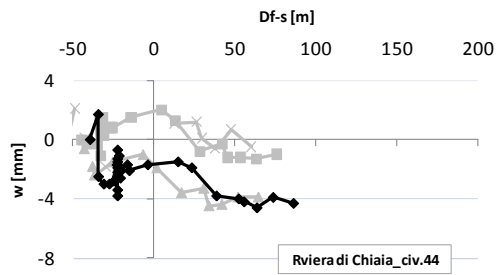
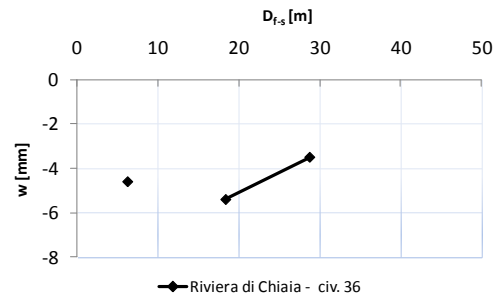
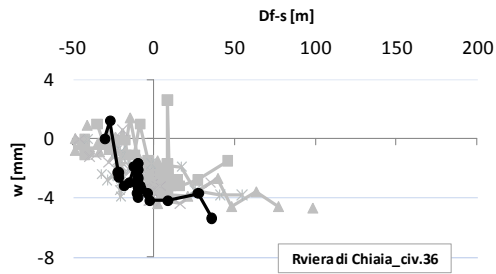
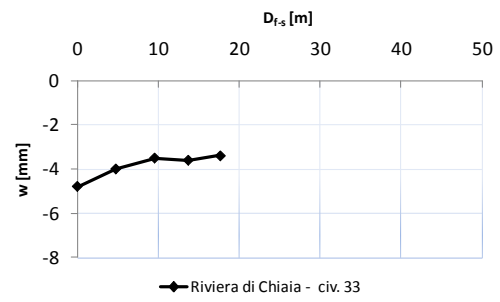
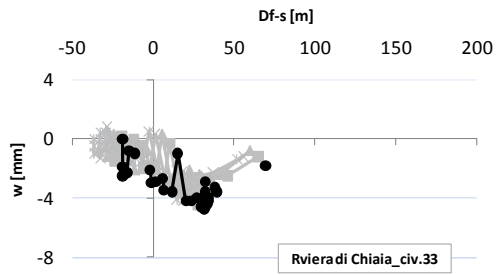
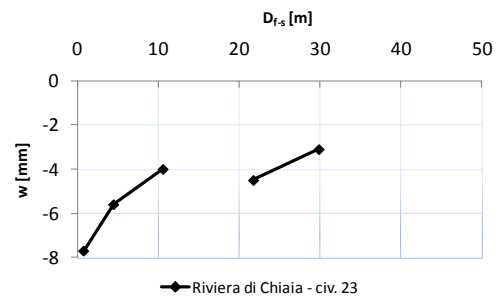
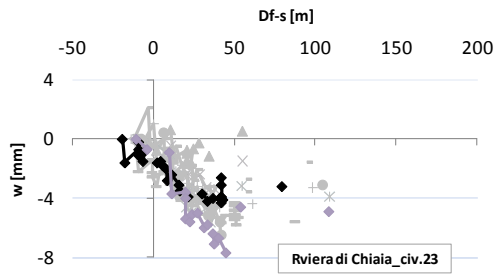
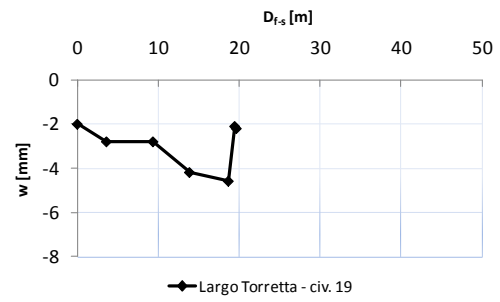
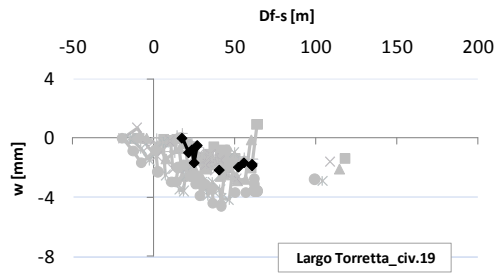
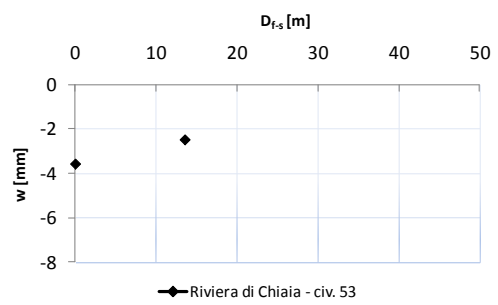
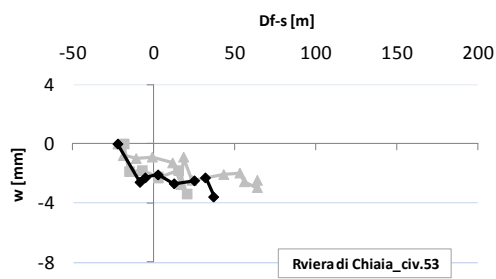
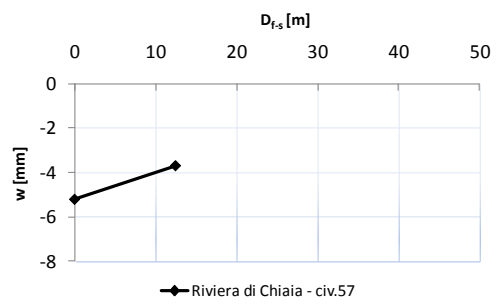
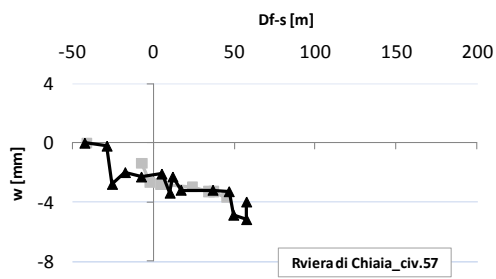
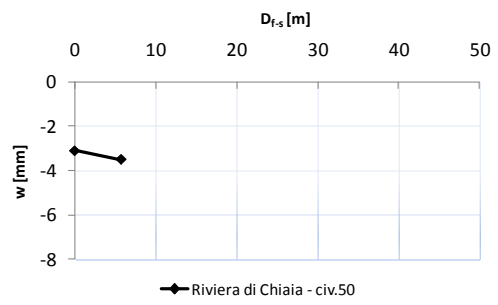
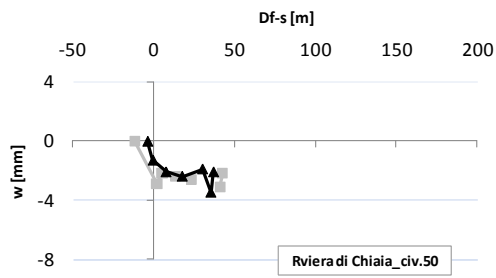
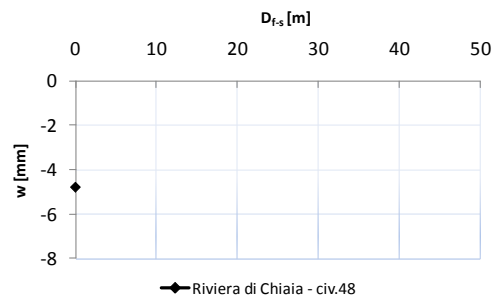
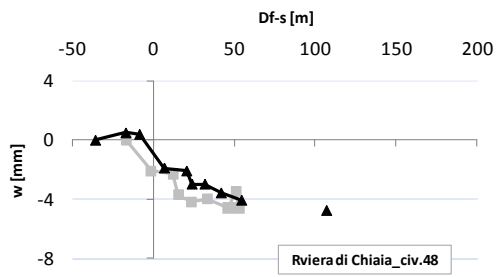


Fig.3-23. Via Piedigrotta: landmarks measured displacements and buildings deformations related to the maximum measured displacement







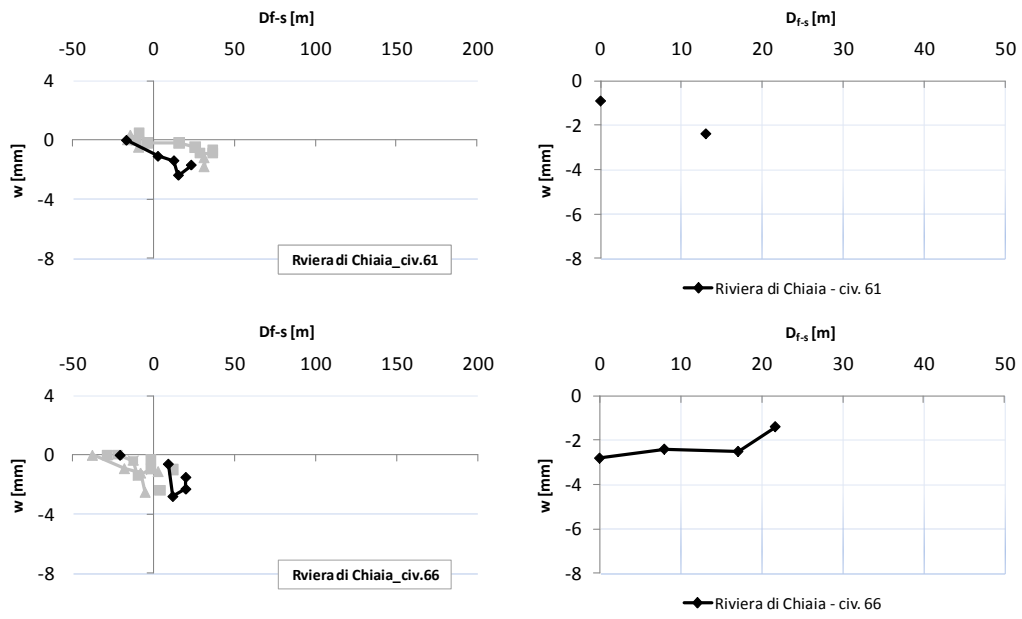


Fig.3-24. P.za Repubblica, Via C. Cucca, L.go Torretta and Riviera di Chiaia: landmarks measured displacements and buildings deformations related to the maximum measured displacement

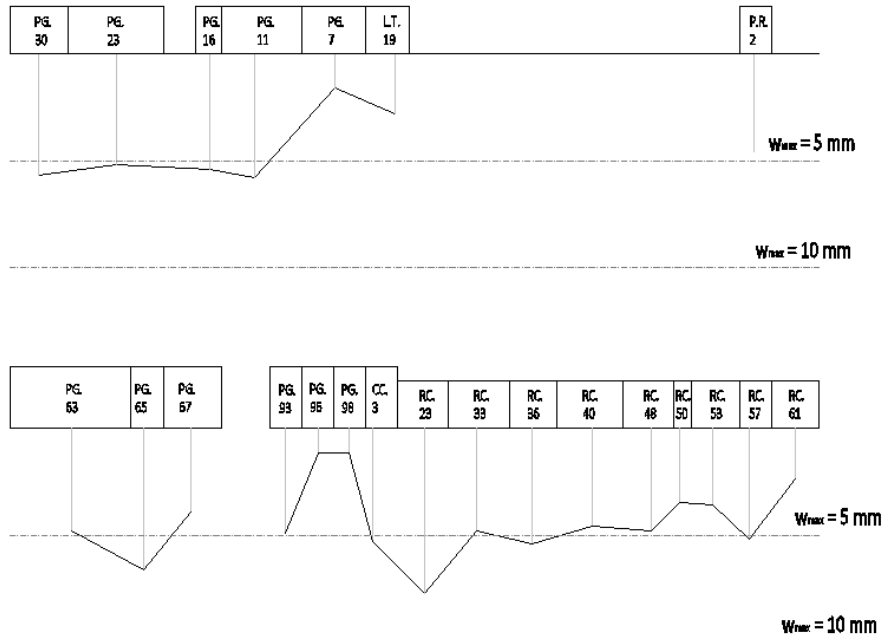


Fig.3-25. Buildings maximum settlements longitudinal contour along Via Piedigrotta and Riviera di Chiaia: sea side (above) and inland side (below)

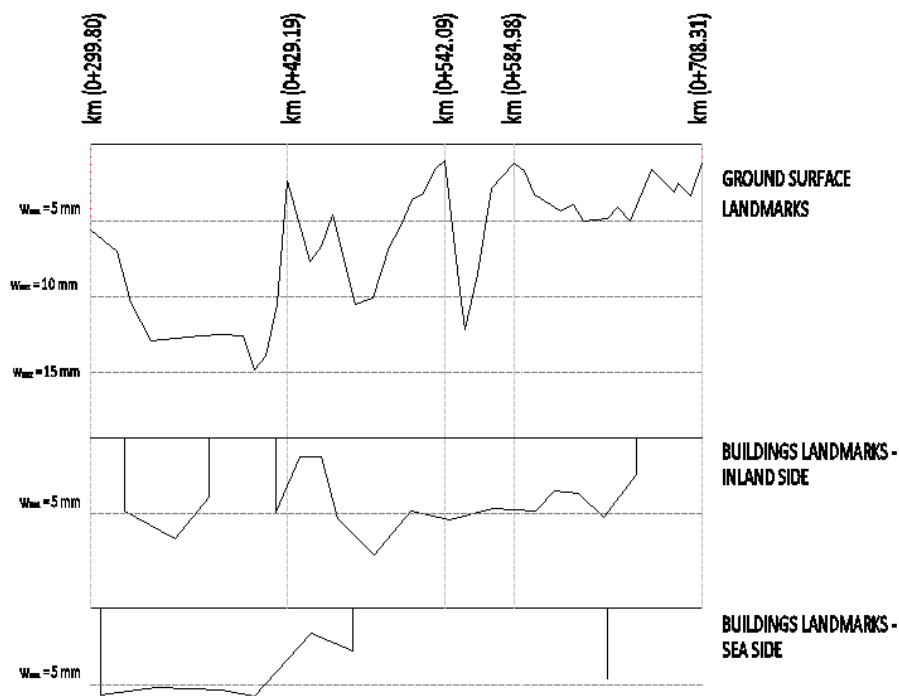


Fig.3-26. Maximum settlements: longitudinal contours for landmarks on ground surface and on buildings facades

On the base of the tunnelling induced displacements and on monitoring collected data, for each building the damage analysis has been done respecting the three level analysis as described in Chapter 1. Results are summarized in Tab.3-9 and Tab.3-10.

After the first level analysis based on calculating the rotation θ and the maximum displacements $S_{v,max}$, for buildings civ.63 along Via Piedigrotta, buildings civ.3 along Via. C. Cucca and civ.23 along Riviera di Chiaia a more detailed evaluation, based on angular distortion $\beta = \Delta/L$ calculation, has been required. For buildings along Via Piedigrotta and Riviera di Chiaia, not any more detailed analysis have been needed, being the maximum angular distortion lower than the maximum admissible value (1/500), whereas for buildings in Via C. Cucca a more advanced definition of the level of damage is required. To carry on this kind of analysis the horizontal deformations are needed; because of the lack of monitoring data offering the horizontal buildings displacements a detailed damage analysis is impossible and on the damage abacus (after Burland, 1995) corresponding to the specific building L/H

value, only the calculation of the limit horizontal strain ε_h for each category of damage, corresponding to the measured deflection ratio Δ/L is possible (Fig.3-27).

1 st STEP ANALYSIS					
BUILDING	$\Theta=\Delta/L$			$S_{v,max}$ [mm]	
	VIA PIEDIGROTTA	57	0.000701	no dam	-3.8
60vp ¹		0.000338	no dam	-2.9	< 10 mm
60		0.000294	no dam	-2.9	< 10 mm
63vp²		0.107407	>1/500	-6	< 10 mm
63		0.000327	no dam	-6	< 10 mm
65		0.000790	no dam	-6.6	< 10 mm
67		0.000237	no dam	-3.9	< 10 mm
96		0.000149	no dam	-1.2	< 10 mm
98		0.000093	no dam	-1.2	< 10 mm
34		0.000711	no dam	-3.7	< 10 mm
30		0.000954	no dam	-5.7	< 10 mm
23		0.000690	no dam	-5.2	< 10 mm
16		0.001152	no dam	-5.4	< 10 mm
11		0.000681	no dam	-5.8	< 10 mm
7		0.000344	no dam	-1.9	< 10 mm

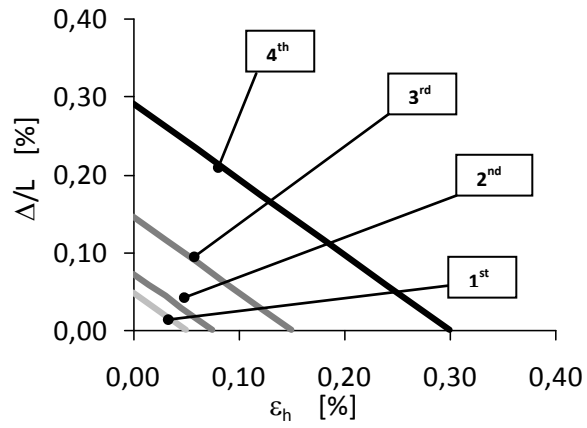
Tab.3-9. Via Piedigrotta: buildings damage analysis

1 st STEP ANALYSIS						2 nd STEP ANALYSIS	
BUILDING	$\Theta=\Delta/L$			$S_{v,max}$ [mm]		$\beta=\Delta/L$	
	P.za REPUBBLICA	2	0.0002	no dam	-2.2	< 10 mm	-
Via C. CUCCA	3	0.0150	>1/500	-5.3	< 10 mm	0.0150	>1/500
L.go TORRETTA	19	0.0005	<1/500	-4.6	< 10 mm	-	-
RIVIERA DI CHIAIA	23	0.0059	>1/500	-7.7	< 10 mm	0.0002	<1/500
	33	0.0003	no dam	-4.8	< 10 mm	-	-
	36	0.0011	no dam	-5.4	< 10 mm	-	-
	44	0.0011	no dam	-4.6	< 10 mm	-	-
	48	0.0001	no dam	-4.8	< 10 mm	-	-
	50	0.0005	no dam	-3.5	< 10 mm	-	-
	53	0.0004	no dam	-3.6	< 10 mm	-	-
	57	0.0001	no dam	-5.2	< 10 mm	-	-
	61	0.0002	no dam	-2.4	< 10 mm	-	-
	66	0.0002	no dam	-2.8	< 10 mm	-	-

Tab.3-10. P.za Repubblica, Via C. Cucca, L.go Torretta and Riviera di Chiaia: building damage analysis

¹ 60vp and 63vp refer to Vico Piedigrotta side of the buildings

² Because of the lack of landmarks measurements along the building facade the β calculation is not possible



Class of damage	L/H = 1.4	
	Δ/L [%]	$\varepsilon_{h,lim}$ [%]
1	0.0150	0.035
2		0.060
3		0.135
4		0.285

Fig.3-27. Building civ.3_Via C.Cucca: category of damage for L/H=1.4 and corresponding $\varepsilon_{h,lim}$ defining the thresholds between the categories of damage

Chapter 4. THREE-DIMENSIONAL FINITE ELEMENT ANALYSIS

4.1. Introduction

In order to understand the tunnelling induced effects of Line 6, a number of finite elements analyses have been performed by the use of Plaxis 3D Tunnel, especially designed for the analyses of tunnel projects whereas it can be thoroughly used for others geotechnical problems.

Although the limitations of the programs in defining a “real” 3D geometry (the final 3D model is a consequence of the 2D geometry, extended on defined planes in tunnel axis direction), the used software allows to simulate the real 3D tunnel excavation process by defining different parameters for each calculation step, such as excavation lengths and duration, grouting and front pressure and volume losses.

Advanced constitutive models can be implemented to simulate non-linear and time-dependent soil behaviour and consolidation and safety analyses can be performed too.

In the following pages, details about the software potentialities and the performed 3D analyses will be presented after a brief discussion on the main properties and functionalities of the program, useful for the elaborated analyses.

4.2. Plaxis 3D Tunnel: useful informations for Line 6 application

As briefly mentioned in the introduction, the 3D model is a consequence of the 2D geometry defined in a cross-section in the (x,y) plane and copied in all the planes defined in the z-direction (Fig. 4-1).

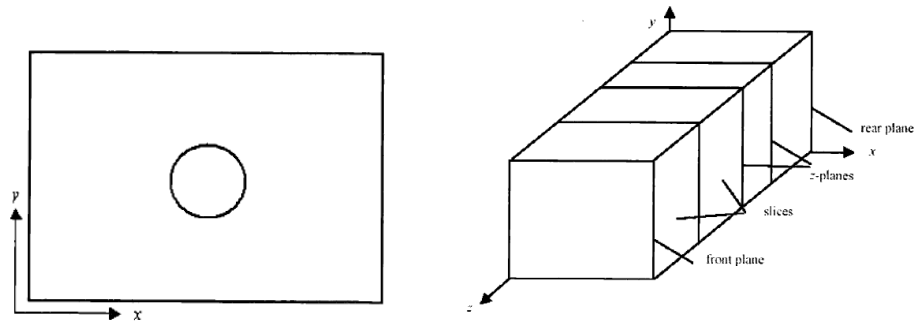


Fig. 4-1. Plane section and 3D model (planes and slices)

In defining the 2D model, soil layers, water table, structural elements, loads and boundary conditions have to be specified in order to let the program generate the 2D mesh, according to the defined general settings in regards to the type of elements (triangular, 15 nodes elements with 6 stress points each - Fig. 4-3) and the model dimensions (defined by the user in order to prevent the boundary conditions influence on the problem). The 2D mesh is then linearly extended in the z-direction to generate the 3D mesh Fig. 4-2.



Fig. 4-2. 2D and 3D mesh

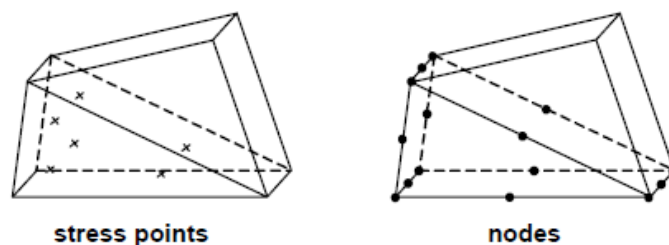


Fig. 4-3. Triangular mesh elements: nodes and stress points

Before the 3D mesh is generated, material properties have to be defined and so applied to each structural or soil elements. Five soils models are available in the program: *Elastic Model*, *Mohr-Coulomb Model*, *Hardening Soil Model*, *Soil Soft Creep Model* and *Jointed Rock Model*. Except from the Jointed Rock Model used to simulate stratified or jointed rock behaviour, the remaining mentioned soil models can be applied to the soils. Since the Elastic Model, based on the Hook's law of isotropic elasticity is primarily applied for structural elements, the Mohr-Coulomb Model defined by five soil parameters (Young's Modulus E , Poisson's ratio ν , cohesion c , friction angle φ and dilatancy angle ψ) is considered a good approximation in describing the soil behaviour and the Soft Soil Creep Model is useful in describing time-dependant behaviour of normally consolidate soils, the Hardening Soil Model is the model chosen for Line 6 tunnel affected soils, since it involves compression hardening to simulate irreversible compaction of soil under primary compression and is particularly used for sands and gravels.

When a water table is defined into the model, in order to describe at best the water pressure influence on soil response, *Drained*, *Undrained* or *Non-Pouros* behaviour for defined soil has to be chosen, depending on the type of soil (granular or cohesive). Because the soils affected by the Line 6 tunnel excavation are essentially granular soils on a Tuff bedrock, *Drained* behaviour has been set to describe their behaviour. It is especially suitable when no excess pore pressure generate, for instance in cases of dry or high permeable soils (sands), low rate of loading and/or for long term behaviour when there is no need to simulate the history of undrained loading or consolidation. The *Non-Pouros* behaviour is indeed used for describing concrete or structural elements (i.e. concrete tunnel lining) often in combination with the *Linear Elastic Model*.

4.2.1. The Hardening Soil Model

The basic idea for the Hardening Soil Model is the hyperbolic relationship between the vertical strain ε_1 and the deviatoric stress q observed in the primary triaxial loading tests (Fig. 4-4). It is related to the decreasing in stiffness and to the plastic strains developing when primary deviatoric loading is applied (Kondner & Zelascko, 1963).

In order to use this soil model, a number of soil parameters have to be defined. Despite some of them are the same as those used in the non-hardening Mohr-Coulomb model, such as φ_p , c and ψ_p , the below additional parameters for using the model have to be defined:

- E_{50}^{ref} , secant stiffness in standard triaxial test
- E_{50}^{ref} , tangent stiffness for primary oedometer loading
- m , power of stress-level dependency of stiffness
- E_{ur}^{ref} , unloading/reloading stiffness
- E_{50}^{ref} , secant stiffness in standard triaxial test
- ν_{ur} , Poisson's ratio for unloading-reloading
- p^{ref} , reference stress for stiffnesses,
- K_0^{NC} , K_0 value for normal consolidation
- R_f , failure ratio q_f/q_a .

In the following pages, the main equations describing the Hardening Soil Model are reported.

The yield curves obtained by the standard triaxial tests can be described by equation (4.1) for $q < q_f$ where q_f is the ultimate deviatoric stress, derived by Mohr-Coulomb failure criterion, involving the strength parameters c and φ_p ; it is defined by equation (4.2).

$$\varepsilon_1 = \frac{q_a}{2 \cdot E_{50}} \cdot \frac{(\sigma_1 - \sigma_3)}{q_a - (\sigma_1 - \sigma_3)} \quad (4.1)$$

As soon as $q = q_f$ the failure criterion is satisfied and perfectly plastic yield occurs. The relation between q_a , given by equation (4.3), and q_f is expressed by the failure ratio $R_f < 1$, representing the percentage of failure deviatoric stress q_f reached, usually automatically set equal to 0.9.

(4.2)

$$q_f = \frac{6 \cdot \sin\varphi_p}{3 - \sin\varphi_p} \cdot (p - c \cdot \cot\varphi_p)$$

(4.3)

$$q_a = \frac{q_f}{R_f}$$

The stress strain behaviour for primary loading is highly non linear. Instead of using the tangent stiffness modulus for primary loading E_i , difficult to determine, the secant Young's modulus E_{50} is defined. It is expressed by:

(4.4)

$$E_{50} = E_{50}^{ref} \cdot \left(\frac{\sigma_3 + c \cdot \cot\varphi_p}{\sigma^{ref} + c \cdot \cot\varphi_p} \right)^m$$

where E_{50}^{ref} is the reference stiffness modulus corresponding to a reference stress p^{ref} , and m represents the amount of stress dependency of the actual stiffness on the minor principal stress σ'_3 (the effective confining pressure in a triaxial test). E_{50}^{ref} is determined from triaxial stress-strain-curve for a 50% mobilization of the maximum shear strength q_f .

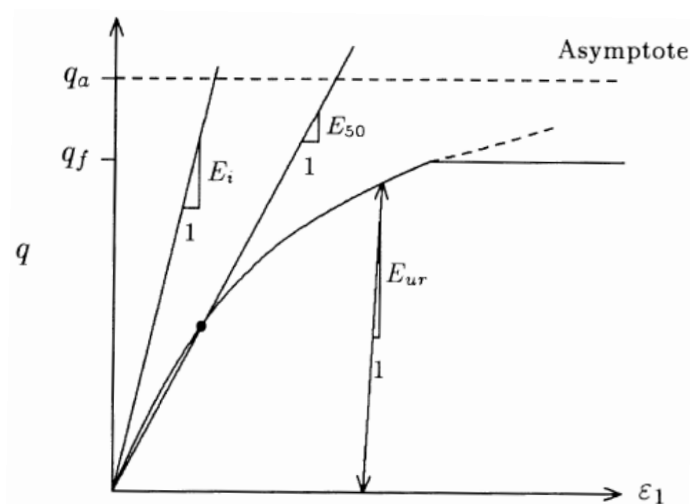


Fig. 4-4. Hyperbolic stress-strain relation in primary loading for a standard drained triaxial test

From experimental data on sandy soils $E_{50}^{ref} = E_{oed}^{ref}$ relation has been found (Fig. 4-5), whereas for clay $E_{50}^{ref} = 2 \cdot E_{oed}^{ref}$.

For un-reloading stress paths, the stress-dependent E_{ur}^{ref} stiffness modulus is used. It is expressed by equation (4.5) and defined as the unloading-reloading Young's modulus in a wide unloading-reloading cycle (Fig. 4-7), corresponding to the reference pressure $\sigma^{ref} = 100 \text{ kPa}$. From drained triaxial tests relations between the unloading-reloading stiffness modulus and the loading stiffness modulus were found (Fig. 4-8).

$$E_{ur} = E_{ur}^{ref} \cdot \left(\frac{\sigma_3 + c \cdot \cot\phi_p}{\sigma^{ref} + c \cdot \cot\phi_p} \right)^m \quad (4.5)$$

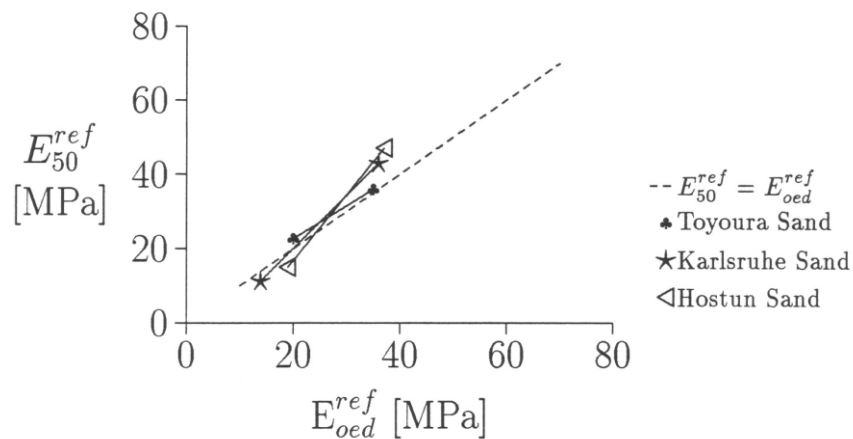


Fig. 4-5. E_{50}^{ref} vs E_{oed}^{ref} relationship from experimental data for sandy soils

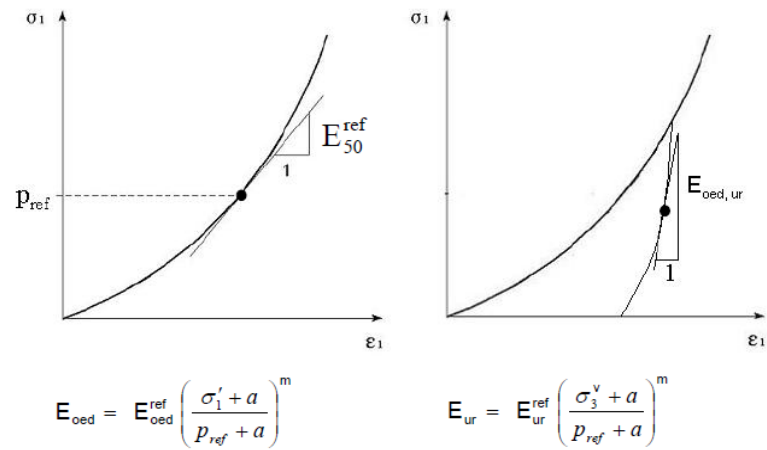


Fig. 4-6. Loading and unloading stiffness Young's moduli

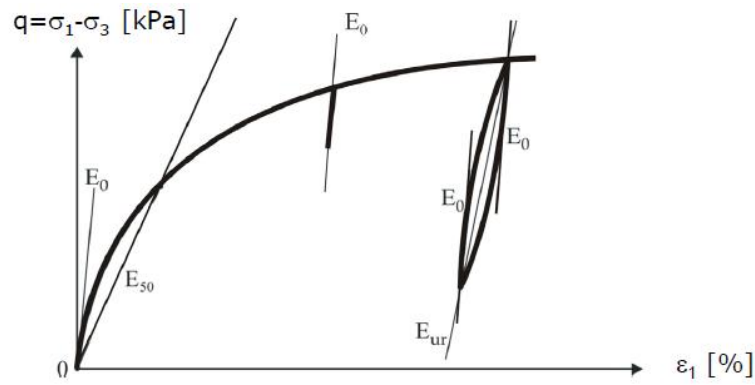


Fig. 4-7. Loading and unloading stiffness moduli

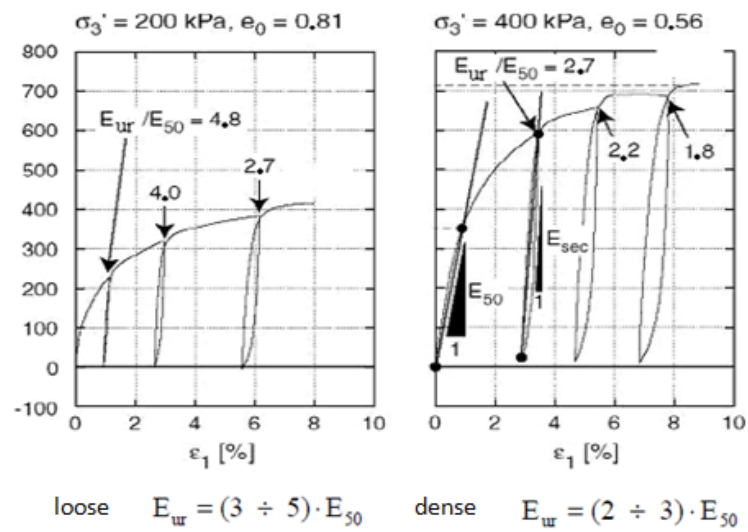


Fig. 4-8. Relation between E_{ur} and E_{50} for loose and dense soils from drained triaxial tests

E_{ur} is even used in defining the shear modulus G_{ur} , as expressed by equation (4.6) and represented in Fig. 4-9.

$$G_{ur} = \frac{1}{2 \cdot (1 + \nu_{ur})} \cdot E_{ur} \tag{4.6}$$

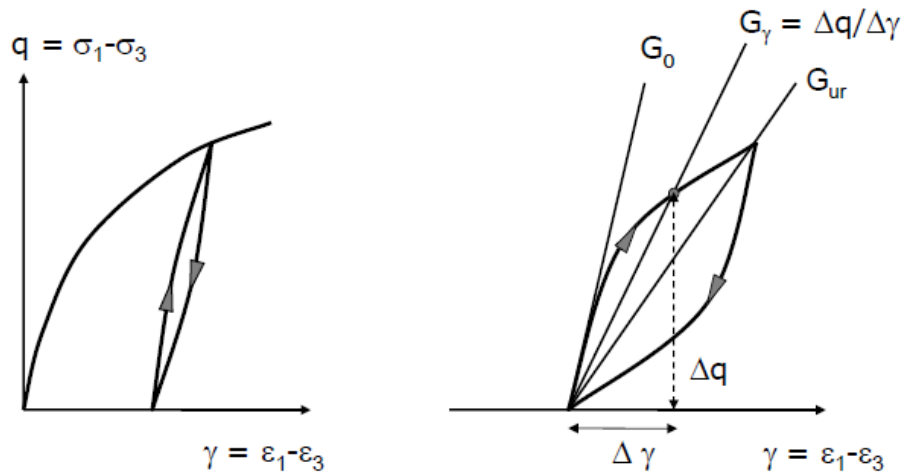


Fig. 4-9. Shear stiffness modulus

The un-reloading path is modeled as purely (non-linear) elastic and the elastic component ε^e is calculated using equations (4.5) and (4.6) for a constant value for the Poisson's ratio ν_{ur} . Relations expressed by formula (4.7) and (4.8) have been obtained.

$$\varepsilon_1^e = \frac{q}{E_{ur}} \tag{4.7}$$

$$\varepsilon_2^e = \varepsilon_3^e = \nu_{ur} \cdot \frac{q}{E_{ur}} \tag{4.8}$$

The yield surfaces for such a model are defined by equations (4.9) and (4.10) depending on plastic shear strain γ_p and plastic volumetric strains ε_v^p , and depicted in Fig. 4-10. The approximation in equation (4.10) is accurate since for hard soils plastic volume changes tend to be small when compared with the axial strain.

$$f_{12} = \frac{q_a}{E_{50}} \cdot \frac{(\sigma_1 - \sigma_2)}{q_a - (\sigma_1 - \sigma_2)} - \frac{2 \cdot (\sigma_1 - \sigma_2)}{E_{ur}} - \gamma^p \tag{4.9}$$

$$f_{13} = \frac{q_a}{E_{50}} \cdot \frac{(\sigma_1 - \sigma_3)}{q_a - (\sigma_1 - \sigma_3)} - \frac{2 \cdot (\sigma_1 - \sigma_3)}{E_{ur}} - \gamma^p$$

$$\gamma^p = \varepsilon_1^p - \varepsilon_2^p - \varepsilon_3^p = 2\varepsilon_1^p - \varepsilon_v^p \approx 2\varepsilon_1^p \tag{4.10}$$

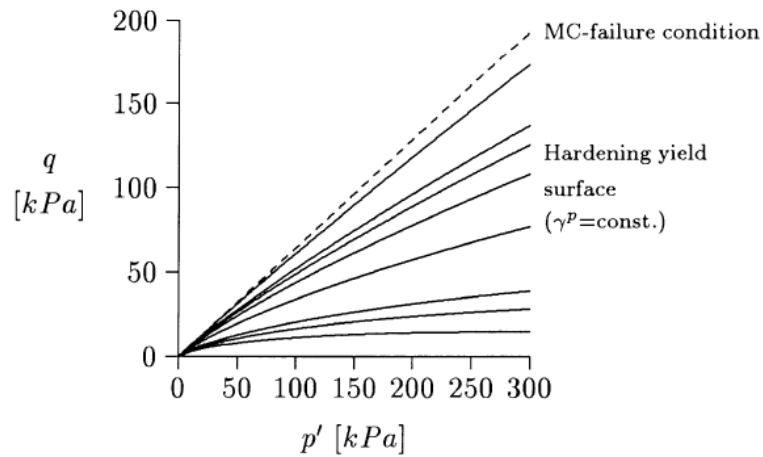


Fig. 4-10. Successive yield loci for various values of the hardening parameter γ_p and failure surface

For given γ_p values equations $f_{12} = f_{13} = 0$ can be plotted in (p', q) plane by means of yield locus whose shapes depend by m values being linear for $m = 1$ and slightly curved for lower values. Fig. 4-10 represents yield loci for $m = 0.5$, typical for hard soils.

Since the Hardening Soil Model involves plastic strains such as γ^p and ε_v^p , attention has to be focused on the relationship (*flow rule*) occurring between them, expressed by equation:

$$\dot{\varepsilon}_v^p = \sin\psi_m \dot{\gamma}^p \quad (4.11)$$

where ψ_m is the mobilized dilatancy angle given by expression (4.12) depending on the critical state friction angle φ_{cv} and on the mobilized friction angle φ_m (equation (4.13)).

$$\sin\psi_m = \frac{\sin\varphi_m - \sin\varphi_{cv}}{1 - \sin\varphi_m \sin\varphi_{cv}} \quad (4.12)$$

$$\sin\varphi_m = \frac{\sigma_1 - \sigma_3}{\sigma_1 + \sigma_3 - 2c \cdot \cot\varphi_p} \quad (4.13)$$

The above mentioned equations correspond to the stress-dilatancy theory by Rowe (1962) and Rowe (1971), as explained by Schanz & Vermeer (1996), based on the observed material contraction for small stress ratios and on the observed dilatancy for high stress ratios ($\varphi_m < \varphi_{cv}$). At failure, when ($\varphi_m = \varphi_{cv}$) equation (4.12) becomes:

$$(4.14)$$

$$\sin\psi_{cv} = \frac{\sin\varphi_p - \sin\psi_p}{1 - \sin\varphi_p \sin\psi_p}$$

hence the critical state angle can be derived from the failure ones φ_p and ψ_p .

4.3. Three-dimensional analyses of the Line 6 tunnel

In this section 3D Finite Elements analyses of Line 6 tunnel performed by means of Plaxis 3D Tunnel will be discuss. Description of the geometric model, details on materials, constitutive model and the kind of analysis performed will be discuss in order to show results of parametric studies on the effects of both soil and machine parameters, and of back-analysis performed on the basis of collected monitoring data. The realized tunnel up to August the 31st was analyzed and a reference plane section has been chosen along Via Piedigrotta to perform such analyses.

4.3.1. The input model

Since Plaxis 3D Tunnel draws the 3D geometry on the basis of the plane-strain section defined in (x, y) plane and reproduced all along the tunnel axis direction (z) (cfr. Paragraph 4.2), the choice of a representative section along the longitudinal profile of the line has been required.

The analyzed section in the (x, y) plane is made by 18 m depth tunnel axis and 14 m thick loose soil layer on the Tuff bedrock with 3 m a.m.s.l. groundwater table (Fig. 4-11). As and no buildings have been considered for the 3D analyses, a symmetric section was possible for the analyses, in order to minimize the calculation time strictly depends by the number of elements in the 3D mesh, hence by the model dimensions.

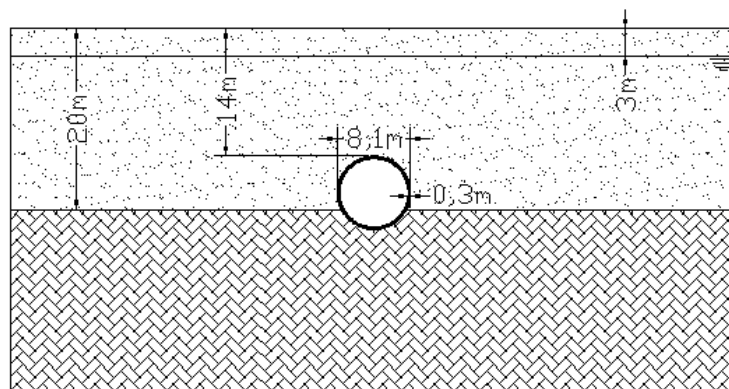


Fig. 4-11. Plane reference section in (x, y) plane for FE analyses

To prevent the border effects influence on the excavation process, a plane section size $B \times H = 5D \times 5D$ was defined. The number of planes in z-direction was fixed as to reproduce at best the real excavation process in respect of the real progress of the final lining and of the tunnel excavation day by day; in such a way an $L = 125\text{ m} = 15.5D$ model in z-direction was constructed (Fig. 4-12). The resulted 3D model is then featured by 44268 elements and 122688 nodes.

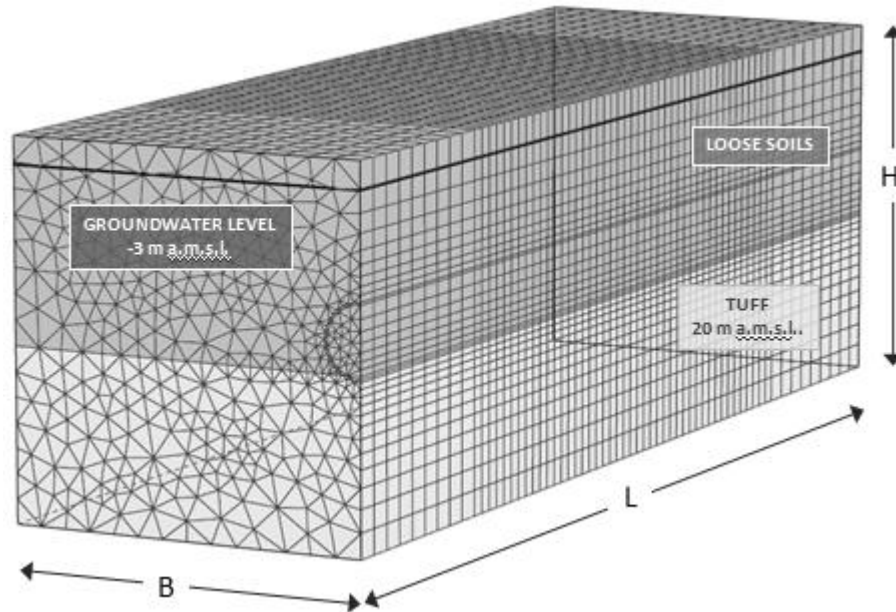


Fig. 4-12. Plaxis 3D geometric model for the FE analyses ($B = 5D, H = 5D, L \approx 15D$)

Since the tunnel excavation affects at the most the upper loose grounds layer, mainly made by sandy soils, “drained” analyses were performed in order to not produce excess pore pressure resulting from the tunnel excavation process.

The Hardening Soil Model was used to define the soils’behaviour and the Linear Elastic Model for the structural elements (EPB shield and concrete final lining); 0 resumes both soils and structural elements properties besides the type of elements chosen to simulate the tunnel lining segments (*clusters*) and the EPB shield (*shell*) (Fig. 4-13).

Hardening Soil Model	LOOSE SOILS	TUFF	Linear Elastic	LINING SEGMENTS	EPB
			Soil Model	"concrete"	"beam"
γ_d [kN/m ³]	13	14	γ [kN/m ³]	25	38.1
γ' [kN/m ³]	8	9	ν [-]	0.25	-
γ_{sat} [kN/m ³]	18	19	RcK [MPa]	45	-
ν [-]	0.3	0.3	d [m]	-	-
c' [kPa]	0	500	Lung. [m]	1.7	8.16
ϕ' [°]	35	27	Larg. [m]	1.5	-
k [m/sec]	1.00E-04	1.00E-04	s [m]	0.3	-
k [m/day]	8.64E+00	8.64E+00	l [m]	8.9	-
k_D [-]	0.426	0.546	E [kN/m ²]	3.82E+07	-
k_A [-]	0.271	0.376	A [m ²]	0.45	-
k_F [-]	3.690	2.663	I [m ⁴]	3.83E-03	-
E_{vc} [kPa]	5.00E+04	1.00E+06	EA [kN/m]	1.72E+07	2.46E+07
E_{ed} [kPa]	6.73E+04	1.35E+06	EI [kNm ² /m]	1.46E+05	2.51E+05
$E_{ur}=3 \cdot E_{vc}$ [kPa]	2.02E+05	4.04E+06	d_{eq} [m]	0.32	0.35

Tab.4-1. Soil parameters used for the 3D analyses

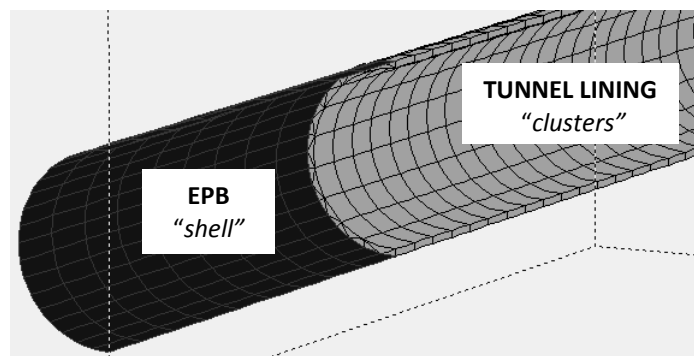


Fig. 4-13. Structural elements for the EPB shield ("beam") and the lining segments ("cluster")

In order to model the soil-tunnel interaction, implying a reduction in soils strength parameters, the same soils materials have been defined also using the R_{inter} parameter, useful to describe the interface and/or soil reduction in friction and adhesion if lower than 1. The materials with reduced strength parameters have been applied to that slices where the tunnel was already excavated, the EPB shield was already been and the soil-tunnel interface properties were consequently reworked.

4.3.2. The effects of soil parameters on surface subsidence

In order to analyze the soils parameters influence on the surface subsidence, a number of FE analyses have been performed on simplified geometric model made by a single loose soils layer (being the Tuff bedrock at the tunnel invert, its effect on the surface displacements can be reasonably considered to be negligible).

The Hardening Soil Model and the “drained” analysis were set to describe the soil behaviour. For such a constitutive model, apart from the strength parameters γ , c , φ and ψ , both the loading E and un-reloading E_{ur} Young’s modulus are requested.

All strength and stiffness parameters (except from c , since analyses focus on sandy soils), together with un-reloading on loading stiffness moduli ratio $P = E_{ur}/E$, were varied within realistic ranges of values, as to investigate their influence on tunnelling induced soil behaviour and to identify that parameters affecting at the most the surface subsidence.

Because of the “drained” soil behaviour, different volume losses at the tunnel crown and at the ground surface were expected. Though a volume loss controlled analysis would be possible (by setting an user value in that planes where a defined volume loss is required), in performed analyses cases not any volume loss at the tunnel depth was imposed. Fig. 4-14_a and Fig. 4-14_b show the obtained volume losses and maximum settlements at the tunnel crown related to the loading stiffness modulus while Fig. 4-15_a and Fig. 4-15_b depict, for the analyzed section, the ratios between the volume losses and the maximum settlements at the ground surface than at the tunnel crown. A linear relationship can be detected between the volume losses and the maximum settlements ratios ($V_L/V_{L,axis}$ and $w_{max}/w_{max,axis}$) and the loading stiffness modulus, with the surface volume loss increasing up to 2.5 the volume loss at the tunnel crown, and the maximum surface settlements being between (0.5 ÷ 1) the crown settlement, depending on $P = E_{ur}/E$ ratio.

All the results plotted in the next pages, concerning the others parameters influence (γ , φ , ψ) on the ground surface displacements, refer to the volume loss on the ground surface rather than to the volume loss at the tunnel crown. For more results about the

mentioned soil parameters influence on the volume loss at the tunnel depth see *Appendix V* (Fig. IV-1 up to Fig. IV-6).

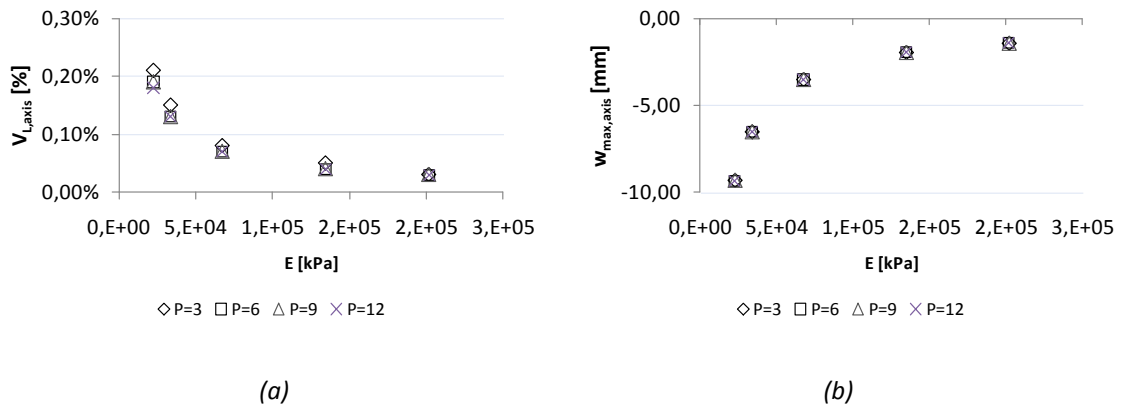


Fig. 4-14. Volume loss (a) and maximum settlement (b) at the tunnel crown

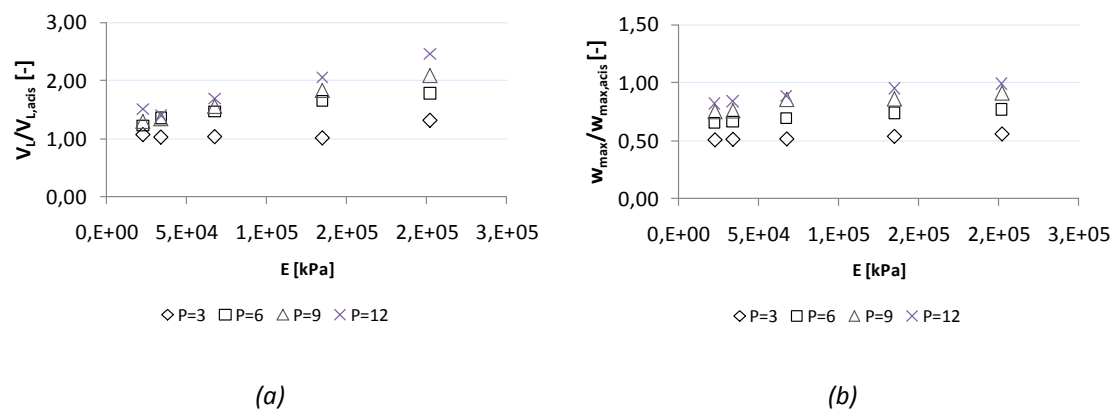


Fig. 4-15. Volume loss at the ground surface on volume loss at the tunnel depth (a) and maximum surface settlements on the maximum settlements at the crown (b)

The range of variations for each soil parameter, together with the reference analyses parameters, are resumed in Tab.4-2, while more details about any specific analysis used parameters together with the obtained numerical results are reported in specific tables in *Appendix IV*.

Concerning to the stiffness moduli ratio E_{ur}/E , although 3 is the Plaxis default value and $(3 \div 5)$ is a reliable range for sandy soils, a number of analyses were performed in

order to analyze the effects of the un-reloading stiffness modulus increase up to 12 times the loading one. In such a way a kind of Hardening Soil Small Model is simulated, since increasing in E_{ur}/E ratio leads the soil behaviour to move towards the small strain field.

SOIL PARAMETERS		REFERENCE VALUES	RANGE OF VARIATION
REFERENCE ANALYSES	E [kPa]	$6.75 \cdot e^4$	$(1/3 \div 3) \cdot E_{rif}$
	E_{ur} [kPa]	$2.02 \cdot e^5$	$(1/3 \div 3) \cdot E_{rif}$
	E_{ur}/E	3	$(3 \div 12)$
RANGES OF VARIATIONS	γ_d [kN/m ³]	13	$\pm(20\%) \cdot \gamma_{rif}$
	γ_{sat} [kN/m ³]	18	$\pm(20\%) \cdot \gamma_{rif}$
	φ [°]	35	$(-40 \div 0)\% \cdot \varphi_{rif}$
	ψ [°]	0	$(0^\circ \div 10^\circ)$

Tab.4-2. Soil parameters in the reference analyses and respective ranges of variations for the performed parametric analyses

As widely described in the first chapter of this thesis, results from numerical FE simulations of tunnel excavation often show a surface subsidence curves too wide if compared to collected monitoring data. For such a reason, in this section, attention is mainly drawn on the effects of soil parameters on k values. Moreover to investigate the advancing effects along the tunnel axis direction, the output results were extrapolated and plotted on three planes: “Plane O” coinciding with the tunnel front plane, “Plane U” and “Plane AE” respectively 1D and 3D from it. Since the observed effects in the three planes are quite similar to each other, the graphs below on E and E_{ur}/E effects, only depict results concerning the tunnel front plane (Plane O); see *Appendix IV* for results on Plane U and Plane AE (cfr. *Appendix IV* - Fig. IV-1).

From the performed analyses, clear relations between k and the soil parameters E , E_{ur} , $P = E_{ur}/E$, γ , φ were detected. The main results about their effects on the surface subsidence are resumed in the following pages, although further informations are reported in the *Appendix IV* (Fig. IV-7, Fig. IV-8, Fig. IV-9).

Fig. 4-16 shows the relations linking E and $P = E_{ur}/E$ to the subsidence maximum displacements, the volume loss and the subsidence width. The figures demonstrate a significant effect of E variations on w_{max} and V_L , rather than on the width parameter k .

Contrarwise a more evident effect on k values is played by the stiffness moduli ratio P ; as a matter of fact Fig. 4-16_c depicts the observed behaviour describing a wider range in the $(\Delta E/E_{rif}, \Delta k/k_{rif})$ plane than in the others cases (Fig. 4-16_a and Fig. 4-16_b). Actually, focusing the attention on k , the graphs show reductions in surface subsidence width (k) by increasing the loading stiffness modulus and an opposite effects by raising the P ratio; for such a reason the Plaxis default value $P = 3$ has been chosen to perform the Line 6 back-analyses. The same informations derived from the just described graphs can be deduced also by $\Delta E_{ur}/E_{ur,rif}$ dependent curves, as shown in Fig. IV-8 in Appendix IV.

More graphs on the stiffness moduli effects are resumed in Appendix, showing relations in $(\Delta P/P_{rif}, \Delta w_{max}/w_{max,rif})$, $(\Delta P/P_{rif}, \Delta V_L/V_{L,rif})$ and $(\Delta P/P_{rif}, \Delta k/k_{rif})$ planes. Linear relationships can be highlighted between the observed parameters and the stiffness moduli ratio (cfr. Appendix IV - Fig. IV-9).

In the same way as described above, in Fig. 4-17 and Fig. 4-18 the effects of γ variations on w_{max} and V_L and k and of φ on k are depicted (not any particular trend between φ , w_{max} and V_L were identified for the analyzed cases, as a consequence not any graph was reported). Increments or reductions in γ lead to analogous variations in w_{max} and in V_L (Fig. 4-17_a and Fig. 4-17_b), contrariwise not any increments in k are related to analogous increments in γ , whereas a 20% γ reduction leads to a 46% k decrease (Fig. 4-17_c).

Tab.4-3 synthesizes the obtained results, resuming the maximum w_{max} , V_L and k variations induced by changes in E , $P = E_{ur}/E$ and γ .

Maximum variations		$\Delta w_{max}/w_{max,rif}$ [%]	$\Delta V_L/V_{L,rif}$ [%]	$\Delta k/k_{rif}$ [%]
$\Delta E/E_{rif}$ [%]	$(-1/3 - 3) E_{rif}$ (-67 - 200)%	(+156 ÷ -49)%	(+171 ÷ -44)%	(-2 ÷ +10)%
$\Delta P/P_{rif}$ [%]	(0 - 300)%	(0 ÷ +15)%	(0 ÷ +70)%	(0 ÷ +52)%
$\Delta \gamma/\gamma_{rif}$ [%]	(± 20%)	(-51 ÷ +29)%	(-73 ÷ +32)%	(-46 ÷ +10)%

Tab.4-3. Maximum variations on w_{max} , V_L and k induced by maximum variations of E , $P = E_{ur}/E$ and γ

Finally, Fig. 4-18 depicts the effects of φ and ψ on the subsidence width: a 40% reductions in friction angle leads approximately to a 25% linear increase in k (the surface subsidence curve becomes wider by reducing the soil friction angle), conversely a non-linear trend relation is detected in the ψ dependent graphs. Up to $\Delta\psi/\varphi_{rif} = 10\%$ not any effects on $\Delta k/k_{rif}$ is identified, while for $\Delta\psi/\varphi_{rif} = 15\%$ an instantaneous 15% increase in k is observed. The same behaviour is noticed in ψ dependent graphs for w_{max} and V_L (cfr. Appendix IV - Fig. IV-10).

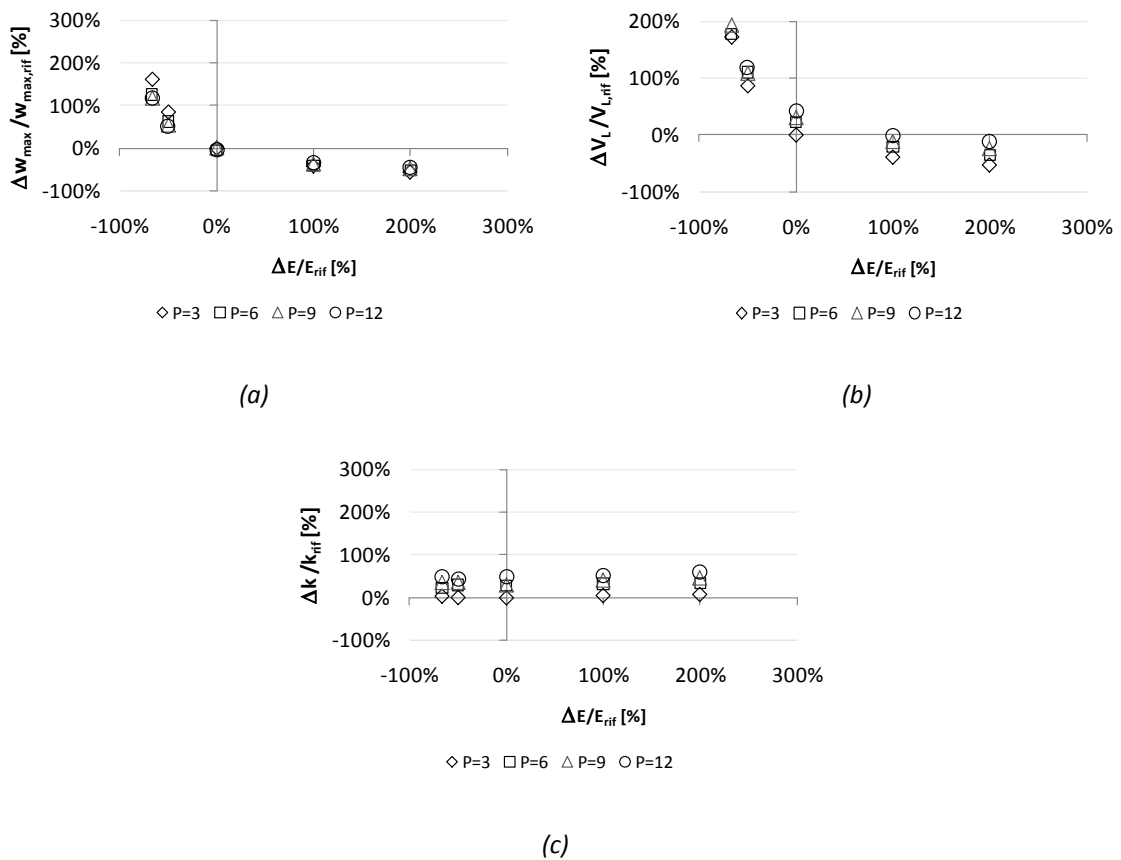


Fig. 4-16. Effects of loading stiffness modulus variations on surface subsidence, on tunnel front plane (Plane O): maximum displacements (a), volume loss (b) and k (c)

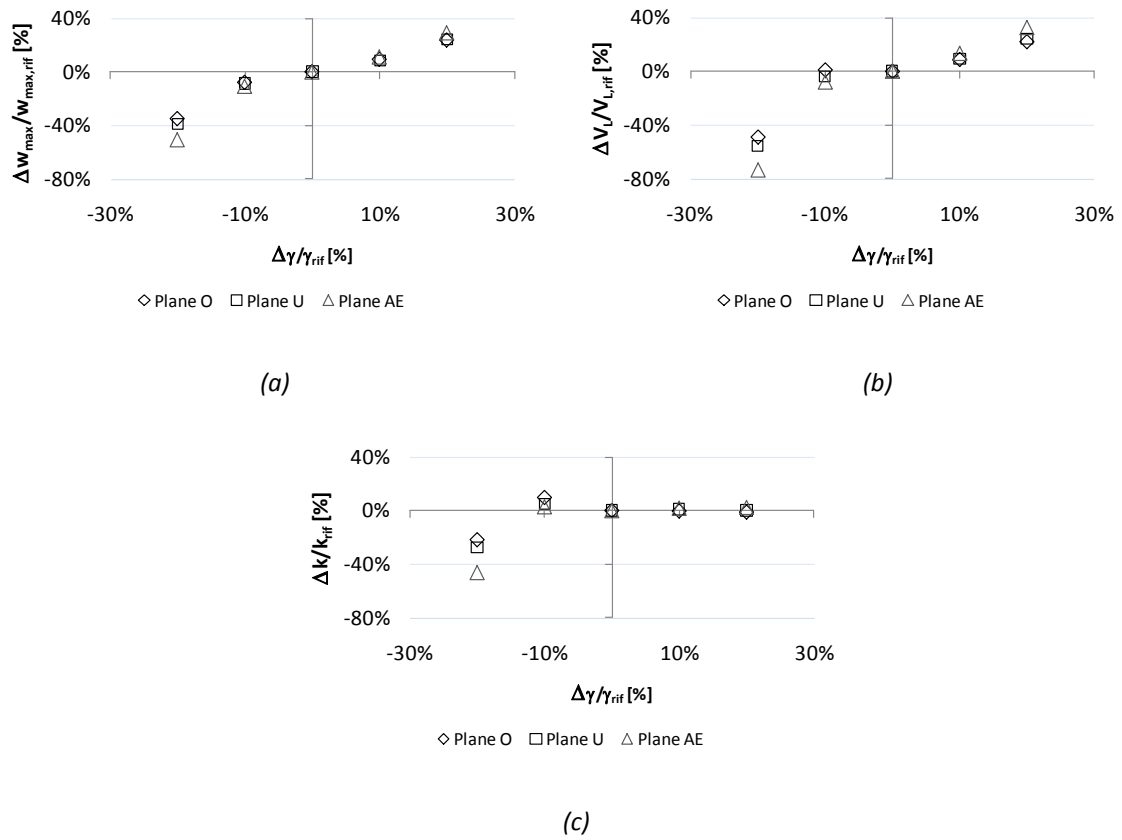


Fig. 4-17. Effects of γ on surface subsidence: maximum displacements (a), volume loss (b) and k (c)

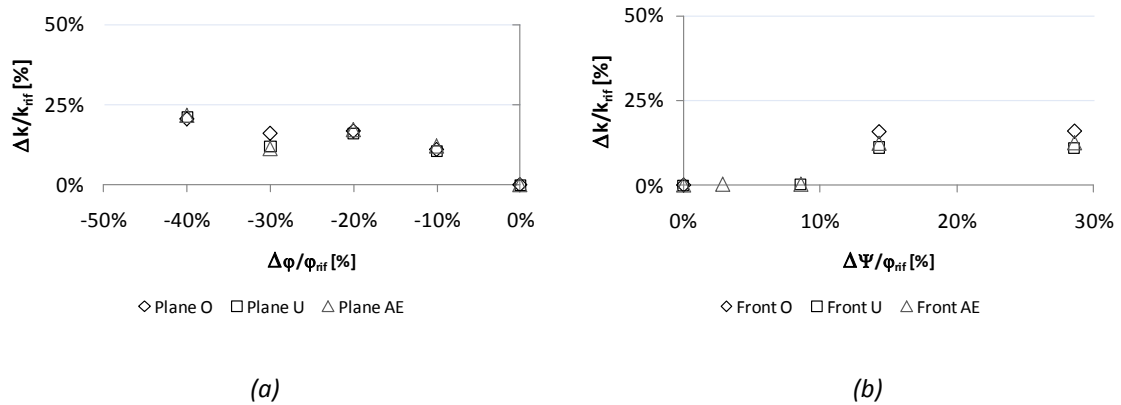


Fig. 4-18. Effects of ϕ (a) and ψ (b) on subsidence width k

4.3.3. Parametric analyses on the EPB front and grouting pressures

The EPB operating principle is based on the use of the front pressure (FP), to prevent the tunnel face collapse, the grouting pressure (GP) to fill the soil-shield gap and of the hydraulic jacks forces to ensure the machine advance. Since both the front and the grouting pressures are used to prevent tunnel collapse phenomena as to minimize the volume loss, a parametric study to observe the effects of each pressure on the induced tunnelling surface displacements was considered useful, as to define the technological parameters importance compared to the soils 'properties ones.

In order to apply to the Line 6 case the results obtained by such a parametric study on the machine pressures, the geometric model described in *Section 4.3.1*. (Fig. 4-11), made by two soil layer, the upper loose soils layer and the Yellow Neapolitan Tuff bedrock, was used, as to not overlook the pressures 'effects applied even in the underlie portion of the tunnel where the Yellow Neapolitan Tuff is located. The reference properties for both the soils 'layers, used in the analyses discussed in the following pages are resumed in the table below.

SOIL PARAMETERS		REFERENCE VALUES	
		LOOSE SOILS	TUFF
REFERENCE VALUES	E [kPa]	$6.75 \cdot e^4$	$1.35 \cdot e^6$
	E_{ur} [kPa]	$2.02 \cdot e^5$	$4.04 \cdot e^6$
	E_{ur}/E	3	3
	γ_d [kN/m ³]	13	14
	γ_{sat} [kN/m ³]	18	19
	c [kPa]	0	500
	φ [°]	35	27
	ψ [°]	0	0

Tab.4-4. Soil parameters for the performed analyses

A number of analyses were performed keeping as constant the “input” parameters soil properties, the excavation phases and volume loss¹ at the crown and varying within the ranges resumed in Tab.4-5 the front and the grouting pressures (*cf.* Appendix IV - Tab. IV-1). Results will be discussed in the following pages highlighting the single front pressure effects as the grouting pressures ones.

EPB PARAMETERS		RANGE OF VARIATION
REFERENCE ANALYSES	Front Pressure (FP) [kPa]	(100 – 500)
	Grout Pressure (GP) [kPa]	(100 – 500)
	Hydraulic Jack Pressure [kPa]	(635 – 2255)
	GP/FP	(0.2 – 5)

Tab.4-5. Ranges of variations of the machine pressures

For both the front and the grouting pressures clear trends of the maximum surface settlement and the volume loss both at tunnel depth and at the ground surface are evident.

Despite volume loss controlled analyses were performed by applying specific volume loss at the tunnel depth, the realized volume loss at that location is clearly affected by the applied front pressures (more than by the grouting pressure). Indeed Fig. 4-19_a shows the volume loss at the crown referred to the applied pressure at the tunnel face. Despite the imposed volume loss at the crown was always the same (0.1%) the figure reveals how the realized² volume loss may exceed such a value for the lower front pressures, as the opposite can occur for high pressures. Such a phenomenon can be explained by the three-dimensional effects related to the tunnelling, much more evident for low front pressures at the tunnel, since the tunnelling induced displacements affect longer distance from the tunnel front because of the higher displacements toward the excavation.

¹ A reference value for the volume loss at the crown was chosen in reference to the parametric study on soil properties effects described in Section 5.3.2. For the design stiffness modulus $E = 6.75 \cdot e^4 kPa$, reliable value for that volume loss is 0.1% (Fig. 4-14(a)_a).

² For each calculation step the used software provides the realized volume loss at the tunnel depth, depending on the relative tunnel–soil stiffness. Such a value represents the final volume loss at the end of each calculation phase, including the effects induced by previous steps.

At the same time Fig. 4-19_b shows the pressure influence on volume loss at the surface than the volume at the tunnel depth. Such a ratio can increase up to 4 by raising the front pressure and for the lowest grouting pressure. The same figures finally reveal the front pressure being much more influential than the grouting pressure on the volume loss at the tunnel depth, and contrariwise the grouting pressure affecting much more the induced surface behaviour.

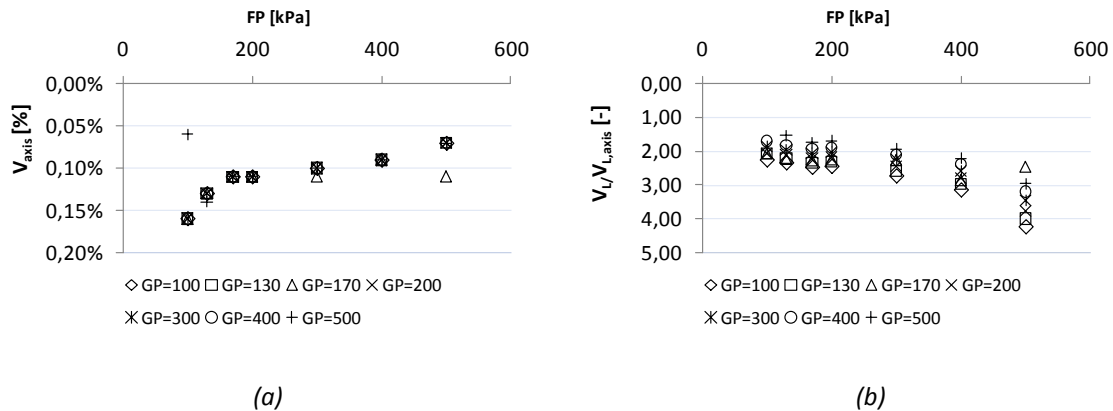


Fig. 4-19. Front and grouting pressure effect on the realized volume loss at tunnel depth (a) and on the ratio between the volume loss at the crown and the volume loss at the ground surface (b)

Focusing the attention on the pressures influence on the surface effects in terms of surface volume loss and maximum settlement, dimensionless and brief graphs are plotted in the next pages, showing the front pressures proportioned to the minimum value of the range (100 kPa) related to the relative surface settlement and volume loss ratios. For specific graphs plotting the numerical values of such parameters, rather than their variations, see the *Appendix IV*.

Fig. 4-20_a and Fig. 4-20_b show the front pressure dependent results. A range of behaviour for both w_{max} and V_L can be identified, by varying the applied grout pressure. Indeed both the figures show initial reduction for both the w_{max} and the V_L for increasing front pressure up to a specific value, than gradual increases with lower gradient. The same behaviour is highlighted in Fig. 4-21 where for each grouting pressure value, both the settlement and volume loss variations are plotted in reference to that value corresponding to the minimum front pressure applied (100 kPa). A reduction up to 30% of the surface maximum settlement and up to 10% of the volume loss are measured for

front pressure increase up to 100% (FP = 200 kPa), after that reductions up to 10% for the settlements and 5% for volume losses are caused by further front pressure increments.

The observed behaviour can be justified by some considerations, resumed below:

- shear strength achievement at the tunnel face for low front pressures, within the range (100 – 130 kPa), leads to local Mohr-Coulomb and Hardening Soil yielding points (*cf.* Appendix IV – Fig. IV-18 and Fig. IV-19), thus face plasticization and higher settlements
- for low front pressure the tunnel face plasticization is the predominant effect, leading to high surface settlements and volume losses; raises in such a pressure up to a defined (200 kPa) value, reflect on reduction of both w_{max} and V_L
- further increase of the front pressure leads to plasticization of the tunnel contour giving rise to new increment in w_{max} and V_L
- horizontal displacements along the tunnel axis are strictly connected to the applied pressure. They go toward the excavated tunnel until the front pressure reaches a sort of “equilibrium” value (170 kPa) at which no z-axis displacements are detected; when the front pressure exceeds such a value opposite horizontal displacements, up to 20 mm, are measured toward the soil (*cf.* Appendix IV – Fig. IV-15).

A different behaviour is observed in the grouting pressure dependent graphs (Fig. 4-23): linear relationships between the grouting pressure and the relative surface settlements and volume losses are detected, showing 25% in w_{max} and 30% in V_L reductions for grouting pressure increments up to 400%.

Furthermore, dimensionless graphs in Fig. 4-24 show the predominant effect of the front pressure on both the surface maximum settlement and volume loss, up till 200% of pressures increments, contrariwise the predominant effect of the grouting pressure is pronounced for the highest increment (FP=GP=500 kPa).

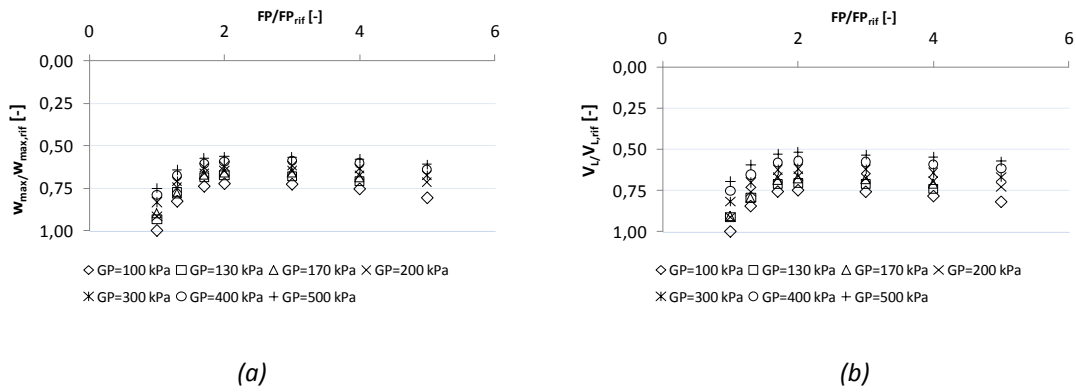


Fig. 4-20. Front pressure (FP) effects on maximum surface settlement (a) and on surface volume loss (b): range of values depending on the applied grouting pressure

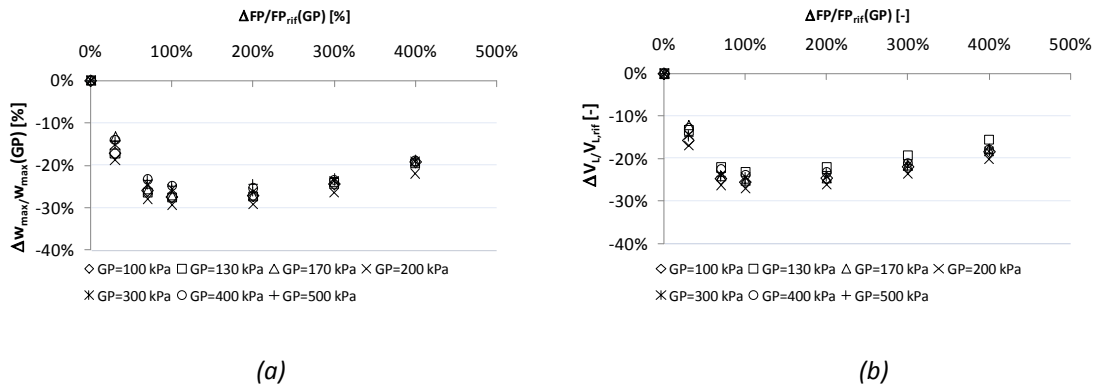


Fig. 4-21. Front pressure (FP) effects on maximum surface settlement (a) and on surface volume loss (b): total dimensionless graphs

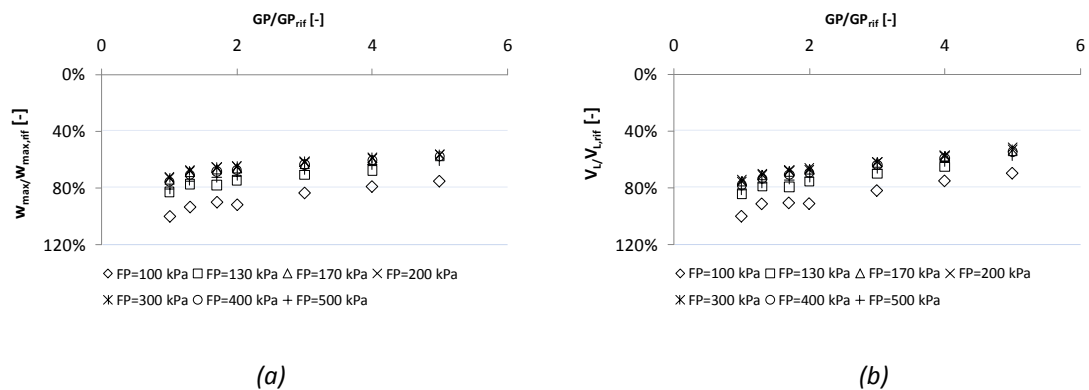


Fig. 4-22. Grout pressure (GP) effects on maximum surface settlement (a) and on surface volume loss (b): range of values depending on the applied front pressure

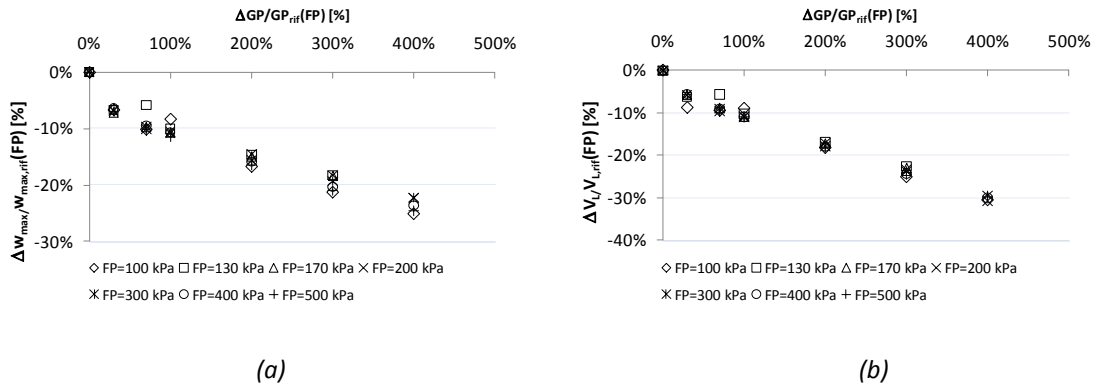


Fig. 4-23. Grout pressure (GP) effects on maximum surface settlement (a) and on surface volume loss (b): dimensionless graphs

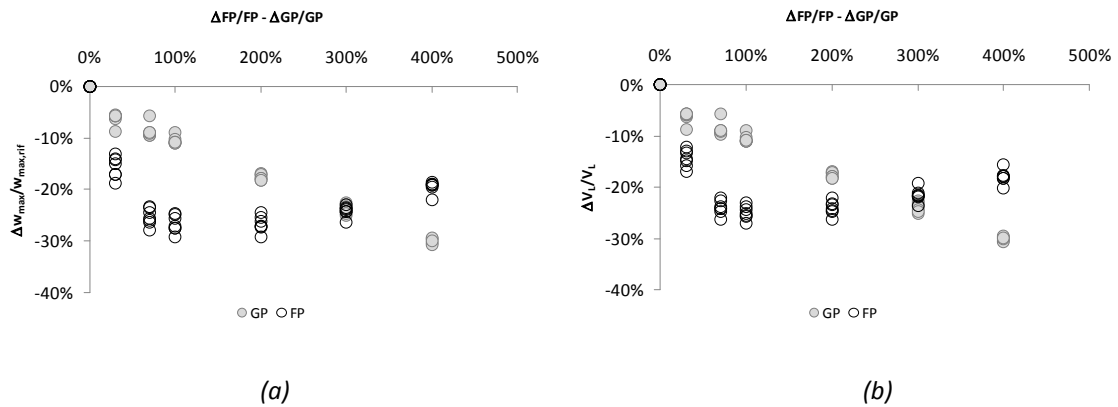


Fig. 4-24. Comparison between the grout pressure (GP) and front pressure (FP) effects on maximum surface settlement (a) and surface volume loss (b)

Trying to resume the informations collected up to now, figures below represent the effects of the pressures ratio GP/FP, on w_{max} and V_L variations. Linear relationships can be identified (Fig. 4-26).

As Fig. 4-26 show the pressures ratio influence on the surface subsidence is more pronounced on the volume loss ($\Delta w_{max}/w_{max,rif} = -25\%$) rather on the settlement ($\Delta w_{max}/w_{max,rif} = -30\%$) and a sort of linear effect can be detected, in a range of values defined by the minimum and maximum front pressure values.

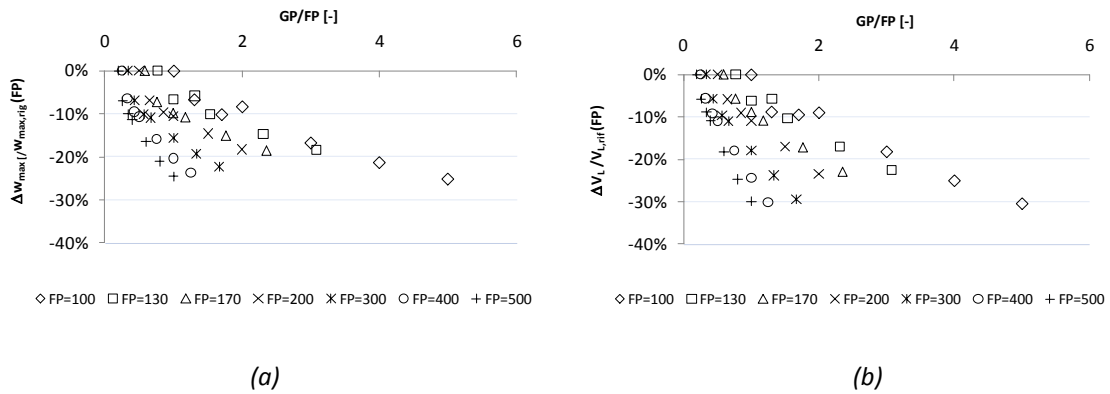


Fig. 4-25. Relation between the front than the grouting pressure ratio, the surface settlement (a) and volume loss (b)

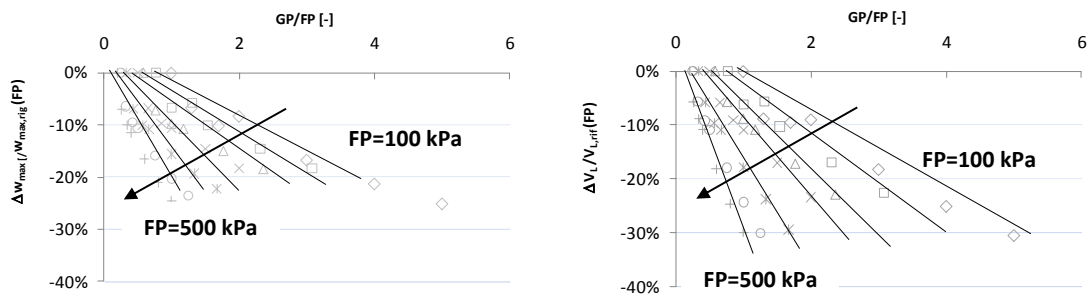


Fig. 4-26. Influence of the grouting than the front pressure ratio on surface volume loss and maximum settlement

4.3.4. Back-analysis of observed effects of Line 6 tunnelling

In order to perform a back-analysis of the observed Line 6 tunnelling effects the geometric model, the material properties for the loose soil layer and the Tuff bedrock described in *Section 4.3.1* were used.

In defining the analyses calculation steps, the real construction process was simulated and the *volume loss* or *contraction method* was used. In such a way, 13 calculation “*Staged construction*” (Tab.4-6) phases have been defined as to reproduce about 100 m tunnel excavation length, respecting the real excavation process.

In each phase the same procedure to simulate the tunnel construction process is repeated by:

- deactivating the soil clusters inside the tunnel lining and draining the water within the EPB shield
- activating the shell elements representing the EPB shield behind the tunnel face
- applying the concrete properties to the clusters representing the installed final lining
- applying the face and the grout pressure to prevent the tunnel collapse, and the forces the hydraulic jack driving the EPB machine exert on the already installed lining (Fig. 4-27)
- modelling the soil-tunnel interaction by assigning modified properties, with reduced strength parameters, to loose soils and tuff in the slices where the tunnel has already been built, by means of $R_{inter} < 1$ parameter
- defining a tunnel contraction.

STEP	FRONT		FINAL LINING	
	Plane ID	Plane position [m]	Plane ID	Plane position [m]
1	H	-36.90	C	-28.40
2	I	-38.60	D	-30.10
3	K	-42.00	F	-33.50
4	N	-47.10	I	-38.60
5	R	-53.90	M	-45.40
6	V	-60.70	Q	-52.20
7	X	-64.10	S	-55.60
8	AB	-70.90	W	-62.40
9	AG	-79.40	AB	-70.90
10	AH	-81.10	AC	-72.60
11	AK	-86.20	AF	-77.70
12	AP	-94.70	AK	-86.20
13	AS	-99.80	AN	-91.30

Tab.4-6. 13 “staged construction” phases defined for Plaxis simulation

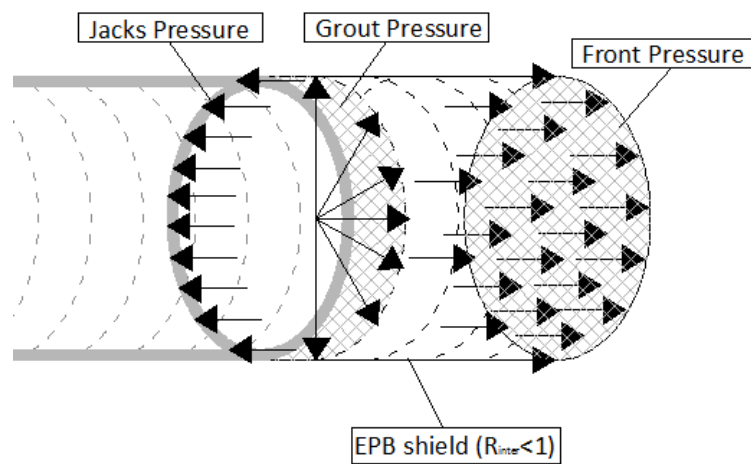


Fig. 4-27. EPB pressures on the tunnel face (Front Pressure), around the cavity (Grout Pressure) and on the final lining (Jack Pressure)

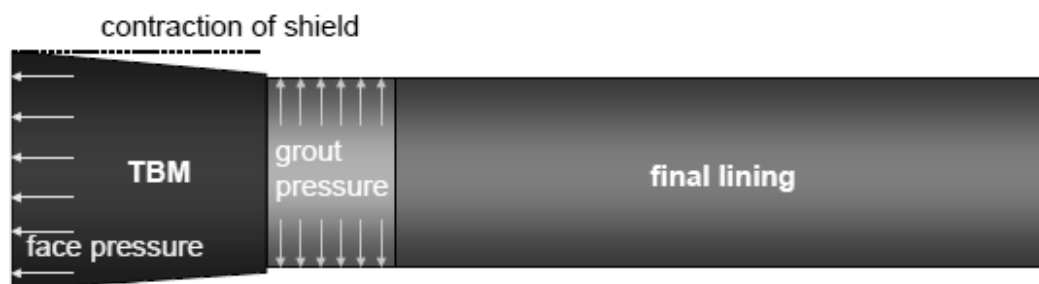


Fig. 4-28. Construction stages of a tunnel shield

For each defined calculation step the gap between the tunnel face and the last installed lining segments was kept equal to the machine length (8.5 m). Except from the first slice next to the last mounted lining segment, where the grout pressure is applied, the EPB shield was installed by activating shell elements all along the slices included in the gap, in order to prevent the tunnel cable collapse. Fig. 4-28 schematically shows the procedure for defining each staged construction phase.

In order to reduce the influence of boundary conditions on the excavation process, 25 m of tunnel have been excavated at the start of the model and the tunnelling induced displacements have been set to zero before the first calculation phase of the observed tunnel construction process started. Fig. 4-29 depicts a generic calculation step.

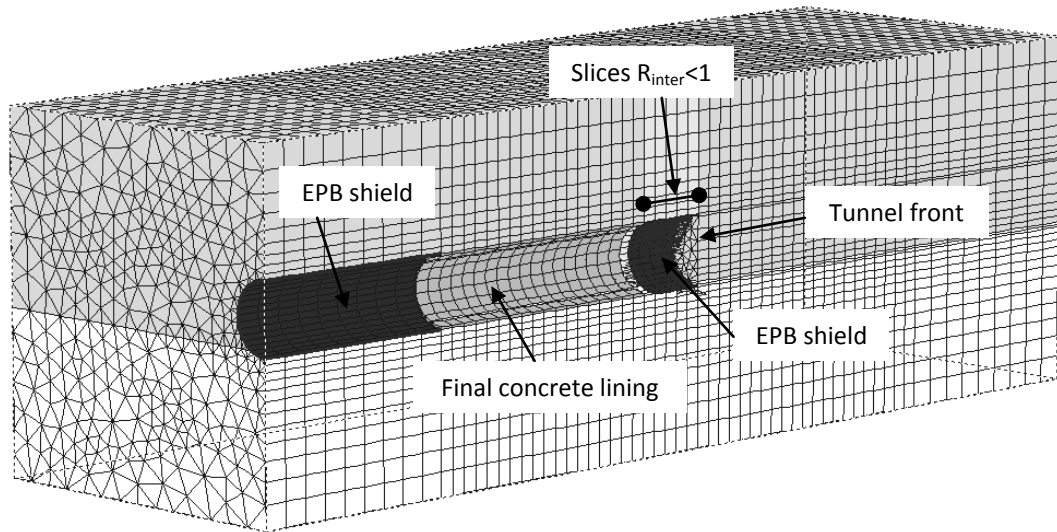


Fig. 4-29. 3D plot of a generic input phase

Both the front and grouting pressure linearly increase with depth; starting from a reference pressure values at the tunnel crown, a gradient of 14 kPa (the specific weight of the bentonite used for supporting the face) was defined for the front pressure and of 20 kPa (depending on the used mixture for the mortar injections) for the grouting pressure. Contrariwise the hydraulic jacks pressure on the final lining is not depth dependent; a constant value is defined, related to the applied front pressure.

The monitoring data collected during the tunnel excavation have been resumed in *Chapter 3*. The landmarks sections on the ground surface have been used to calibrate the model. As discussed in the chapter expressly dedicated to the monitoring data analysis, up to August the 31st 45 ground landmarks sections were installed along Via Piedigrotta, following the tunnel track; according to the maximum measured settlements, such sections were collected into the groups resumed in the table below.

GROUP	ID	W_{max} [mm]
1	AT01 – SP01 (zone A)	5 ÷ 8
	AT12 – AT16 (zone B)	
	AT18 – AT19 (zone B)	
	AT26 (zone B)	
2	AT02 – AT10 (zone A)	8 ÷ 14
	AT17 (zone B)	
	AT25 (zone B)	
	SC01 (zone B)	
3	AT11 (zone B)	≤ 5
	AT20 – AT23 (zone B)	
	AT27 – AT42 (zone B - C)	
SINGULAR CASES	AT04 (zone A)	42.40
	AT24 (zone B)	62.30

Tab.4-7. Landmarks sections on the ground surface grouped according to the maximum measured settlement

As discussed in the previous sections, the machine applied pressures and the volume loss at the tunnel depth have a considerable influence on the tunnelling induced effects on the ground surface, the same goes for the volume loss imposed at tunnel depth.

While for the machine pressures the collected data, pointed out in Chapter 3 (*cf. Section 3.3.1.*), were used as to define the input values for the analyses, not any monitoring data about the volume loss at the ground surface nor at the tunnel depth is available. Referring to the parametric analyses results discussed in the previous sections, according to the soil stiffness parameters (*cf. Section 4.3.2.*), a 0.1% volume loss was considered an initial reliable value to impose at the tunnel depth. Nevertheless, since the geometric model for the analyses did not change (according to the reference section described in *Section 4.3.1.*- Fig. 4-11) and the effects to be reproduced are significantly different from each other, being the soil parameters and the machine pressures known and well defined, different values for the volume loss at the tunnel crown were needed in order to reproduce the different measured subsidence surface. Tab.4-8. resumes the final volume loss values to reproduce the observed displacements; the highest value was required to reproduce the Group 1 displacements and the lowest for the Group 3 ones. The obtained subsidence's are plotted in Fig. 4-30. Looking at the maximum settlement, the analyses results are in good agreement with the monitoring data in terms of maximum settlements reproduced, while a less accurate accordance results regarding the subsidence width, especially for the first group of data (Fig. 4-30_a), showing an abnormal

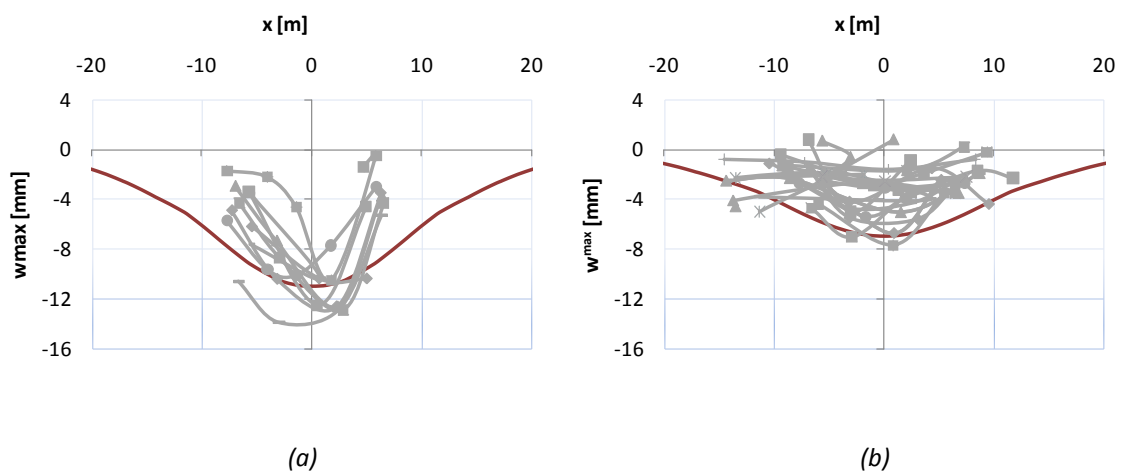
behaviour if compared to the remaining groups of sections. Anyway, such a result confirms the collected indications from literature about the difficulties in reproducing the subsidence width by means of numerical simulations.

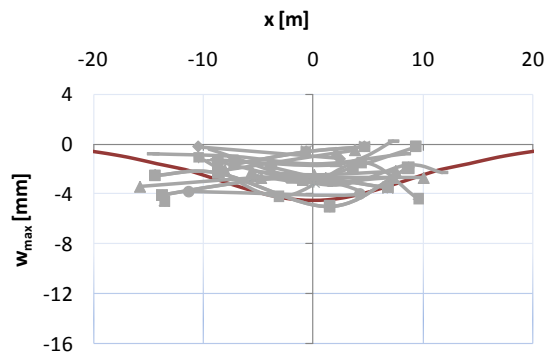
	GROUP 1 (AT01 – AT07)	GROUP 2 (AT09 – AT21)	GROUP 3 (AT27 – AT42)
Front Pressure [kPa]	150	190	240
Grouting Pressure [kPa]	160	150	370
Hydraulic Jacks Pressure [kPa]	877.6	999	1202
Volume loss at the tunnel depth	0.25 %	0.15%	0.10%
Volume loss at the ground surface	0.52%	0.34%	0.21%
Maximum obtained settlements [mm]	-11	-6.99	-4.53

Tab.4-8. Input and output parameters for the analyses reproducing the measured landmarks sections displacements

The analyses accuracy was confirmed also by comparing the obtained results to displacements in longitudinal direction. Fig. 4-31 shows how all the settlements longitudinal profiles for the three groups, belong to the range narrowed by monitoring data.

As shown in Fig. 4-32, for the analyzed case, the volume loss at the surface is always twice the volume loss at tunnel depth.





(c)

Fig. 4-30. Transversal subsidence surfaces obtained by the back-analyses for the three groups of sections: Group 1 (a), Group 2 (b) and Group 3 (c)

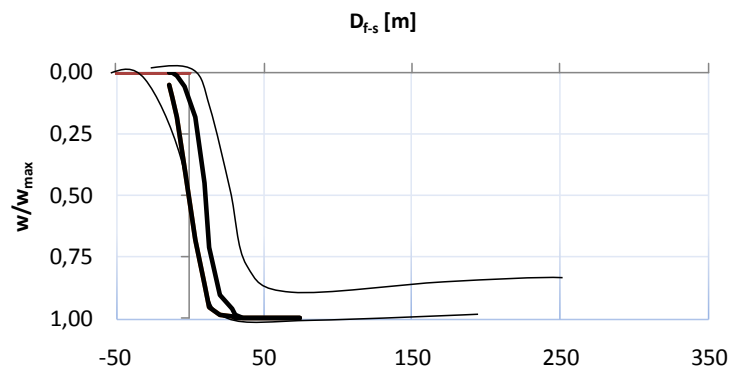


Fig. 4-31. Longitudinal displacements obtained by the back-analyses compared to the range defined by the collected monitoring data

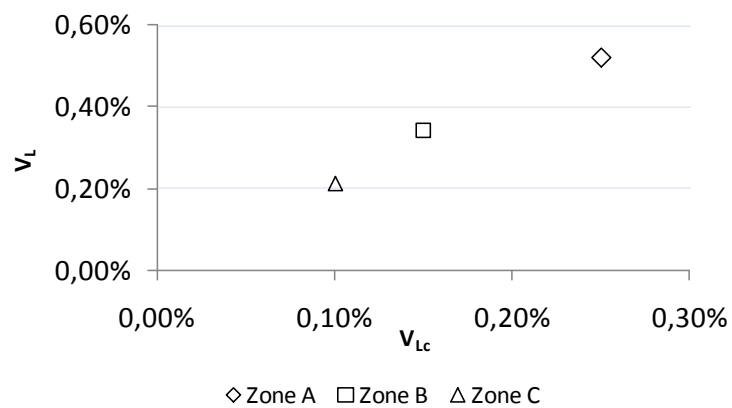


Fig. 4-32. Relation between the volume loss at the tunnel depth and the volume loss at the ground surface

CONCLUSIONS

Tunnelling in urban areas is of increasing importance over the past few decades. The lack of existing facilities, considering the continuously increasing demand in transports, asks for new solutions. In such a way deep excavations (tunnels and vertical shafts) started to spread even more throughout the urban areas, as to realize new underground lines. Because of the high urbanization of the largest cities, where such excavations take place, the prediction and the analyses of the induced effects, by means of analytical, numerical or sperimental methods, play an even more important role, in order to prevent distortions and, in severe cases, damage to the overlying buildings and services. The conventional design methods to assess the induced deformations on buildings are based on empiricism gained from Greenfield sites. Such methods lead to define the tunnelling induced displacement field in very simple hypothesis roughly accounting of the number of technological factors affecting the induced displacements. However literature data reveal that the role of the excavation technique is far from negligible. Indeed, an initial distinction between the effects induced by traditional and mechanical tunnelling methods can be defined. Moreover looking at the tunnel excavations realized by means of complex excavation machines, a significant reduction in the induced effects due to the excavation techniques improvement over the years has been revealed. Numerical analyses, by means of Finite Element codes, represent an useful tool to account for the excavation method in the design process, since they enable the whole excavation process. In this context, the objective of this thesis has been to assess the influence of technological factors on tunnelling induced displacements. This has been done from a numerical point of view by a parametric study aimed to investigate the role played factors. In a second stage of the research, the results have been used to back-analyze at the best the observed behavior, in terms of surface settlements, during the Line 6 tunnel excavation process. The availability of a huge amount of monitoring data, in terms of ground displacements and machine parameters (over all, front and grouting pressure) allowed to perform several 3D Finite Element Analyses by Plaxis 3D Tunnel.

Looking at the soil parameters influence, main results of the parametric studies can be summarized in the following:

1. as expected the soil stiffness mainly affects the volume loss and maximum settlement at the ground surface. Also, it influences the subsidence width in a lesser degree. Nevertheless an increase in the subsidence width is observed for increasing in such a modulus (by increasing the stiffness modulus the basin subsidence becomes wider)
2. the un-reloading to loading stiffness moduli ratio does not significantly affects the ground maximum settlement. An increase in the ratio leads to enlargement of the basin subsidence, thus increasing the volume loss (the higher is the un-reloading stiffness modulus with respect to the loading one, the more the ground subsidence becomes wider)
3. an increase in the soil unit weight leads to an increase in the maximum settlement and volume loss, and not in the subsidence width. On the contrary, significant decrease in such a parameter yields a shrinkage of the subsidence basin, thus reductions in both the volume loss and the maximum settlement
4. no clear relationships has been detected between the friction angle and the dilatancy angle with the volume loss nor with the maximum surface settlement; conversely, reductions in friction angle leads to a sort of linear increase in subsidence width, whereas the dilatancy effect is evident only above a certain value when the subsidence width suddenly increases.

Looking at the pressures effects on the surface volume loss and maximum settlement, the main considerations can be resumed in the ensuing. Clear relationships between such pressures and the induced surface volume loss and maximum settlement have been observed. In order to investigate the pressures' influence also at the tunnel depth, the volume losses at that locations were extrapolated, showing the noticeable influence played by low values of the front pressures due to a development of an active failure mechanism. On the contrary, with reference to the grouting pressure effects, results reveal the influence played only on surface volume losses. No effects were detected on the volume loss at the tunnel depth. To this point the main results can be resumed as follows:

1. a linear relationship between the grouting pressure and the effects on the ground surface can be defined, on the opposite side a non-linear but clear relation links the front pressure to the same effects

2. the positive effect of the front pressure on the induced displacements is evident up to a certain value of such a pressure, related to the front equilibrium, after which further increases leads to plasticization around the tunnel lining implying later growing in settlements and volume loss
3. the front pressure governs the tunnel front behaviour leading to active or passive failure mechanism, thus strongly affecting the displacements at the ground surface
4. the front pressure influence on both the volume loss and the maximum settlement at the ground surface, is much more pronounced than the grouting pressure one, up to a certain value, when the observed behaviour changes and the grouting pressure becomes more influent in reducing the tunnelling induced effects
5. looking at the pressures ratio, linear relationships with both the volume loss and settlement variations have been detected within a range defined by the minimum and maximum front pressure used.

Due to the large number of influencing factors on the observe behaviour (soil profile, soil properties, constitutive laws, machine parameters, etc.), the back-analysis has been performed necessarily fixing some of the above factors, and changing the others.

For the analyses presented in this thesis, the Hardening Soil Model was used to numerically simulate the excavation process. The input values of the soil parameters were determined from geotechnical investigation. The used machine parameters came from continuously monitored and recorded data. Thus, the values of volume loss at tunnel depth were defined, and a surface settlement along the tunnel axis was reproduced.

As general conclusion, it seems reasonable to state that the design of tunnel cannot neglect (as usually done) technological factors, which have a strong influence on the tunnelling induced settlement.

In other words, good soil modelling coupled with advances numerical analyses, could give wrong results if technological aspects (grouting and front pressures) are not well considered at design stage and not well implemented at construction stage. A good design is based on a “right” balance of all above.

REFERENCES

- Attewell, P. B. (1978). Ground movements caused by tunnelling in soil. *Pages 812-948 of: Large ground movements and structures*. Pentech Press, London.
- Attewell, P. B., Yeates, J. and Selby, A. R. (1986). *Soil movements induced by tunnelling and their effects on pipelines and structures*. Blackie, Glasgow.
- Attewell, P.B. and Selby, A.R. (1989). Tunnelling in compressible soils: Large ground movements and structural implications. *Tunnelling and Underground Space Technology*, 4 (4)
- Attewell, P. B. and Woodman, J.P. (1982). Predicting the dynamics of ground settlement and its derivatives caused by tunnelling in soil. *Ground Engineering*, 15 (8), 13-22.
- Bloodworth A. G. (2002). *Three-dimensional analysis of tunnelling effects on structures to develop design methods*. Thesis (PhD). University of Oxford.
- Broms, B. B. and Bennermark, H. (1967). Stability of clay in vertical openings. *Journal of Soil Mechanics and Foundations, ASCE*, 193, 71-94.
- Davis, E. H., Gunn, M. J., Mair, R. J. and Seneviratne, H. N. (1980). The stability of shallow tunnels and underground openings in cohesive material. *Géotechnique*, 30(4), 397-416.
- Franzius, J. N. (2003). *Behaviour of buildings due to tunnel induced subsidence*. Thesis (PhD). Imperial College, University of London.
- Lake, L. M., Rankin, W. J. and Hawley, J. (1992). *Prediction and effects of ground movements caused by tunnelling in soft ground beneath urban areas*. CIRIA Funders Report / CP / 5.
- Macklin, S. R. and Field, G. R. (1999). The response of London clay to full-face TBM tunnelling at West Ham, London. *In: Proc. Int. Conf. On Urban Ground Engineering*, Hong Kong, 11-12 November 1998. London: Thomas Telford
- Mair, R. J. (1979). *Centrifugal modelling of tunnel construction in soft clay*. Thesis (PhD). University of Cambridge.

- Mair, R. J. and Taylor, R. N. (1993). Prediction of clay behaviour around tunnel using plasticity solutions. *In: Predictive Soil Mechanics: Proc. Wroth Memorial Symposium*, Oxford, 27-29 July 1992. London: Thomas Telford, 449-463.
- Morton, K. and Au, E. (1975). Settlement observation on eight structures in London. *In: Proc. Conf. Settlement of Structures*, Cambridge, April 1974. London: Pentech Press, 183-203.
- O'Reilly, M. P. and New, B. (1982). Settlements above tunnels in the United Kingdom – their magnitude and prediction. *In. Proc. Int. Symposium Tunnelling '82*, London: 7-11 June. London: Institution of Mining and Metallurgy, 173-181.
- Nyren, R. J. (1998). Field measurements above twin tunnels in London clay. Thesis (PhD). Imperial College, University of London.
- Peck, R. B. (1969). Deep excavation and tunnelling in soft ground. *In: Proc. 7th ICSMFE, State-of-the-art Volume*, Mexico City. Mexico: Sociedad Mexicana de Mecànica de Suelos, 225-290.
- Peck & Schmid (1960)
- Simons, N. E. and Som, N. N. (1970). *Settlements of structures on clay with particular emphasis on London clay*. CIRIA Report 22.

APPENDIX

APPENDIX II

SITE AND LABORATORY INVESTIGATIONS

INVESTIGATION CAMPAIGN 1990

BOREHOLE	GROUND LEVEL	DEPTH	SAMPLES	SPT	GROUNDWATER		TUFF	
	[m a.m.s.l.]				[m]	[N°]	[m a.m.s.l.]	[m]
B52	2.3	17.00		5				
B54	2.3	30.00		5			24.20	-21.90
S176	2.28	25.50	3	4				
B55	2.28	25.00	1	3				
S194	2.26	36.00	1	3			31.50	-29.24
B56	2.26	31.00		3				
B190	2.4	40.00	2	4			36.20	-33.80
S114	2.55	38.00	3	4			33.00	-30.45
B81	2.7	25.00	2	5				
B40	3.2	25.00						
B84	3.15	25.00	1	1			9.00	-5.85
S220	3.3	20.20		4	3.4		14.50	-11.20
B85	3.2	25.00	1	3			18.00	-14.80
S222	3.18	29.00		7	3.4		24.00	-20.82
B86	3.2	25.00	1	5				
S227		31.00	1	8	1.8			
B87	3.4	25.00	1	5				
S196	2.3	39.50	2	4				
S197	2.3	39.50		5				
S198	2.3	45.00	1	5			40.20	-37.90
S199	2.3	45.00	1	5			38.50	-36.20
B88	3.4	25.00	1	5				
B89	3.4	26.50	1	5				
B90	3.6	25.00	2	5				
B91	3.7	26.00	2	5				
S211	3.6	50.00		5				
S208	3.6	50.00	1	5				
S200	3.6	50.00		5				
S210	3.6	50.00		5				
A3	3.302	7.00			2.2			
A1	3.329	15.50			2.5			
S101	3.6						36.90	-33.30
B1	3.329			6	3.3		28.50	-25.17
A4	3.518	7.00			2.6			
S102	3.64						25.20	-21.56

B2	3.812	25.00		5		5	20.00	-16.19
B3	3.891	20.00				3	15.50	-11.61
S106	5.03					3.6	11.90	-6.87
A5	5.426	14.00				4	7.00	-1.57
B4	4.687	12.00				4.5	4.00	0.69
A6	5.02	15.00				3.8	3.00	2.02
B5	5.349	11.00				3	3.00	2.35
S103	3.66	26.00				3	18.40	-14.74
S105bis	6.23	40.80				4.5	36.50	-30.27
S104	3.7	20.40				3.1	17.80	-14.10

Tab.II-1. Site investigation from 1990

CPT	GROUND LEVEL [m a.m.s.l.]	DEPTH [m]
CPT 82	3	29.20
CPT 83	3.2	29.20
CPT 86	3.2	25.00
CPT 88	3.4	24.20
CPT 90	3.6	24.80

Tab.II-2. CPT from the site investigation campaign in 1990

BOREHOLE	N°	DEPTH [m]	SOIL	W	γ [kN/m ³]	S	γ_s [kN/m ³]	K [cm/sec]	TESTS	σ'_3 [kPa]	$\sigma_1-\sigma_3$ [kPa]
S176	1	7.25	SAND	0.362	17.1	0.941	12.55		TRIAXIAL	75	536
		7.25		0.63	15.43	0.863	10.55			150	751
		7.25		0.389	15.53	0.908	11.89			300	1402
S176	2	16.25	PIROCLASTITI	0.38	15.94	0.943	12.27		TRIAXIAL	150	886
		16.25		0.382	17.05	0.958	12.23			300	1624
		16.25		0.384	17.88	0.963	12.34			450	2117
S176	3	22.25	PIROCLASTITI	0.302	17.83	0.943	13.7				
		22.25		0.379	16.76	0.918	12.16		TRIAXIAL	200	909
		22.25		0.379	16.89	0.911	12.1			350	1476
		22.25		0.386	16.4	0.887	11.84			500	1851
B55	1	15.75	PIROCLASTITI	0.491	16.52	0.993	11.08				
PP55	1	8.45	CINERITE	0.495	16.64	1	11.13				
		8.45		0.471	16.6	0.975	11.29		TRIAXIAL	80	367
		8.45		0.477	16.49	0.968	11.16			150	793
		8.45		0.491	16.51	0.983	11.07			300	1602
S194	1	26.3	PIROCLASTITI	0.276	17.55	0.88	13.75				
		26.3		0.288	17.38	0.878	13.49		TRIAXIAL	200	1225
		26.3		0.271	17.87	0.91	14.05			300	1699
		26.3		0.27	17.66	0.883	13.9			400	2233
S190	1	8.7	CINERITE	0.324	18.05	1	13.63				
		8.7		0.325	18.03	1	13.6		TRIAXIAL	100	404

APPENDIX

		8.7		0.309	18.21	1	13.9			200	846
		8.7		0.337	17.87	0.995	13.36			300	1177
	2	23.3	PIROCLASTITI	0.468	15.81	0.902	10.77		TRIAXIAL	200	859
		23.3		0.457	16.32	0.947	11.2			300	1602
		23.3		0.434	16.24	0.917	11.32			400	1890
S114	1	5.25	SAND	0.299	17.45	0.791	13.44				
	2	23.3	PIROCLASTITI	0.587	14.02	0.811	8.83				
	3	30.45	PIROCLASTITI	0.312	16.22	0.749	12.36				
		30.45		0.323	16.66	0.803	12.6		TRIAXIAL	300	1554
		30.45		0.362	16.47	0.833	12.89			400	1922
		30.45		0.371	16.79	0.874	12.25			500	2259
B81	2	20.25	PIROCLASTITI	0.561	15.41	0.936	9.87				
		20.25		0.523	15.8	0.95	10.37		TRIAXIAL	200	876
		20.25		0.536	15.76	0.955	10.27			350	1453
		20.25		0.756	15.02	1	8.56			500	2044
B82	2	15.3	PIROCLASTITI	0.532	15.13	0.882	9.87				
		15.3		0.512	15.85	0.941	10.48		TRIAXIAL	100	492
		15.3		0.562	15.64	0.955	10.02			250	1046
		15.3		0.489	16.04	0.942	10.77			400	1659
		15.3		0.631	15.62	0.997	9.58		TRIAXIAL	100	384
		15.3		0.602	15.61	0.979	9.74			250	842
		15.3		0.604	15.71	0.99	9.79			400	1290
	3	20.225	PIROCLASTITI	0.542	16.18	0.998	10.49				
		20.225		0.526	15.83	0.949	10.37		TRIAXIAL	200	845
		20.225		0.498	16.01	0.947	10.69			350	1237
		20.225		0.517	15.9	0.95	10.48			500	1868
B83	1	15.25	PIROCLASTITI	0.292	16.32	0.762	12.63				
		15.25		0.339	15.92	0.782	11.89		TRIAXIAL	150	699
		15.25		0.288	16.01	0.726	12.43			300	1300
		15.25		0.331	16.05	0.786	12.06			450	1954
B84	1	6.75	CINERITE	0.378	16.72	0.866	12.13	1.6E-03			
B85	1	15.25	CINERITE	0.218	19.51	1	16.02		TRIAXIAL	100	616
		15.25		0.211	19.61	1	16.2			250	1339
		15.25		0.235	19.25	1	15.58			400	2273
B86	1	14.2	SAND	0.321	17.52	0.843	13.27	1.4E-05			
B87	1	11.45	SAND	0.489	16.38	0.924	11	7.0E-03			
S196	1	15.75	SAND	0.231	19.24	0.938	15.63				
		15.75		0.23	19.49	0.967	15.85		TRIAXIAL	150	968
		15.75		0.233	19.55	0.984	15.85			300	1674
		15.75		0.231	19.51	0.975	15.84			450	2497
	2	23.7	PIROCLASTITI	0.361	17.43	0.956	12.81				
		23.7		0.374	16.78	0.9	12.21		TRIAXIAL	200	686
		23.7		0.366	17.14	0.93	12.55			300	997
		23.7		0.351	17.08	0.905	12.65			400	1350
S198	1	24.75	PIROCLASTITI	0.348	17.11	0.897	12.69				
		24.75		0.356	17.22	0.919	12.71		TRIAXIAL	200	714
		24.75		0.354	17.15	0.908	12.67			300	1003
		24.75		0.342	17.25	0.905	12.86			400	1536
B88	1	10.2	SAND	0.267	18.72	1	14.78	3.7E-05			

B90	1	10.3	SAND	0.265	19.04	0.902	15.05	3.4E-03		
	2	20.15	SAND	0.41	16.71	0.917	11.85	3.7E-05		
B91	1	5.2	SAND	0.307	16.78	0.757	12.84	1.8E-03		
S208	1	25.75	PIROCLASTITI	0.335	17.32	0.927	12.97			
		25.75		0.347	17.29	0.94	12.84			
		25.75		0.461	16.73	0.994	11.45			
		25.75		0.449	16.77	0.989	11.58			

Tab.II-3. Laboratory tests on loose soils from investigation campaign in 1990

INVESTIGATION CAMPAIGN 1998 - 2000

BOREHOLE	GROUND LEVEL [m a.m.s.l.]	DEPTH [m]	SAMPLES	SPT	GROUNDWATER		TUFF	
					[m a.m.s.l.]	[m]	[m]	[m a.m.s.l.]
T0	22.5	29.8		8	5.5	17		
T1	22.3	30		8	4.8	17.5		
T2	25	30		8	5.5	19.5		
T3	24	30		8	6	18		
P0	2.7	31		5	1.7	1	30.5	-27.8
P1	2.1	34.5		5	1	1.1	30.7	-28.6
P2	2.2	35.5		6	1.1	1.1	30.4	-28.2
P3	2.6	35		6	0.9	1.7		
P4	2.6	35		6	0.9	1.7		
P5	2.6	59			1.1	1.5	41.5	-38.9
F1	14.6	40			0.8	13.8	5.8	8.8
F2	14.8	40			0.9	13.9	7.8	7
F3	41.5	60			1.5	40	18.9	22.6
F4	35.2	60			1.7	33.5	17.6	17.6
F5	30.7	40			1.7	29	16	14.7
F6	23.7	30			-1.3	25	14.2	9.5
F7	19	40			4	15	16	3
F8	16.3	50			2.8	13.5	13.3	3
F9	21.8	26.5					23.5	-1.7
F10	20	19.1					13	7
F11	19.1	18.2					14	5.1
F12	23.5	15.5			11.8	11.7	10.2	13.3
F13	32.2	28.7					22.9	9.3
F14	10.8	12.5					8	2.8

Tab.II-4. Site investigation between 1998 and 2000

CPT	LOCATION	GROUND LEVEL [m a.m.s.l.]	DEPTH [m]
PP0	Arco Mirelli	2.70	32
PP1	Arco Mirelli	2.10	32
PP2	Arco Mirelli	2.20	25.2
PP3	San Pasquale	2.60	35
PP4	San Pasquale	2.60	35
PP5	San Pasquale	2.60	43.60

Tab.II-5. CPT from the site investigation campaign between 1998 and 2000

PIEZOMETER	LOCATION	GROUND LEVEL [m a.m.s.l.]	DEPTH [m]	GROUNDWATER LEVEL	
				[m a.m.s.l.]	[m]
Ma	Riviera di Chiaia - Via Arco Mirelli	2.00	29.20	0.8	1.20
Mb	Vico delle fiorentine a Chiaia	11.70	40	10.30	1.40
Mc	Via Andrea d'Isernia	24.30	40	22.30	2.00
Sa	Riviera di Chiaia - Rone Sirignano	2.30	40	1.28	1.02
Sb	fine Rione Siringano	6.80	20	5.35	1.45
Sc	Via Martucci - Gradini dei Nobili	17.30	22	15.44	1.86
Ca	Riviera di Chiaia - Via Carducci	2.30	10	1.31	0.99
Cb	Via Carducci - Via Cuoco	5.20	14	4.18	1.02
Cc	Via Carducci - Via Torelli	10.00	50	9.04	0.96
Cd	Via Carducci - Via dei Mille	17.25	50	15.85	1.40
Va	Riviera di Chiaia - via Satriano	2.50	57	1.94	0.56
Vb	Via Bisignano -Vico Sospiri	7.40	30	6.32	1.08
Vc	Via Bisignano -via Cavallerizza	10.40	30	9.38	1.02

Tab.II-6. Piezometers from the site investigation campaign between 1998 and 2000

BOREHOLE	TESTING STRETCH [m below ground level]	SOIL	K [cm /sec]
P1	18.50 - 20.00	PIROCLASTITI	2.76E-05
P2	10.70 - 11.70	SAND	1.22E-05
P2	14.40 - 16.30	PIROCLASTITI	6.11E-05
P2	21.50 - 23.00	PIROCLASTITI	2.16E-05
P3	9.00 - 10.00	SAND	5.81E-05
P3	15.00 - 16.50	SAND	1.03E-04
P3	21.50 - 23.00	PIROCLASTITI	6.41E-05
P4	9.00 - 10.00	SAND	8.37E-05
P4	14.60 - 16.50	SAND	4.99E-05
P4	21.00 - 22.50	PIROCLASTITI	5.19E-06
P5	15.50 - 16.20	SAND	6.40E-05
P5	22.00 - 23.00	SAND	6.43E-06
P5	42.00 - 44.00	TUFF	2.14E-05
F1	13.00 -14.50	TUFF	1.03E-04
F1	19.20 - 21.00	TUFF	6.46E-05
F2	14.00 - 15.50	TUFF	1.07E-04
F2	20.00 - 21.00	TUFF	2.59E-04

Tab.II-7. Permeability tests (Lefranc) from the site investigation campaign 1998 - 2000

BOREHOLE	SAMPLE	DEPTH [m]	γ [kN/m ³]	γ_s [kN/m ³]	UNIAXIAL COMPRESSIVE STRENGTH
					[MPa]
F6	1	14.00-14.35	1.62	1.32	3.86
	2	14.35-14.72	1.60	1.31	3.96
	3	15.00-15.39	1.70	1.38	4.65
	4	19.50-19.90	1.73	1.41	5.06
	5	19.90-20.25	1.71	1.40	5.89
	6	21.20-21.50	1.69	1.39	7.16
	7	21.50-21.80	1.78	1.42	7.2
	8	22.00-22.30	1.76	1.38	8.99
	9	22.30-22.70	1.73	1.43	8.62
	10	23.75-23.95	1.67	1.41	3.63
	11	25.65-26.00	1.76	1.40	4.55
	12	28.35-28.70	1.71	1.38	2.78
	13	29.30-30.00	1.71	1.38	4.12
F1	1	10.10-10.50	1.71	1.39	5.69
	2	10.70-11.20	1.74	1.38	5.87
	3	11.40-11.85	1.70	1.40	5.11
	4	14.00-14.50	1.70	1.41	5.83
	5	16.70-17.00	1.71	1.41	7.13
	6	19.32-19.62	1.66	1.38	3.71
	7	22.30-22.70	1.68	1.40	4.17
	8	23.03-23.38	1.77	1.40	3.51
	9	24.00-24.29	1.69	1.37	3.24
	10	25.60-26.00	1.72	1.40	2.95
	11	27.80-28.01	1.77	1.39	3.80
	12	28.75-29.05	1.65	1.38	2.78
	13	31.00-31.65	1.70	1.38	4.08
	14	33.30-33.60	1.75	1.40	5.74
	15	35.50-35.80	1.78	1.42	3.23
F2	1	17.75-18.00	1.62	1.32	2.58
	2	19.00-19.22	1.60	1.31	3.17
	3	23.30-23.60	1.56	1.36	1.90
	4	23.80-24.15	1.67	1.37	3.19
	5	24.15-26.25	1.62	1.35	2.46
	6	26.25-26.55	1.79	1.38	4.40
	7	26.55-26.85	1.71	1.38	4.13
	8	27.00-27.31	1.78	1.39	4.59
	9	29.50-29.81	1.77	1.39	5.00
	10	30.10-30.50	1.74	1.40	8.86
	11	30.80-31.28	1.69	1.40	3.03
	12	32.77-33.20	1.71	1.35	1.96

Tab.II-8. Laboratory tests on Tuff from investigation campaign in 1998 -2000

INVESTIGATION CAMPAIGN 2005

BOREHOLE	GROUND LEVEL [m a.m.s.l.]	DEPTH [m]	SPT	GROUNDWATER [m a.m.s.l.]	TUFF	
					[m]	[m a.m.s.l.]
S1	2.13	45.0	10	1.2	33.20	-31.07
S2	2.08	40.5	8	1.2	30.50	-28.42
SG1	2.11	37	9	1.2	29.20	-27.09
SG2	2.13	37.40	8	1.2	32.40	-30.27
SG3	2.12	35	7	1.2	30.90	-28.78
SG4	2.16	35	8	1.2	30.70	-28.54
SG5	2.41	40	9	1.2	34.80	-32.39
SG6	2.23	35.80	7	1.2	30.70	-28.47
SG7	2.04	35	8	1.2	29.70	-27.66
SG8	2.09	34	8	1.2	29.30	-27.21

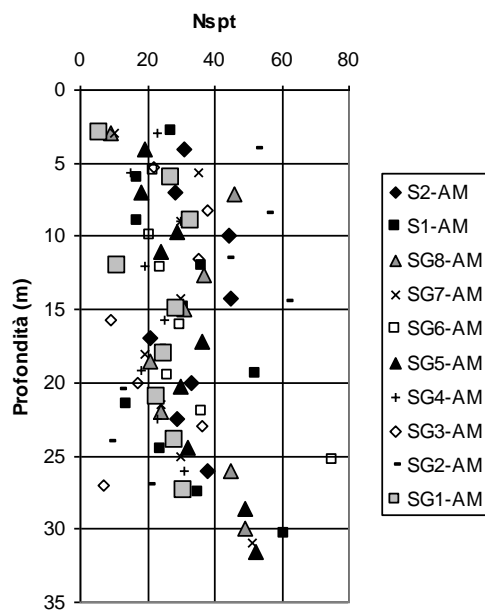
Tab.II-9. Arco Mirelli Station: site investigation in 2005

BOREHOLE	GROUND LEVEL [m a.m.s.l.]	DEPTH [m]	SPT	GROUNDWATER [m a.m.s.l.]	TUFF	
					[m]	[m a.m.s.l.]
S1	2.23	44.5	8	1.2	34.2	-31.97
S2	2.06	45	9	1.2	41	-38.94
SG1	2.27	45	9	1.2	40.7	-38.43
SG2	2.27	49	9	1.2	44.5	-42.23
SG3	2.27	52.5	9	1.2	47.5	-45.23
SG4	2.29	43	8	1.2	38	-35.71
SG5	2.03	41	8	1.2	36	-33.97
SG6	2.37	45		1.2	40	-37.63
SG7	2.29	41.5	8	1.2	36.5	-34.21
SG8	2.01	50	9	1.2	45.5	-43.49

Tab.II-10. San Pasquale Station: site investigation in 2005

BOREHOLE	GROUND LEVEL [m a.m.s.l.]	DEPTH [m]	SPT	GROUNDWATER [m a.m.s.l.]	TUFF	
					[m]	[m a.m.s.l.]
S1						
S1bis		35	2		16	
S2		26	6		21.5	
S3		15	3			
S4		15	3			
SG1		27	5		22.5	
SG2		22	5		17.10	

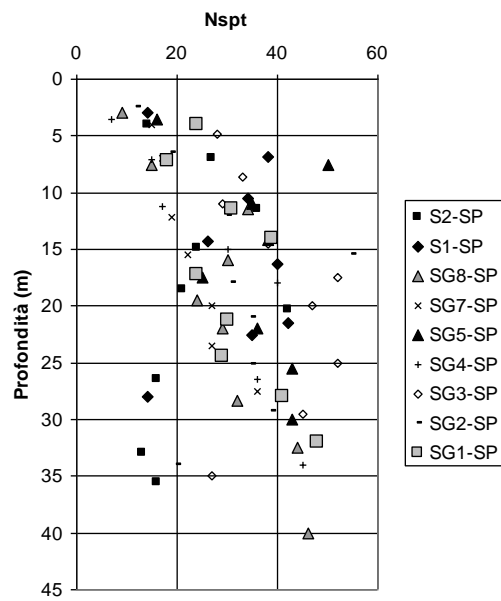
Tab.II-11. Chiaia Station: site investigation in 2005



Tab.II-12. Arco Mirelli Station: SPT from the site investigation campaign in 2005

BOREHOLE	TESTING STRETCH [m a.m.s.l.]	SOIL	K [cm/sec]
S1	33.50-35.50	TUFF	1.93E-05
S1	35.50-37.50	TUFF	7.87E-06
S1	37.80-39.80	TUFF	8.67E-06
S1	40.30-42.30	TUFF	1.42E-04
S1	42.50-44.50	TUFF	1.23E-04
S2	30.50-32.50	TUFF	3.15E-06
S2	32.50-34.50	TUFF	4.50E-07
S2	34.50-36.50	TUFF	8.84E-07
S2	36.50-38.50	TUFF	1.33E-06
S2	38.50-40.50	TUFF	1.68E-06

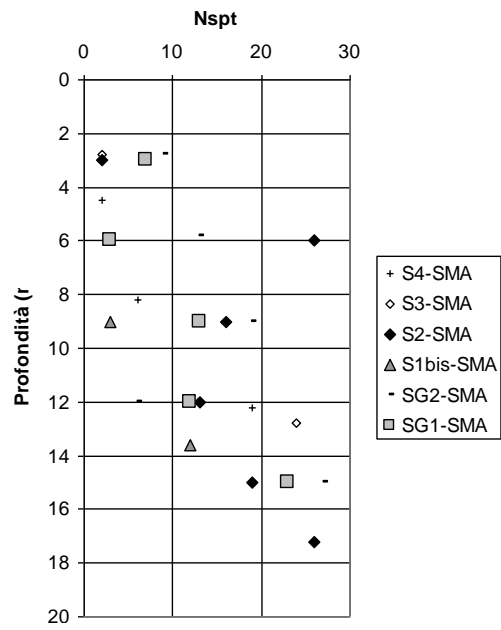
Tab.II-13. Arco Mirelli Station: permeability tests (Lugeon) from the site investigation campaign in 2005



Tab.II-14. San Pasquale Station: SPT from the site investigation campaign in 2005

BOREHOLE	TESTING STRETCH [m a.m.s.l.]	SOIL	K [cm /sec]
S1	34.00-36.00	TUFF	1.66E-04
S1	36.20-38.20	TUFF	1.53E-05
S1	38.50-40.50	TUFF	4.38E-05
S1	40.30-42.50	TUFF	4.22E-05
S1	42.50-44.50	TUFF	5.18E-05
S2	41.50-43.50	TUFF	8.40E-05
S2	43.50-45.50	TUFF	2.03E-05
S2	45.50-47.50	TUFF	2.28E-05
S2	47.50-49.50	TUFF	3.86E-05

Tab.II-15. San Pasquale Station: permeability tests (Lugeon) from the site investigation campaign in 2005



Tab.II-16. Chiaia Station: SPT from the site investigation campaign in 2005

APPENDIX III

	DATE	EXCAVATION [m]	TUNNEL PRODUCTION/ DAY [m]	TOTAL TUNNEL PRODUCTION [m]	LINING SEGMENTS [m]	N° LINING SEGMENTS/DAY [m]	N° TOTAL LINING SEGMENTS [m]
APRIL	7-apr-10	292.90	-	-	283.65	1	1
	8-apr-10	294.60	1.70	1.70	283.65	0	1
	9-apr-10	296.30	1.70	3.40	287.05	2	3
	12-apr-10	298.00	1.70	5.10	288.75	1	4
	13-apr-10	301.40	3.40	8.50	292.90	2	6
	14-apr-10	303.10	1.70	10.20	294.60	1	7
	15-apr-10	304.80	1.70	11.90	296.30	1	8
	16-apr-10	308.20	3.40	15.30	299.70	2	10
	19-apr-10	313.30	5.10	20.40	304.80	3	13
	20-apr-10	320.10	6.80	27.20	311.60	4	17
	21-apr-10	326.90	6.80	34.00	318.40	4	21
	22-apr-10	330.30	3.40	37.40	321.80	2	23
	23-apr-10	330.80	0.50	37.90	322.30	0	23
	26-apr-10	337.10	6.30	44.20	328.60	4	27
	27-apr-10	345.60	8.50	52.70	337.10	5	32
	28-apr-10	352.40	6.80	59.50	343.90	4	36
	29-apr-10	360.90	8.50	68.00	352.40	5	41
	30-apr-10	367.70	6.80	74.80	359.20	4	45
	30-apr-10	367.70	0.00	74.80	359.20	0	45
	MAY	3-mag-10	376.20	8.50	83.30	367.70	5
3-mag-10		379.60	3.40	86.70	371.10	2	52
4-mag-10		383.00	3.40	90.10	374.50	2	54
5-mag-10		386.40	3.40	93.50	377.90	2	56
6-mag-10		389.80	3.40	96.90	381.30	2	58
7-mag-10		391.50	1.70	98.60	383.00	1	59
10-mag-10		401.70	10.20	108.80	393.20	6	65
11-mag-10		411.90	10.20	119.00	403.40	6	71
12-mag-10		418.70	6.80	125.80	410.20	4	75
13-mag-10		432.30	13.60	139.40	423.80	8	83
14-mag-10		437.40	5.10	144.50	428.90	3	86
17-mag-10		445.90	8.50	153.00	437.40	5	91
18-mag-10		457.80	11.90	164.90	449.30	7	98
19-mag-10		466.30	8.50	173.40	457.80	5	103
20-mag-10		473.10	6.80	180.20	464.60	4	107
21-mag-10		478.20	5.10	185.30	469.70	3	110
24-mag-10		486.70	8.50	193.80	478.20	5	115
25-mag-10		488.33	1.63	195.43	479.83	1	116
26-mag-10		496.83	8.50	203.93	488.33	5	121
27-mag-10		496.83	0.00	203.93	488.33	0	121
28-mag-10	496.83	0.00	203.93	488.33	0	121	
31-mag-10	499.50	2.67	206.60	491.00	2	123	

	DATE	EXCAVATION [m]	TUNNEL PRODUCTION/DAY [m]	TOTAL TUNNEL PRODUCTION [m]	LINING SEGMENTS [m]	N° LINING SEGMENTS/DAY [m]	N° TOTAL LINING SEGMENTS [m]	
JUNE	1-giu-10	500.80	1.30	207.90	492.30	1	123	
	3-giu-10	504.20	3.40	211.30	495.70	2	125	
	4-giu-10	508.30	4.10	215.40	499.80	2	128	
	7-giu-10	510.41	2.11	217.51	501.91	1	129	
	8-giu-10	511.80	1.39	218.90	503.30	1	130	
	9-giu-10	513.70	1.90	220.80	505.20	1	131	
	10-giu-10	514.50	0.80	221.60	506.00	0	131	
	11-giu-10	517.23	2.73	224.33	508.73	2	133	
	14-giu-10	521.72	4.49	228.82	513.22	3	136	
	15-giu-10	522.30	0.58	229.40	513.80	0	136	
	16-giu-10	527.40	5.10	234.50	518.90	3	139	
	17-giu-10	530.83	3.43	237.93	522.33	2	141	
	18-giu-10	535.90	5.07	243.00	527.40	3	144	
	21-giu-10	536.02	0.12	243.12	527.52	0	144	
	22-giu-10	539.33	3.31	246.43	530.83	2	146	
	23-giu-10	542.73	3.40	249.83	534.23	2	148	
	24-giu-10	545.50	2.77	252.60	537.00	2	150	
	28-giu-10	547.40	1.90	254.50	538.90	1	151	
	29-giu-10	547.83	0.43	254.93	539.33	0	151	
	30-giu-10	547.83	0.00	254.93	539.33	0	151	
Stop excavation for no ordinary yard operations in the excavation chamber								
JULY	19-lug-10	548.80	0.97	255.90	540.30	1	152	
	19-lug-10	549.55	0.75	256.65	541.05	0	152	
	20-lug-10	550.00	0.45	257.10	541.50	0	152	
	21-lug-10	553.90	3.90	261.00	545.40	2	155	
	22-lug-10	555.10	1.20	262.20	546.60	1	155	
	23-lug-10	566.50	11.40	273.60	558.00	7	162	
	27-lug-10	585.23	18.73	292.33	576.73	11	173	
	28-lug-10	593.70	8.47	300.80	585.20	5	178	
	29-lug-10	609.00	15.30	316.10	600.50	9	187	
	30-lug-10	622.73	13.73	329.83	614.23	8	195	
	AUGUST	2-ago-10	626.04	3.31	333.14	617.54	2	197
3-ago-10		634.00	7.96	341.10	625.50	5	202	
4-ago-10		644.00	10.00	351.10	635.50	6	208	
5-ago-10		663.50	19.50	370.60	655.00	11	219	
6-ago-10		663.50	0.00	370.60	655.00	0	219	
Stop excavation for vacancies								
23-ago-10		668.53	5.03	375.63	660.03	3	222	
24-ago-10		682.13	13.60	389.23	673.63	8	230	
25-ago-10		694.03	11.90	401.13	685.53	7	237	
26-ago-10		724.23	30.20	431.33	715.73	18	255	
27-ago-10		709.33	-14.90	416.43	700.83	-9	246	
30-ago-10	709.33	0.00	416.43	700.83	0	246		
31-ago-10	716.13	6.80	423.23	707.63	4	250		

Tab.III-1. Tunnel excavation process

APPENDIX IV

PARAMETRIC ANALYSES ON STIFFNESS MODULI (E , E_{ur}) AND THEIR RATIO (P)

INPUT PARAMETERS						OUTPUT VALUES									OUTPUT RESULTS RELATED TO REFERENCE ANALYSES RESULTS									
ANALYSES ID		E		E_{ur}	$P=E_{ur}/E$	V_i [%]			$k = i/Z_0$			w_{max} [mm]			$\Delta E/E_{rif}$	$\Delta V_i/V_{L,rif}$ [%]			$\Delta k/k_{rif}$ [%]			$\Delta w_{max}/w_{max,rif}$ [%]		
		[kN/m ²]	[kN/m ²]	[-]	Plane O	Plane U	Plane AE	Plane O	Plane U	Plane AE	Plane O	Plane U	Plane AE	[%]	Plane O	Plane U	Plane AE	Plane O	Plane U	Plane AE	Plane O	Plane U	Plane AE	
1	HS	E	6.73E+04	2.02E+05	3	0.08%	0.13%	0.14%	0.52	0.52	0.52	-1.82	-2.92	-3.05	0%	0%	0%	0%	0%	0%	0%	0%	0%	0%
2	HSE1	E_1	2.24E+04	6.73E+04	3	0.23%	0.35%	0.34%	0.54	0.53	0.53	-4.76	-7.47	-7.34	-67%	171%	161%	143%	4%	2%	1%	161%	156%	141%
3	HSE2	E_3	2.02E+05	6.06E+05	3	0.04%	0.07%	0.08%	0.57	0.56	0.57	-0.80	-1.36	-1.55	200%	-52%	-50%	-44%	8%	8%	10%	-56%	-54%	-49%
4	HSE3	E_2	3.37E+04	1.01E+05	3	0.16%	0.24%	0.24%	0.53	0.52	0.53	-3.37	-5.26	-5.28	-50%	86%	82%	74%	1%	1%	0%	85%	80%	73%
5	HSE4	E_4	1.35E+05	4.04E+05	3	0.05%	0.08%	0.09%	0.55	0.54	0.56	-1.06	-1.76	-1.93	100%	-39%	-37%	-33%	5%	4%	6%	-42%	-40%	-37%
6	HS6Eur	E	6.73E+04	4.04E+05	6	0.10%	0.16%	0.20%	0.67	0.66	0.68	-1.75	-2.82	-3.26	0%	23%	23%	40%	28%	27%	31%	-4%	-3%	7%
7	HSE16Eur	E_1	2.24E+04	1.35E+05	6	0.23%	0.38%	0.44%	0.64	0.64	0.67	-4.13	-6.65	-7.44	-67%	177%	182%	213%	22%	24%	28%	126%	128%	144%
8	HSE26Eur	E_3	2.02E+05	1.21E+06	6	0.05%	0.09%	0.11%	0.70	0.69	0.68	-0.87	-1.48	-1.91	200%	-36%	-33%	-19%	34%	33%	29%	-52%	-49%	-37%
9	HSE36Eur	E_2	3.37E+04	2.02E+05	6	0.18%	0.28%	0.33%	0.68	0.67	0.69	-2.96	-4.78	-5.42	-50%	110%	110%	135%	29%	28%	32%	63%	64%	78%
10	HSE46Eur	E_4	1.35E+05	8.08E+05	6	0.07%	0.11%	0.13%	0.69	0.68	0.70	-1.09	-1.83	-2.18	100%	-21%	-18%	-4%	32%	31%	34%	-40%	-37%	-28%
11	HS9Eur	E	6.73E+04	6.06E+05	9	0.11%	0.18%	0.22%	0.68	0.71	0.70	-1.83	-2.83	-3.59	0%	30%	33%	58%	29%	37%	34%	0%	-3%	18%
12	HSE19Eur	E_1	2.24E+04	2.02E+05	9	0.25%	0.39%	0.48%	0.71	0.70	0.73	-3.95	-6.38	-7.38	-67%	193%	194%	239%	35%	35%	40%	117%	118%	142%
13	HSE29Eur	E_3	2.02E+05	1.82E+06	9	0.06%	0.10%	0.14%	0.76	0.75	0.78	-0.94	-1.58	-1.97	200%	-25%	-22%	-4%	46%	44%	50%	-49%	-46%	-36%
14	HSE39Eur	E_2	3.37E+04	3.03E+05	9	0.17%	0.28%	0.34%	0.71	0.70	0.73	-2.80	-4.54	-5.33	-50%	108%	110%	145%	36%	35%	40%	53%	56%	75%
15	HSE49Eur	E_4	1.35E+05	1.21E+06	9	0.07%	0.12%	0.16%	0.74	0.73	0.76	-1.13	-1.90	-2.34	100%	-13%	-8%	12%	41%	40%	46%	-38%	-35%	-23%
16	HSEur	E	6.73E+04	8.08E+05	12	0.12%	0.19%	0.25%	0.77	0.76	0.79	-1.75	-2.88	-3.52	0%	42%	44%	75%	47%	46%	52%	-4%	-1%	15%
17	HSE1Eur	E_1	2.24E+04	2.69E+05	12	0.27%	0.37%	0.52%	0.78	0.76	0.78	-3.98	-5.61	-7.56	-67%	223%	179%	268%	48%	45%	48%	118%	92%	148%

18	HSE2Eur	E ₃	2.02E+05	2.42E+06	12	0.07%	0.12%	0.15%	0.83	0.81	0.83	-1.01	-1.70	-2.10	200%	-12%	-10%	10%	58%	55%	59%	-45%	-42%	-31%
19	HSE3Eur	E ₂	3.37E+04	4.04E+05	12	0.18%	0.29%	0.36%	0.75	0.74	0.77	-2.76	-4.47	-5.37	-50%	117%	118%	160%	44%	42%	48%	51%	53%	76%
20	HSE4Eur	E ₄	1.35E+05	1.62E+06	12	0.08%	0.14%	0.18%	0.80	0.78	0.81	-1.18	-1.98	-2.45	100%	-2%	1%	25%	52%	50%	55%	-35%	-32%	-20%

SOIL GRAVITY WEIGHT (γ)¹

INPUT PARAMETERS				OUTPUT VALUES									OUTPUT RESULTS RELATED TO REFERENCE ANALYSES RESULTS										
ANLAYSSES ID		γ_d	γ_{sat}	V_L [%]			$k = i/Z_0$			w_{max} [mm]			$\Delta\gamma/\gamma_{rif}$ [%]	$\Delta V_L/V_{L,rif}$ [%]			$\Delta k/k_{rif}$ [%]			$\Delta w_{max}/w_{max,rif}$ [%]			
		[kN/m ³]	[kN/m ³]	Plane O	Plane U	Plane AE	Plane O	Plane U	Plane AE	Plane O	Plane U	Plane AE		Plane O	Plane U	Plane AE	Plane O	Plane U	Plane AE	Plane O	Plane U	Plane AE	
1	HS	16.00	21.00	0.08%	0.13%	0.14%	0.52	0.52	0.52	-1.82	-2.92	-3.05	0%	0%	0%	0%	0%	0%	0%	0%	0%	0%	0%
2	HSg1	12.80	17.80	0.04%	0.06%	0.04%	0.41	0.38	0.28	-1.19	-1.78	-1.51	-20%	-49%	-56%	-73%	-22%	-28%	-46%	-35%	-39%	-51%	
3	HSg2	19.20	24.20	0.10%	0.17%	0.19%	0.52	0.52	0.54	-2.25	-3.63	-3.94	20%	22%	25%	32%	-1%	0%	2%	24%	24%	29%	
4	HSg3	14.40	19.40	0.08%	0.13%	0.13%	0.57	0.55	0.54	-1.68	-2.67	-2.72	-10%	1%	-4%	-8%	10%	5%	3%	-8%	-9%	-11%	
5	HSg4	17.60	22.60	0.09%	0.15%	0.16%	0.52	0.53	0.53	-1.99	-3.17	-3.39	10%	9%	10%	13%	0%	1%	2%	9%	9%	11%	

¹ For the parametric study on γ , ϕ and ψ the stiffness moduli values of the reference analysis were used

THREE-DIMENSIONAL FINITE ELEMENT ANALYSES

SOIL FRICTION ANGLE (φ)

INPUT PARAMETERS			OUTPUT VALUES									OUTPUT RESULTS RELATED TO REFERENCE ANALYSES RESULTS									
ANLAYSSES ID	φ [°]	V_L [%]	$k = i/Z_0$			w_{max} [mm]			$\Delta\varphi/\varphi_{rif}$ [%]	$\Delta V_L/V_{L,rif}$ [%]			$\Delta k/k_{rif}$ [%]			$\Delta w_{max}/w_{max,rif}$ [%]					
			Plane O	Plane U	Plane AE	Plane O	Plane U	Plane AE		Plane O	Plane U	Plane AE	Plane O	Plane U	Plane AE	Plane O	Plane U	Plane AE			
1	HS	35	0.08%	0.13%	0.14%	0.52	0.52	0.52	-1.82	-2.92	-3.05	0%	0%	0%	0%	0%	0%	0%	0%	0%	0%
2	HSj1	21	0.10%	0.13%	0.12%	0.63	0.63	0.64	-1.81	-2.36	-2.19	-40%	20%	-2%	-13%	21%	21%	22%	-1%	-19%	-28%
3	HSj2	28	0.10%	0.17%	0.18%	0.61	0.60	0.61	-1.92	-3.12	-3.43	-20%	23%	24%	32%	17%	16%	17%	5%	7%	12%
4	HSj3	24.5	0.08%	0.12%	0.12%	0.61	0.58	0.58	-1.47	-2.35	-2.44	-30%	-6%	-10%	-11%	16%	12%	11%	-19%	-20%	-20%
5	HSj4	31.5	0.10%	0.16%	0.18%	0.58	0.58	0.59	-2.05	-3.23	-3.46	-10%	25%	22%	27%	11%	11%	12%	12%	11%	13%

SOIL DILATANCY ANGLE (ψ)

INPUT PARAMETERS			OUTPUT VALUES									OUTPUT RESULTS RELATED TO REFERENCE ANALYSES RESULTS									
ANLAYSSES ID	Ψ [°]	V_L [%]	$k = i/Z_0$			w_{max} [mm]			$\Delta\Psi/\varphi_{rif}$ [%]	$\Delta V_L/V_{L,rif}$ [%]			$\Delta k/k_{rif}$ [%]			$\Delta w_{max}/w_{max,rif}$ [%]					
			Plane O	Plane U	Plane AE	Plane O	Plane U	Plane AE		Plane O	Plane U	Plane AE	Plane O	Plane U	Plane AE	Plane O	Plane U	Plane AE			
1	HS	0	0.08%	0.13%	0.14%	0.52	0.52	0.52	-1.82	-2.92	-3.05	0%	0%	0%	0%	0%	0%	0%	0%	0%	0%
2	HSY10	10	0.11%	0.17%	0.18%	0.61	0.58	0.59	-2.10	-3.29	-3.43	29%	34%	25%	27%	16%	11%	12%	15%	13%	13%
3	HSY5	5	0.11%	0.17%	0.18%	0.61	0.58	0.59	-2.10	-3.29	-3.43	14%	34%	25%	26%	16%	11%	12%	15%	13%	13%
4	HSY3	3	0.08%	0.13%	0.14%	0.52	0.52	0.52	-1.82	-2.92	-3.05	9%	0%	0%	0%	0%	0%	0%	0%	0%	0%
5	HSY1	1	0.08%	0.13%	0.14%	0.52	0.52	0.52	-1.82	-2.92	-3.05	3%	0%	0%	0%	0%	0%	0%	0%	0%	0%

EFFECTS OF SOIL PARAMETERS ON THE VOLUME LOSS AT THE TUNNEL DEPTH ($V_{L,axis}$)

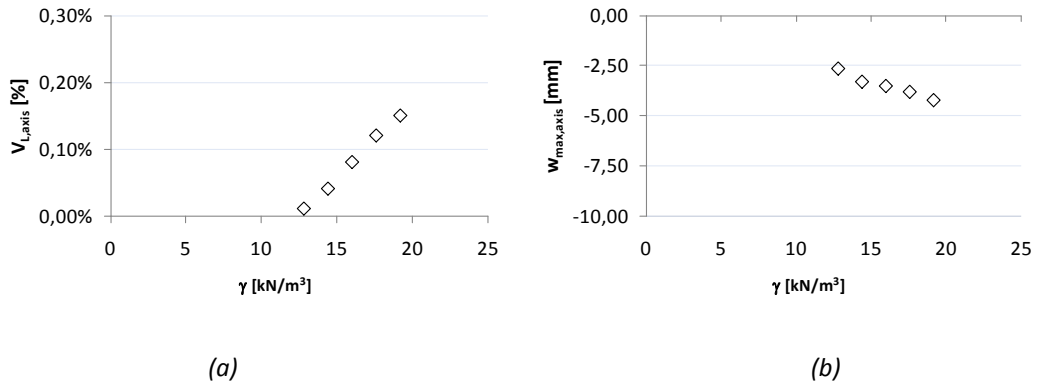


Fig. IV-1: Effects of γ on volume loss (a) and maximum settlement (b) at the tunnel depth

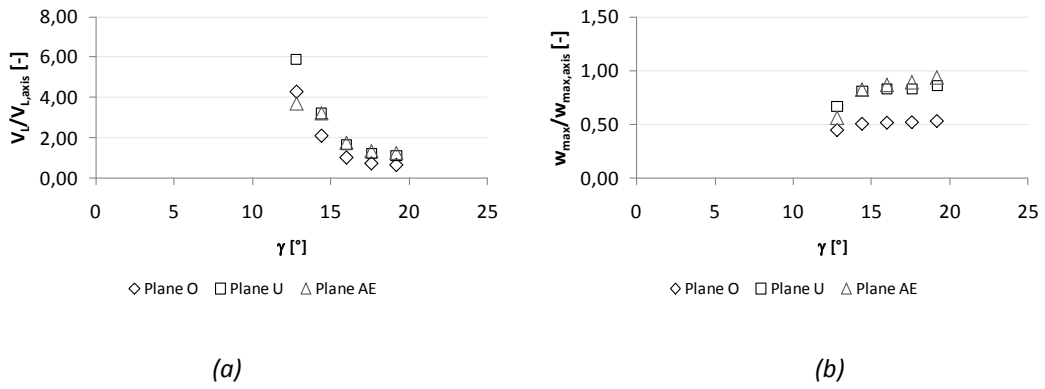


Fig. IV-2: γ vs surface volume losses (a) and maximum settlements (b) ratios

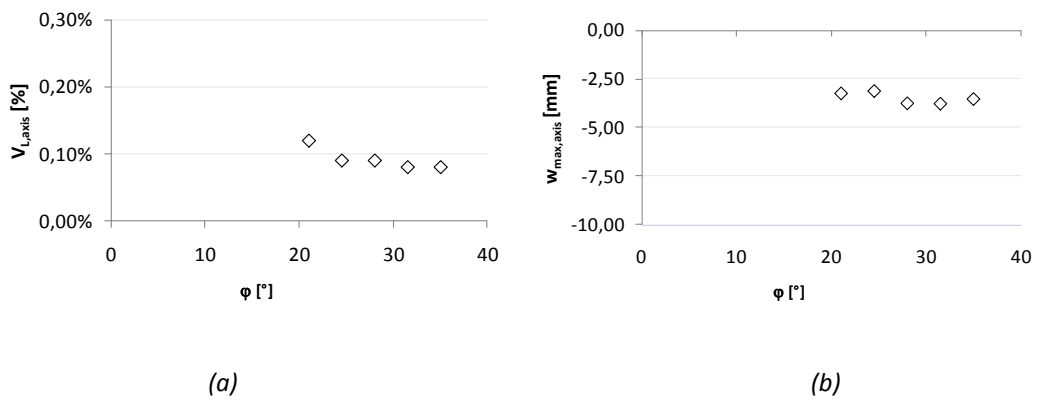


Fig. IV-3: Effects of ϕ on volume loss (a) and maximum settlement (b) at the tunnel depth

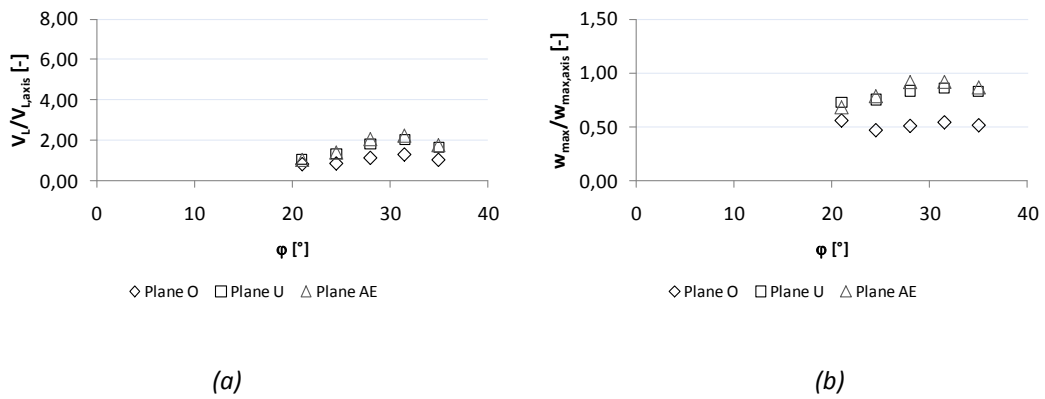


Fig. IV-4: φ vs surface volume losses (a) and maximum settlements (b) ratios

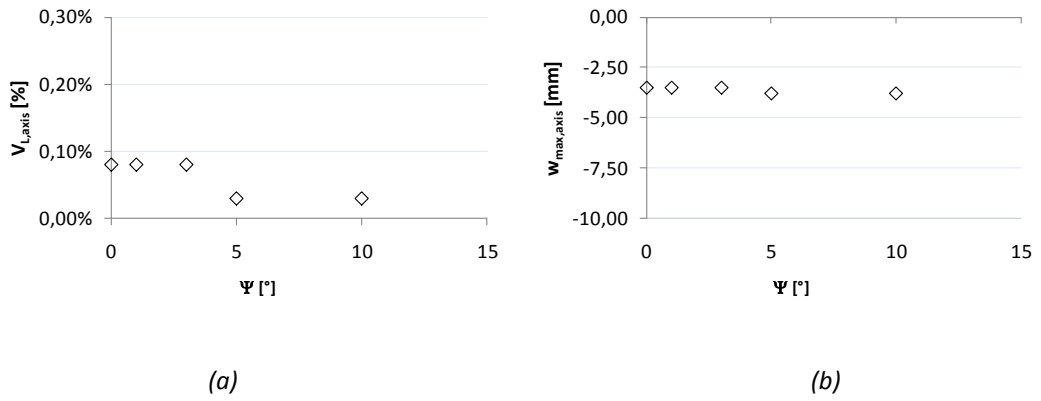


Fig. IV-5: Effects of ψ on volume loss (a) and maximum settlement (b) at the tunnel depth

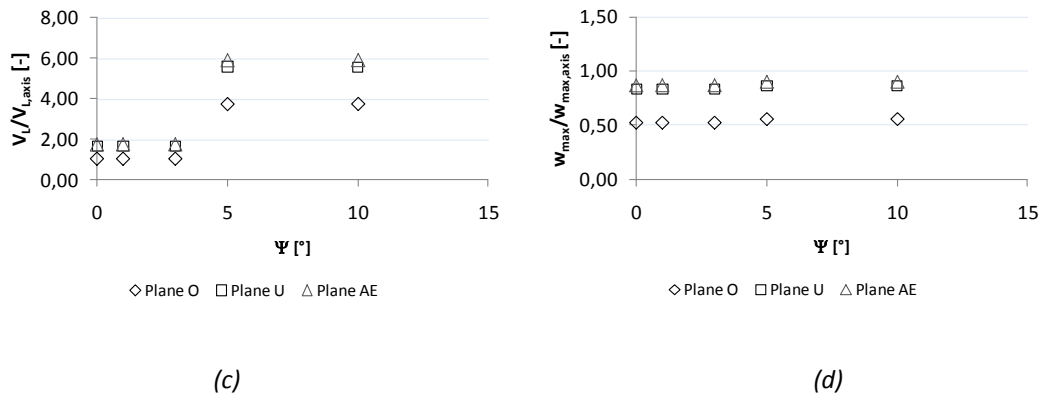


Fig. IV-6: ψ vs surface volume losses (a) and maximum settlements (b) ratios

EFFECTS OF SOIL PARAMETERS ON THE SURFACE VOLUME LOSS (V_L)

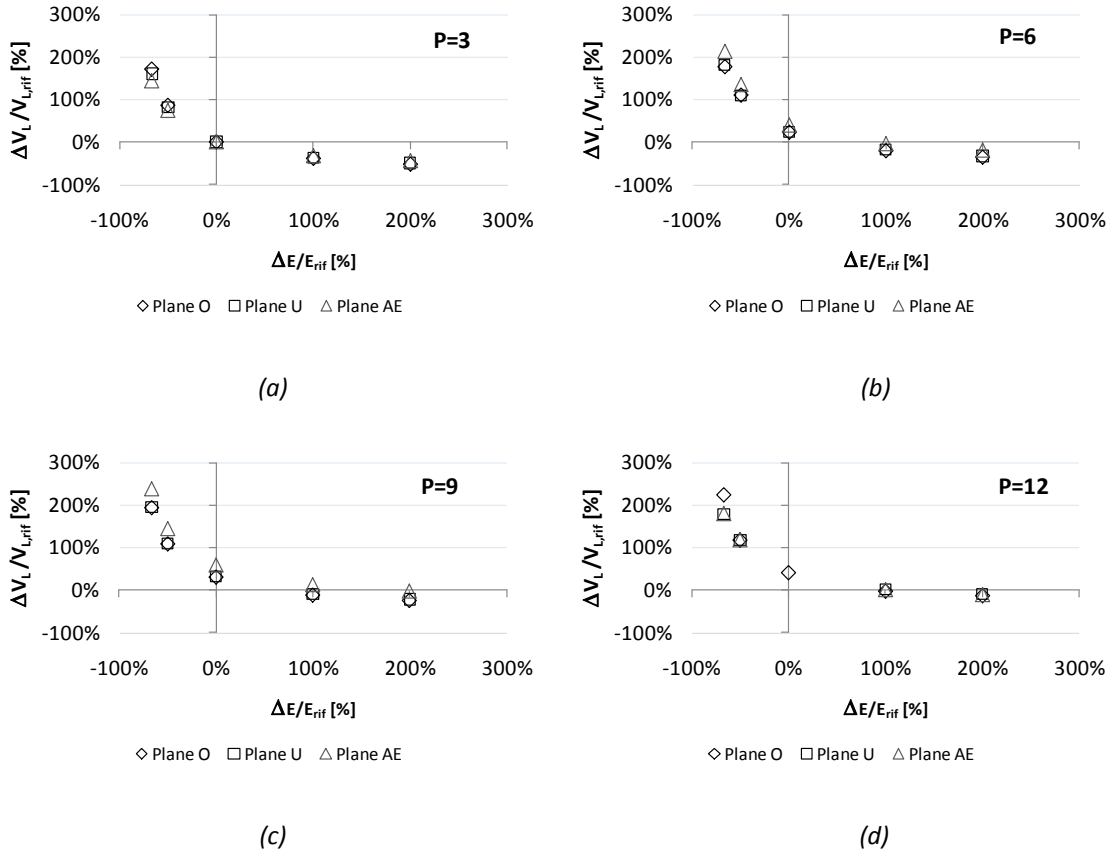


Fig. IV-7: Effects of loading stiffness modulus on V_L along the tunnel axis for constant stiffness moduli ratio (Plane O coinciding with the tunnel front, Plane U and Plane AE respectively 1D and 3D from it)

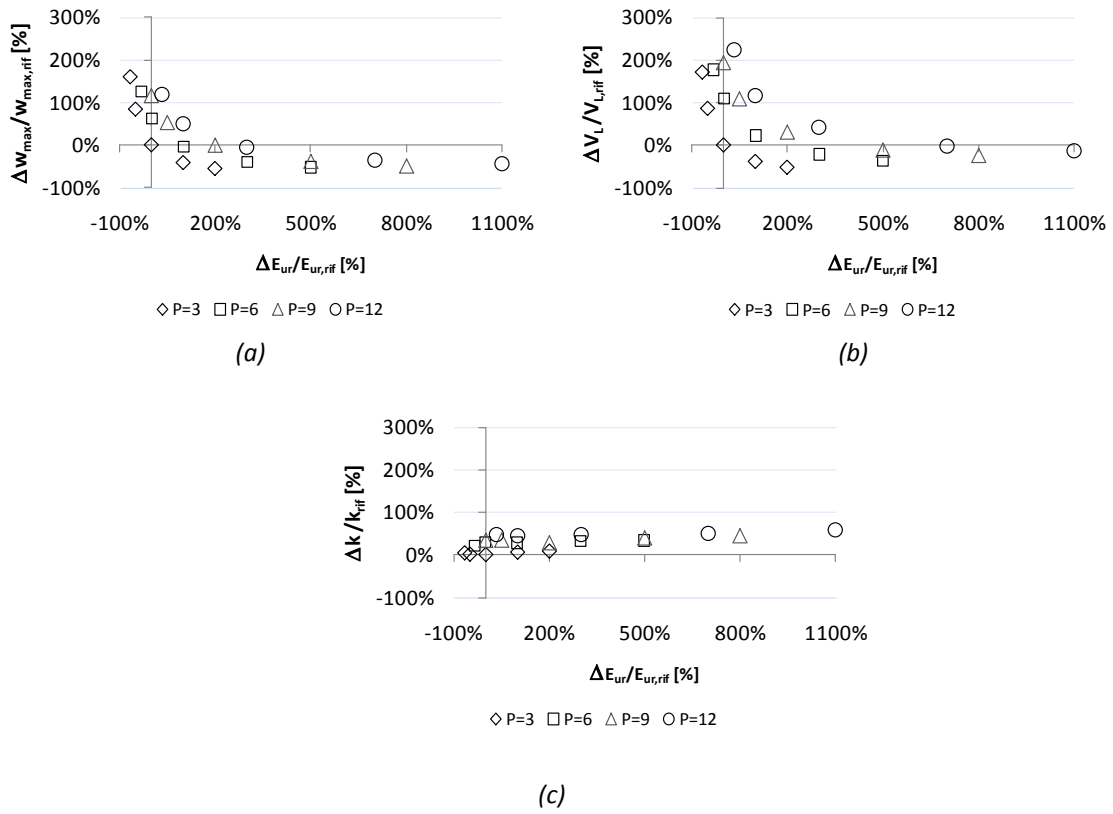
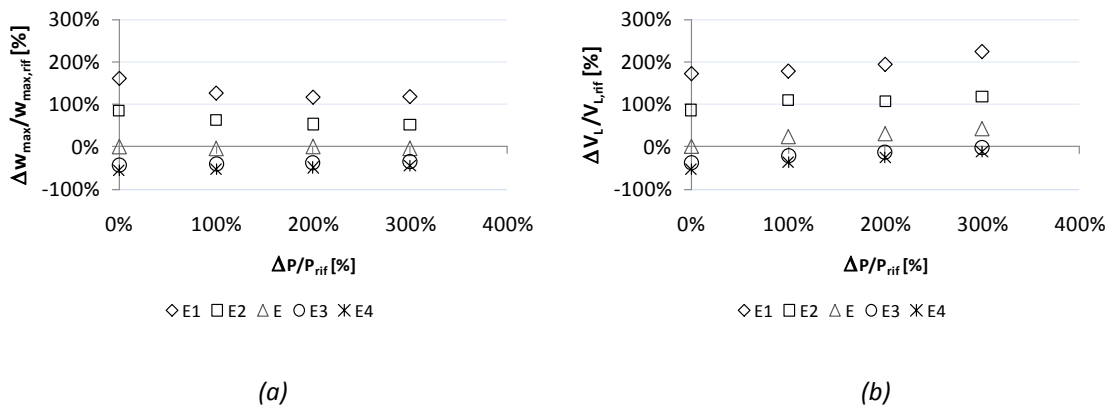
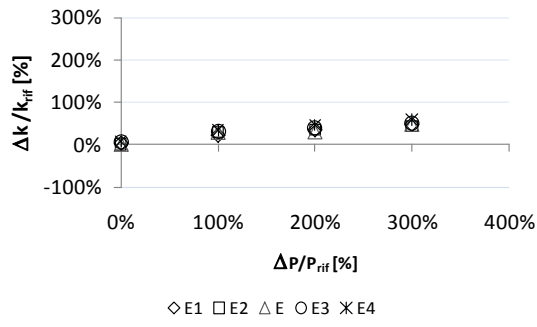


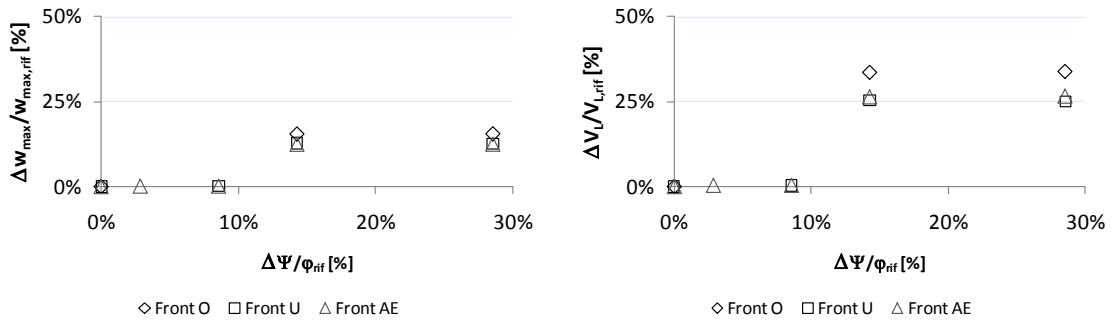
Fig. IV-8: Effects of un-reloading stiffness modulus on V_L along the tunnel axis for constant stiffness moduli ratio (Plane O coinciding with the tunnel front, Plane U and Plane AE respectively 1D and 3D from it)





(c)

Fig. IV-9: Effects of $P = E_{ur}/E_{ref}$ variations up to 300% on w_{max} , V_L and k



(a)

(b)

Fig. IV-10: Effects of ψ on w_{max} and V_L

THREE-DIMENSIONAL FINITE ELEMENT ANALYSES

PARAMETRIC ANALYSES ON MACHINE PRESSURES EFFECTS

ANALYSES ID		INPUT VALUES							OUTPUT VALUES		RESULTS ELABORATIONS						
		FP	FP _{inc}	GP	GP _{inc}	HYDRAULIC JACKS PRESSURE	V _{Lc}	GP/FP	w _{max}	V _L	ΔFP/FP	FP/FP _{rif}	ΔV _L /V _L	Δw _{max} /w _{max}	V _L /V _{Lc}	w _{max} /w _{max,rif}	w _{max} /w _{max,rif} (GP)
		[kPa]	[kPa]	[kPa]	[kPa]	[kPa]	[%]	[-]	[mm]	[%]	[%]	[-]	[%]	[%]	[-]	[-]	[-]
1	PG_HSg1EFP100GP100	100	14	100	20	635	0.1%	1.0	-7.59	0.36%	0.0	1.0	0%	0%	3.63	1.00	1.00
2	PG_HSg1EFP130GP100	130	14	100	20	756	0.1%	0.8	-6.29	0.31%	0.3	1.3	-16%	-17%	3.06	0.83	0.83
3	PG_HSg1EFP170GP100	170	14	100	20	918	0.1%	0.6	-5.62	0.27%	0.7	1.7	-25%	-26%	2.73	0.74	0.74
4	PG_HSg1EFP200GP100	200	14	100	20	1040	0.1%	0.5	-5.50	0.27%	1.0	2.0	-25%	-27%	2.70	0.73	0.73
5	PG_HSg1EFP300GP100	300	14	100	20	1445	0.1%	0.3	-5.53	0.27%	2.0	3.0	-25%	-27%	2.74	0.73	0.73
6	PG_HSg1EFP400GP100	400	14	100	20	1850	0.1%	0.3	-5.74	0.28%	3.0	4.0	-22%	-24%	2.84	0.76	0.76
7	PG_HSg1EFP500GP100	500	14	100	20	2255	0.1%	0.2	-6.13	0.30%	4.0	5.0	-18%	-19%	2.96	0.81	0.81
8	PG_HSg1EFP100GP130	100	14	130	20	635	0.1%	1.3	-7.08	0.33%	0.0	1.0	-9%	-7%	3.31	0.93	1.02
9	PG_HSg1EFP130GP130	130	14	130	20	756	0.1%	1.0	-5.86	0.29%	0.3	1.3	-21%	-23%	2.87	0.77	0.84
10	PG_HSg1EFP170GP130	170	14	130	20	918	0.1%	0.8	-5.21	0.26%	0.7	1.7	-29%	-31%	2.58	0.69	0.75
11	PG_HSg1EFP200GP130	200	14	130	20	1040	0.1%	0.7	-5.13	0.25%	1.0	2.0	-30%	-32%	2.55	0.68	0.74
12	PG_HSg1EFP300GP130	300	14	130	20	1445	0.1%	0.4	-5.15	0.26%	2.0	3.0	-29%	-32%	2.58	0.68	0.74
13	PG_HSg1EFP400GP130	400	14	130	20	1850	0.1%	0.3	-5.37	0.27%	3.0	4.0	-26%	-29%	2.68	0.71	0.77
14	PG_HSg1EFP100GP170	100	14	170	20	635	0.1%	1.7	-6.82	0.33%	0.0	1.0	-9%	-10%	3.29	0.90	0.98
15	PG_HSg1EFP130GP170	130	14	170	20	756	0.1%	1.3	-5.92	0.29%	0.3	1.3	-20%	-22%	2.89	0.78	0.85
16	PG_HSg1EFP170GP170	170	14	170	20	918	0.1%	1.0	-5.07	0.25%	0.7	1.7	-31%	-33%	2.49	0.67	0.73
17	PG_HSg1EFP200GP170	200	14	170	20	1040	0.1%	0.9	-4.97	0.25%	1.0	2.0	-32%	-34%	2.46	0.66	0.71
18	PG_HSg1EFP300GP170	300	14	170	20	1445	0.1%	0.6	-4.97	0.25%	2.0	3.0	-32%	-34%	2.48	0.66	0.71
19	PG_HSg1EFP400GP170	400	14	170	20	1850	0.1%	0.4	-5.19	0.26%	3.0	4.0	-29%	-32%	2.58	0.68	0.75
20	PG_HSg1EFP100GP200	100	14	200	20	635	0.1%	2.0	-6.96	0.33%	0.0	1.0	-9%	-8%	3.30	0.92	1.00
21	PG_HSg1EFP130GP200	130	14	200	20	756	0.1%	1.5	-5.65	0.27%	0.3	1.3	-24%	-25%	2.75	0.75	0.81
22	PG_HSg1EFP170GP200	170	14	200	20	918	0.1%	1.2	-5.01	0.24%	0.7	1.7	-33%	-34%	2.44	0.66	0.72
23	PG_HSg1EFP200GP200	200	14	200	20	1040	0.1%	1.0	-4.92	0.24%	1.0	2.0	-34%	-35%	2.41	0.65	0.71
24	PG_HSg1EFP300GP200	300	14	200	20	1445	0.1%	0.7	-4.93	0.24%	2.0	3.0	-33%	-35%	2.44	0.65	0.71

25	PG_HSg1EFP400GP200	400	14	200	20	1850	0.1%	0.5	-5.12	0.25%	3.0	4.0	-30%	-33%	2.52	0.67	0.74
26	PG_HSg1EFP500GP200	500	14	200	20	2255	0.1%	0.4	-5.43	0.26%	4.0	5.0	-27%	-28%	2.64	0.72	0.78
27	PG_HSg1E	200	14	220	20	1040	0.1%	1.1	-5.16	0.25%	1.0	2.0	-31%	-32%	2.52	0.68	0.00
28	PG_HSg1EFP100GP300	100	14	300	20	635	0.1%	3.0	-6.32	0.30%	0.0	1.0	-18%	-17%	2.97	0.83	1.00
29	PG_HSg1EFP130GP300	130	14	300	20	756	0.1%	2.3	-5.37	0.25%	0.3	1.3	-30%	-29%	2.54	0.71	0.85
30	PG_HSg1EFP170GP300	170	14	300	20	918	0.1%	1.8	-4.77	0.23%	0.7	1.7	-38%	-37%	2.26	0.63	0.76
31	PG_HSg1EFP200GP300	200	14	300	20	1040	0.1%	1.5	-4.70	0.22%	1.0	2.0	-38%	-38%	2.24	0.62	0.74
32	PG_HSg1EFP300GP300	300	14	300	20	1445	0.1%	1.0	-4.67	0.22%	2.0	3.0	-38%	-39%	2.25	0.61	0.74
33	PG_HSg1EFP400GP300	400	14	300	20	1850	0.1%	0.8	-4.82	0.23%	3.0	4.0	-36%	-36%	2.33	0.64	0.76
34	PG_HSg1EFP500GP300	500	14	300	20	2255	0.1%	0.6	-5.12	0.24%	4.0	5.0	-33%	-33%	2.43	0.67	0.81
35	PG_HSg1EFP100GP400	100	14	400	20	635	0.1%	4.0	-5.98	0.27%	0.0	1.0	-25%	-21%	2.72	0.79	1.00
36	PG_HSg1EFP130GP400	130	14	400	20	756	0.1%	3.1	-5.14	0.24%	0.3	1.3	-35%	-32%	2.37	0.68	0.86
37	PG_HSg1EFP170GP400	170	14	400	20	918	0.1%	2.4	-4.58	0.21%	0.7	1.7	-42%	-40%	2.11	0.60	0.77
38	PG_HSg1EFP200GP400	200	14	400	20	1040	0.1%	2.0	-4.50	0.21%	1.0	2.0	-43%	-41%	2.07	0.59	0.75
39	PG_HSg1EFP300GP400	300	14	400	20	1445	0.1%	1.3	-4.46	0.21%	2.0	3.0	-42%	-41%	2.09	0.59	0.75
40	PG_HSg1EFP400GP400	400	14	400	20	1850	0.1%	1.0	-4.57	0.21%	3.0	4.0	-41%	-40%	2.15	0.60	0.76
41	PG_HSg1EFP500GP400	500	14	400	20	2255	0.1%	0.8	-4.84	0.22%	4.0	5.0	-38%	-36%	2.23	0.64	0.81
42	PG_HSg1EFP100GP500	100	14	500	20	635	0.1%	5.0	-5.69	0.25%	0.0	1.0	-30%	-25%	2.52	0.75	1.00
43	PG_HSg1EFP130GP500	130	14	500	20	756	0.1%	3.8	-4.88	0.22%	0.3	1.3	-41%	-36%	2.15	0.64	0.86
44	PG_HSg1EFP170GP500	170	14	500	20	918	0.1%	2.9	-4.35	0.19%	0.7	1.7	-47%	-43%	1.91	0.57	0.77
45	PG_HSg1EFP200GP500	200	14	500	20	1040	0.1%	2.5	-4.27	0.19%	1.0	2.0	-48%	-44%	1.87	0.56	0.75
46	PG_HSg1EFP300GP500	300	14	500	20	1445	0.1%	1.7			2.0	3.0					
47	PG_HSg1EFP400GP500	400	14	500	20	1850	0.1%	1.3			3.0	4.0					
48	PG_HSg1EFP500GP500	500	14	500	20	2255	0.1%	1.0	-4.63	0.21%	4.0	5.0	-43%	-39%	2.08	0.61	0.81

Tab.V-1. Performed analyses aimed at the parametric study on machine pressures

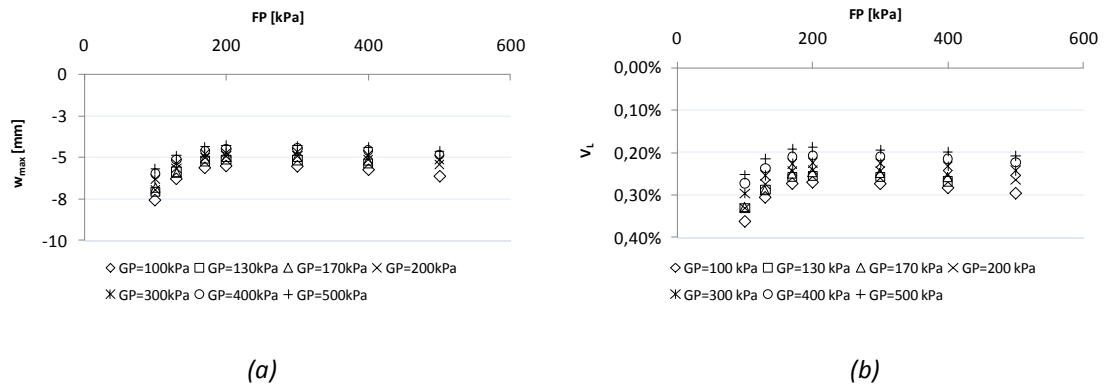


Fig. IV-11: Front pressure (FP) effects on maximum surface settlement (a) and on surface volume loss (b)

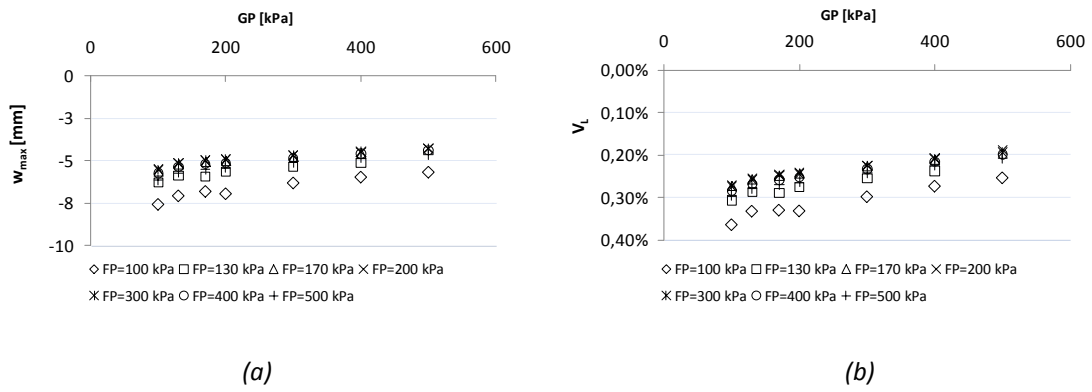


Fig. IV-12: Grout pressure (GP) effects on maximum surface settlement (a) and on surface volume loss (b)

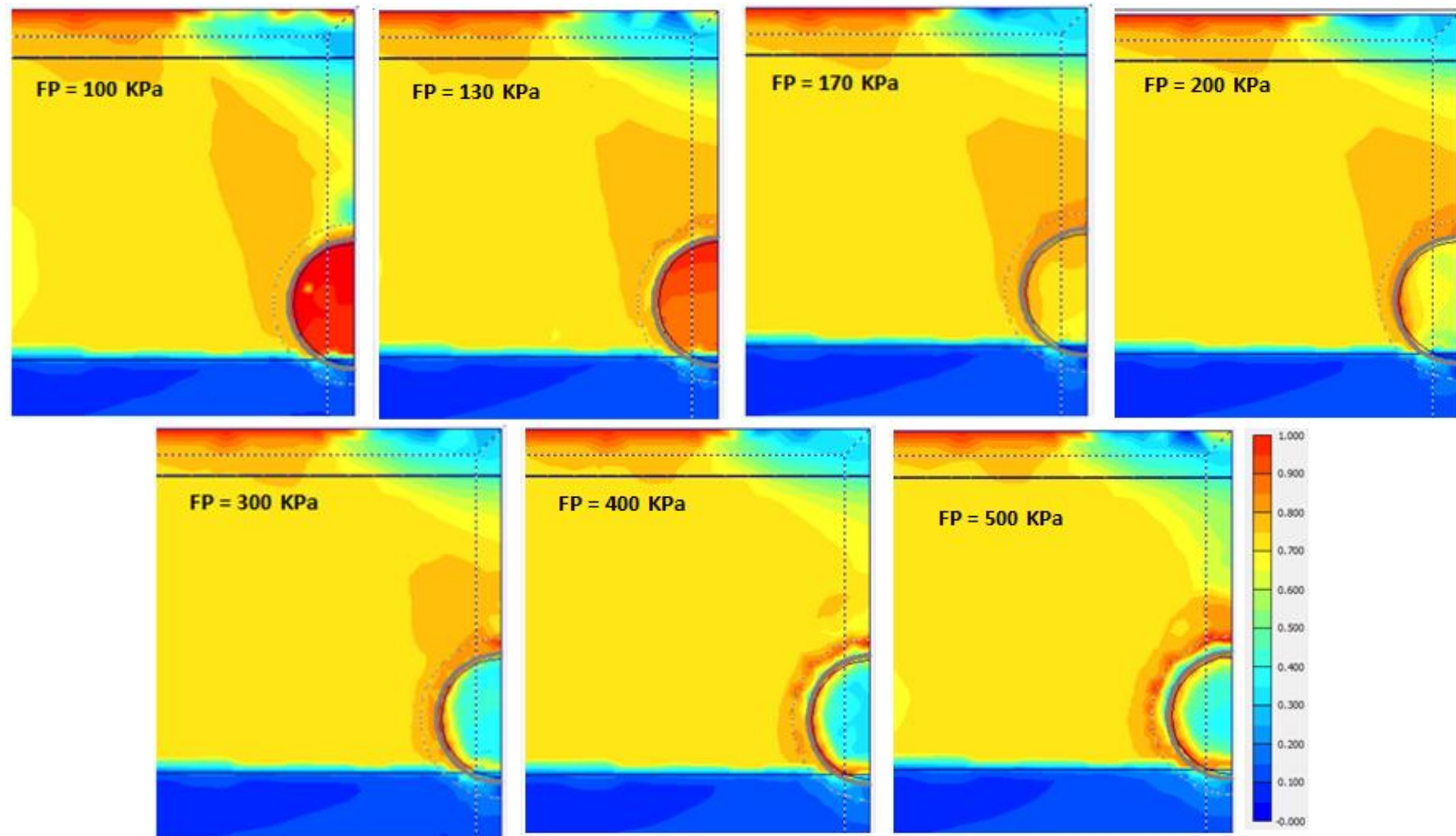


Fig. IV-13: $\tau_{rel} = \tau/\tau_{max}$: relative shear stresses for 100 kPa up to 500 kPa front pressures and constant grouting pressure (100 kPa)

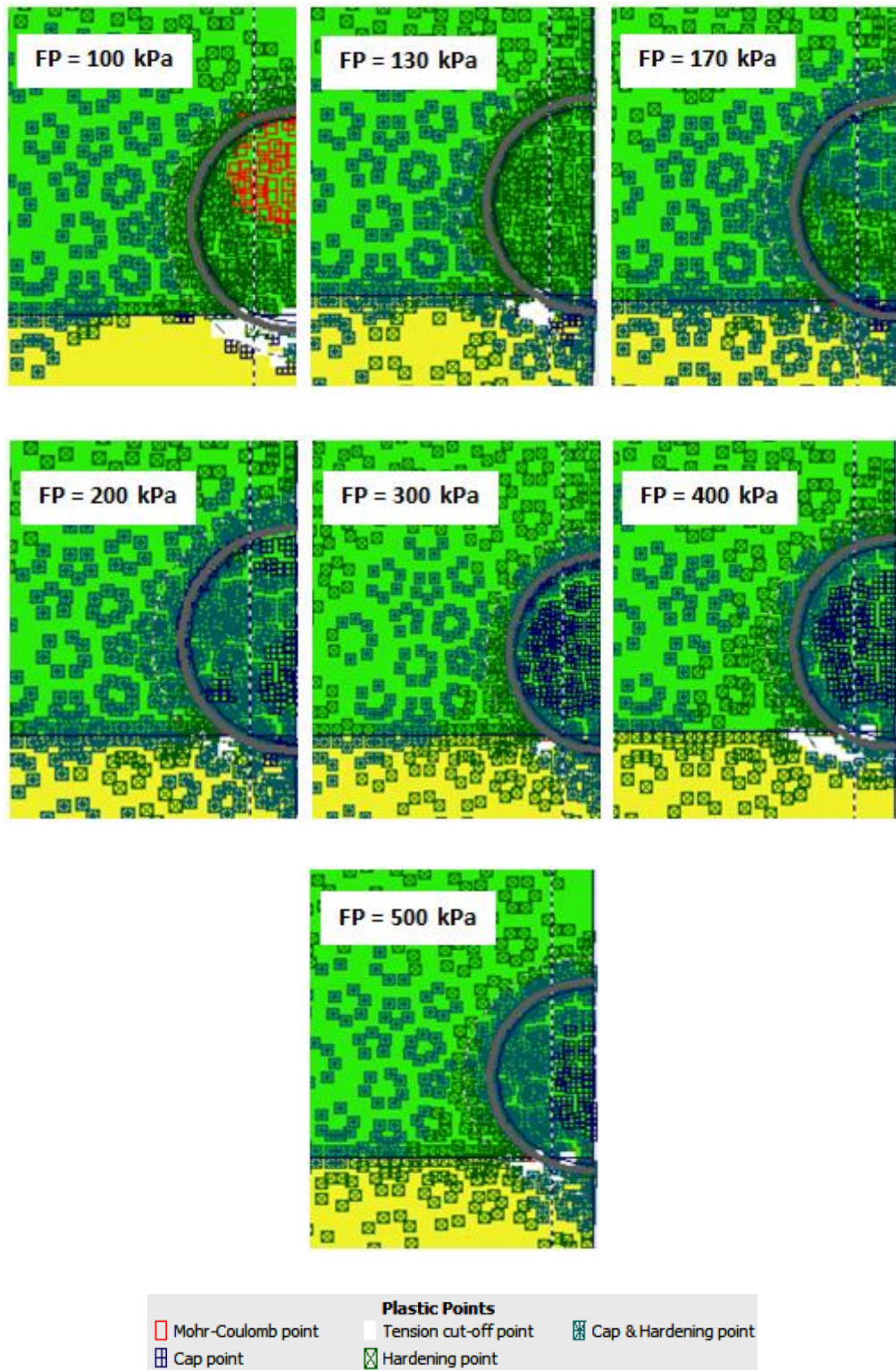


Fig. IV-14: Plastic points for analyses with 100 kPa up to 500 kPa front pressures and constant grouting pressure (100 kPa)

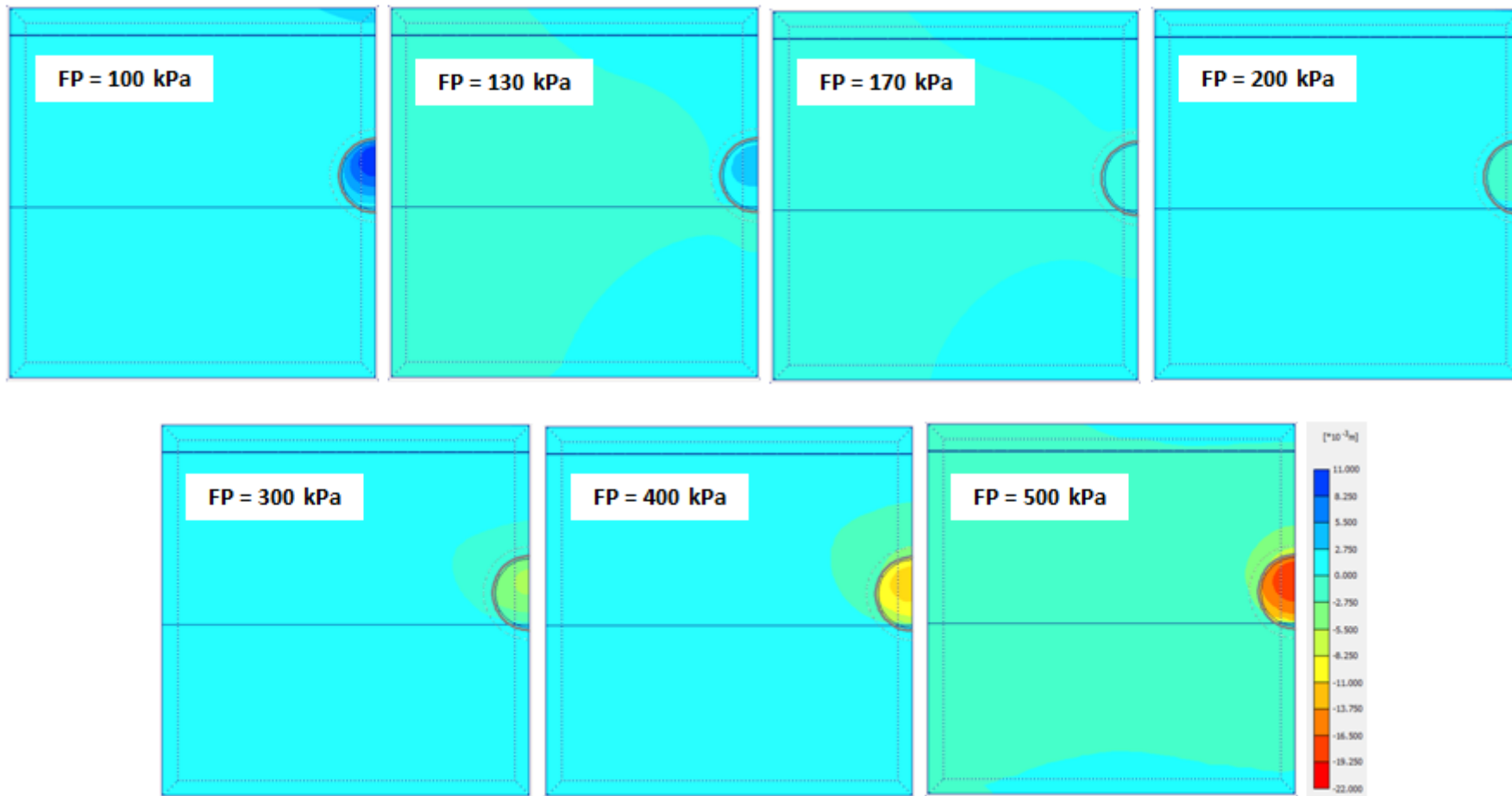


Fig. IV-15: Horizontal displacement along tunnel axis (z-axis) for analyses with 100 kPa up to 500 kPa front pressures and constant grouting pressure (100 kPa)